



# Investigation of regulation of stellar magnetism and rotation

A thesis presented

by

Aditi Sood

to

School of Mathematics and Statistics

in partial fulfillment of the requirements for the degree of

*Doctor of Philosophy*

University of Sheffield, UK

August, 2015

Supervisor: Dr. Eun-jin Kim



# Abstract

Stellar rotation plays an important role in maintaining the magnetic fields inside the stellar interior through convection, and starspots are the most visible manifestation of the interplay between stellar rotation rate and magnetic fields. It is revealed through high end observations of evolution of magnetic fields and rotation rate of the Sun and other solar type stars that they exhibit a wide range of variation among their rotation rates yet there are some common ingredients such as rotational shear, turbulent transport and various nonlinear transport mechanisms which contribute towards the evolution and maintenance of the magnetic activity displayed by them. Also, these observations provide us with valuable information about the dependence of differential rotation and magnetic activity on rotation rate of stars with different ages and different rotation rates. Thus, the main challenge in dynamo theory is to explain these observations which is in fact a very strenuous problem and is challenging to do with full MHD simulations due to the various constraints such as expensive computations in terms of time and resolution. Therefore, it is useful to construct a simple parameterized model in order to understand the evolution of rotation rate and magnetic fields which can provide valuable insight into the various observations.

This thesis discusses the modelling of solar dynamo and spindown of solar-type stars by using ODE and the effect of shear in kinematic dynamo in full MHD. We propose a simple parameterized model to understand the effect of nonlinear transport coefficients as well as mean/fluctuating differential rotation in the generation and destruction of magnetic fields and their capability in the working of dynamo near marginal stability. This model is then utilised to discuss detailed dynamics to understand the self-regulation of magnetic fields in solar/stellar dynamo. This work is further extended to understand the spindown of solar-type stars where the angular momentum loss is dynamically prescribed via equation of evolution of rotation rate and magnetic fields. The results obtained from this model are consistent with observations. Furthermore, regulatory behaviour of a kinematic dynamo by shear flow is investigated. Specifically, we study the induction equation by prescribing small scale velocity field to which a large scale radial/latitudinal shear is added in the direction of zonal flow. The results from numerical simulations are analysed and we conclude that the presence of large scale shear suppresses the small scale flows and results in quenching of a kinematic dynamo.



# Acknowledgement

Undertaking a PhD has been a life-changing experience for me, and I take this opportunity to express my sincere appreciation to everyone who has supported and guided me during this amazing journey.

First and foremost, I am extremely grateful to my supervisor Dr Eun-jin Kim for her continuous support, patient guidance and encouragement during the four years of my PhD. Her deep insights and contagious enthusiasm for her research always helped and motivated me during various stages of my PhD pursuit, even during tough times. I thank her for her unwavering belief in me.

My sincere gratitude is reserved for Prof Rainer Hollerbach for giving me an opportunity to work with him which was an invaluable learning experience. His invaluable insights and suggestions have greatly helped me to improve my research and thesis.

Many thanks to both my examiners, Dr Paul Bushby and Dr Istvan Ballai, for their extremely useful comments and suggestions.

I also greatly appreciate the support received from my advisor Dr Rekha Jain with whom I was always free and welcome to discuss any of my professional or personal problems. And, to my colleagues and friends who were always around me to help me when in need, and to make PhD a fun experience.

A big heartfelt thank you to my mum, dad, my siblings Alpana and Anadi, and my in-laws for believing in me to follow my dreams.

And finally, to my husband, Rishi, who had been by my side throughout this roller-coaster ride, and without whom I would not have the courage to embark on this incredible journey.



# Contents

<b>List of Figures</b>	<b>x</b>
<b>List of Tables</b>	<b>xv</b>
<b>1 Introduction</b>	<b>1</b>
1.1 Magnetism in other stars . . . . .	2
1.2 Fundamentals of dynamo theory . . . . .	5
1.3 Classification of Dynamos . . . . .	7
1.3.1 Kinematic versus dynamical dynamos . . . . .	7
1.3.2 Fast versus slow dynamos . . . . .	8
1.3.3 Large scale versus small scale dynamos . . . . .	8
1.4 Mean Field Theory . . . . .	9
1.5 Kinematic Dynamo . . . . .	11
1.6 Stellar dynamo saturation mechanisms . . . . .	14
1.7 Stellar magnetic activity and dynamical systems . . . . .	15
1.8 Summary . . . . .	16
<b>2 Consistent model of dynamo: activity and rotation</b>	<b>18</b>

2.1	Introduction . . . . .	20
2.2	Model Construction <sup>1</sup> . . . . .	23
2.3	Seventh-Order System . . . . .	25
2.4	Reduced Fifth-Order System . . . . .	31
2.5	Reduced Sixth-Order System . . . . .	35
2.6	Minimal Dynamical Model: parameter dependencies . . . . .	38
2.7	Conclusions . . . . .	42
<b>3</b>	<b>Signature of Self-regulation in a Nonlinear Dynamo</b>	<b>44</b>
3.1	Introduction . . . . .	46
3.2	Model equations . . . . .	48
3.3	Nonlinear effects through transport coefficients . . . . .	52
3.4	Nonlinear effect through mean differential rotation . . . . .	59
3.5	Nonlinear effect through fluctuating differential rotation . . . . .	67
3.6	Self-regulatory behavior of seventh-order system . . . . .	71
3.7	Conclusions . . . . .	72
<b>4</b>	<b>Spindown of solar type stars</b>	<b>74</b>
4.1	Introduction . . . . .	76
4.2	Model . . . . .	78
4.3	Results . . . . .	79
4.3.1	The $\Omega - t$ relationship . . . . .	79

---

<sup>1</sup>The dimensionless model represented by a set of Eqs. (2.1)-(2.4) in the absence of nonlinear transport coefficients is originally obtained by Cattaneo et al. (1983) and Weiss et al. (1984). A detailed derivation of these Eqs. is provided in the Appendix A as noted in Weiss et al. (1984). In present thesis, the model is extended by adding nonlinear transport coefficients represented by a system of Eqs. (2.5) - (2.8) and forms the basis of Chapters 2, 3 & 4, respectively.

4.3.2	The $ B  - \Omega$ relationship . . . . .	80
4.3.3	The Power spectra of $B$ and the $\omega_{cyc} - \Omega$ relationship . . . . .	81
4.3.4	The total shear - $\Omega$ relationship . . . . .	83
4.3.5	The $ B $ - Age Relationship . . . . .	85
4.3.6	The time-scale for spindown . . . . .	87
4.3.7	Summary of results . . . . .	89
4.4	Conclusions . . . . .	89
<b>5</b>	<b>Regulation of kinematic dynamo by shear flow</b>	<b>92</b>
5.1	Introduction . . . . .	94
5.2	Governing Equations . . . . .	96
5.3	Results . . . . .	100
5.3.1	Growth rate as a function of $R_m$ . . . . .	100
5.3.2	Growth rates with shear strength . . . . .	101
5.3.3	Contour plots and energy spectrum . . . . .	102
5.4	Conclusions . . . . .	109
<b>6</b>	<b>Conclusions</b>	<b>112</b>
6.1	Summary of the results . . . . .	112
6.2	Future Work . . . . .	114
<b>Appendix A Derivation of nonlinear dynamical system represented</b>		
	<b>by Eqs. (2.1) - (2.4)</b>	<b>115</b>
<b>Bibliography</b>		<b>120</b>

# List of Figures

1.1	Observational activity-rotation relationship for main sequence stars	3
1.2	Magnetic activity saturation for different stars at different levels .	4
1.3	Stretch-twist-fold . . . . .	9
1.4	Twisting of magnetic field lines due to cyclonic convection and stretching due to solar differential rotation is shown in (a) and (b), respectively. . . . .	12
1.5	Dynamo cycle in an $\alpha\Omega$ dynamo model . . . . .	13
2.1	Frequency of maximum intensity $\omega_M$ , magnetic field strength $ B $ and total shear are plotted as a function of $\Omega$ for $\kappa_1 = 2.5, \lambda_1 = \lambda_2 = 0$ for Case 1 in the seventh-order system. . . . .	28
2.2	Frequency of maximum intensity $\omega_M$ , magnetic field strength $ B $ , and total shear are plotted as a function of $\Omega$ for $\kappa_1 = 0.0, \lambda_1 = \lambda_2 = 2.5$ for Case 2 in the seventh-order system. . . . .	30
2.3	Frequency of maximum intensity $\omega_M$ , magnetic field strength $ B $ , and total shear are plotted as a function of $\Omega$ for $\kappa_1 = \lambda_1 = \lambda_2 = 2.5$ for Case 3 in the seventh-order system. . . . .	32
2.4	$\omega_M,  B $ , and total shear are plotted as a function of $\Omega$ for $\lambda_1 = \lambda_2 = 0, \kappa_1 = 1.0$ for Case 1 in the fifth-order system. . . . .	33

2.5	$\omega_M$ , $ B $ , and total shear are plotted as a function of $\Omega$ for $\lambda_1 = \lambda_2 = 2.5$ , $\kappa_1 = 0.0$ for Case 2 in the fifth-order system. . . . .	34
2.6	$\omega_M$ , $ B $ , and total shear are plotted as a function of $\Omega$ for $\kappa_1 = \lambda_1 = \lambda_2 = 3.5$ for Case 3 in the fifth-order system. . . . .	36
2.7	Frequency of maximum intensity $\omega_M$ and strength of magnetic field $ B $ as a function of rotation rate $\Omega$ for $\kappa_1 = \kappa_2 = \lambda_1 = \lambda_2 = 0.5$ for Case 1 in the sixth-order system. . . . .	37
2.8	Frequency of maximum intensity $\omega_M$ and $ B $ as a function of rotation rate $\Omega$ for $\kappa_1 = 0, \kappa_2 = \lambda_1 = \lambda_2 = 0.5$ for Case 2 in the sixth-order system. . . . .	38
2.9	Case 1: Frequency of maximum intensity $\omega_M$ , magnetic field strength $ B $ , and total shear are plotted as a function of $\Omega$ for $m=n=1$ and $\kappa_1 = \lambda_1 = \lambda_2 = 2.5$ . . . . .	41
2.10	Case 2: Frequency of maximum intensity $\omega_M$ , magnetic field strength $ B $ , and total shear are plotted as a function of $\Omega$ for $m=n=3$ and $\kappa_1 = \lambda_1 = \lambda_2 = 2.5$ . . . . .	42
3.1	Frequency of maximum intensity $p$ , poloidal magnetic field $ A $ and toroidal magnetic field $ B $ as a function of rotation rate $\Omega$ for $F_1 = F, F_2 = F_3 = 1.0$ for Case 1 in the fourth-order system. . . . .	54
3.2	Frequency of maximum intensity $p$ , poloidal magnetic field $ A $ and toroidal magnetic field $ B $ as a function of rotation rate $\Omega$ for $F_1 = 1.0, F_2 = F_3 = F$ for Case 2 in the fourth-order system. . . . .	55
3.3	Frequency of maximum intensity $p$ , poloidal magnetic field $ A $ and toroidal magnetic field $ B $ as a function of rotation rate $\Omega$ for $F_1 = F_2 = F_3 = F$ for Case 3 in the fourth-order system. . . . .	57

3.4	Frequency of maximum intensity $p$ , poloidal magnetic field $ A $ , toroidal magnetic field $ B $ and total shear as a function of rotation rate $\Omega$ for $F_1 = F_2 = F_3 = 1$ for Case 1 in the fifth-order system.	61
3.5	Frequency of maximum intensity $p$ , poloidal magnetic field $ A $ , toroidal magnetic field $ B $ and total shear as a function of rotation rate $\Omega$ for $F_1 = F_2 = F_3 = F$ for Case 4 in the fifth-order system.	64
3.6	Frequency of maximum intensity $p$ , poloidal magnetic field $ A $ , toroidal magnetic field $ B $ and total shear as a function of rotation rate $\Omega$ for $F_1 = F_2 = F, F_3 = 1$ for Case 5 in the fifth-order system.	66
3.7	Frequency of maximum intensity $p$ , poloidal magnetic field $ A $ and toroidal magnetic field $ B $ as a function of rotation rate $\Omega$ for $F_1 = F_2 = F_3 = 1$ for Case 1 in the sixth-order system. . . . .	68
3.8	Local scalings $\xi_1$ for $p$ , $\gamma_1$ for $ A $ , and $\beta_1$ for $ B $ are plotted as functions of rotation rate for different combinations of $F_1$ , $F_2$ , and $F_3$ , where for different combinations, different colours/linestyles are assigned as: for $F_1 = F_2 = F_3 = F$ black/solid line, $F_1 = F_2 = F, F_3 = 1$ green/dot, $F_1 = F_3 = F, F_2 = 1$ gold/dash, $F_1 = 1, F_2 = F, F_3 = F$ pink/dash dot, $F_1 = F, F_2 = F_3 = 1$ turquoise/dash dot dot, $F_1 = F_2 = 1, F_3 = F$ red/long dash, $F_1 = F_3 = 1, F_2 = F$ turquoise/'+'. . . . .	70
3.9	Frequency $p$ of magnetic field and toroidal magnetic field $ B $ are plotted as a function of rotation rate $\Omega$ for $F_1 = F_2 = F_3 = F$ in case of the seventh-order system for $\nu = 0.5$ and $\nu_0 = 35.0$ . . .	72
3.10	Time series of different nonlinear terms for $F_1 = F_2 = F_3 = F$ in case of the seventh-order system for $\nu = 0.5$ and $\nu_0 = 35.0$ . . .	72
4.1	Behaviour of rotation rate $\Omega$ is shown as function of time. . . . .	80

4.2	Magnetic field strength $ B $ is shown as a function of $\Omega$ . Also, fluctuating behavior $ B $ for high rotation rate regime is shown for $\Omega \in [23.30, 23.31]$ . . . . .	81
4.3	Power spectra of magnetic field $B$ is shown as a function of frequency. . . . .	84
4.4	Frequency of maximum intensity $\omega_{cyc}$ , as a function of time and rotation rate, respectively. . . . .	85
4.5	Total shear $1 + w_0$ as a function of rotation rate $\Omega$ . . . . .	85
4.6	Magnetic field strength $ B $ is shown as function of dimensionless time in (a) while (b) depicts the magnetic field strength as a function of age in physical units by scaling the $x$ -axis with age of the Sun. . . . .	87
4.7	Spindown timescale as function of age in Gyrs ( $1G = 10^9$ ) depicted in linear- and log-scale respectively. . . . .	88
5.1	$u_r$ , $u_\theta$ and $u_\varphi$ components in case of Flow1 . . . . .	98
5.2	$u_r$ , $u_\theta$ and $u_\varphi$ components in case of Flow2 . . . . .	99
5.3	Growth rates as function of $R_m$ in case of $(N_r, N_\theta) = (5, 20)$ . . .	102
5.4	Growth rates as function of $R_m$ in case of $(N_r, N_\theta) = (10, 40)$ . .	103
5.5	Growth rate as a function of shear strength for $(N_r, N_\theta) = (5, 20)$ and $(N_r, N_\theta) = (10, 40)$ for fixed values of $R_m$ and $m$ as $R_m = 1000$ , $m = 5, 10$ for Flow1 and Flow2. . . . .	104
5.6	Contour plots for $m = 5, N_r = 5$ . . . . .	105
5.7	Energy spectrum for Flow1 and Flow2 is depicted in (a) and (b) respectively, by taking $m = 5, N_r = 5, R_m = 1000$ . . . . .	106
5.8	Contour plots for $m = 5, N_r = 10$ . . . . .	106

5.9 Energy spectrum for Flow1 and Flow2 is depicted in (a) and (b) respectively, by taking  $m = 5, N_r = 10, R_m = 1000$ . We note that the resolution is marginal here. . . . . 107

5.10 Contour plots for  $m = 10, N_r = 5$  . . . . . 108

5.11 Energy spectrum for Flow1 and Flow2 is depicted in (a) and (b) respectively, by taking  $m = 10, N_r = 5, R_m = 1000$ . . . . . 109

5.12 Contour plots for  $m = 10, N_r = 10$  . . . . . 110

5.13 Energy spectrum for Flow1 and Flow2 is depicted in (a) and (b) respectively, by taking  $m = 10, N_r = 10, R_m = 1000$ . We note that the resolution is marginal here. Shear parameter is denoted by  $sp$  in some of the plots. . . . . 111

# List of Tables

3.1	Scaling exponents for $p$ , $ B $ , and $ A $ for $\Omega \geq 5$ in the cases of the fourth-order system where $p = \Omega^\xi$ , $ B  = \Omega^\beta$ , and $ A  = \Omega^\gamma$ .	59
3.2	Scaling exponents for $p$ , $ B $ , $ A $ , and $1 + w_0$ for $\Omega \geq 5$ in the cases of the fifth-order system where $p = \Omega^\xi$ , $ B  = \Omega^\beta$ , $ A  = \Omega^\gamma$ , and $1 + w_0 = \Omega^\delta$ .	65
3.3	Scaling exponents for $p$ , $ B $ , and $ A $ for $\Omega \geq 5$ in the cases of the sixth-order system where $p = \Omega^\xi$ , $ B  = \Omega^\beta$ , and $ A  = \Omega^\gamma$ .	69
4.1	Power law exponent $n$ for stars with different rotation period in days	79
4.2	Power law exponent $q$ for lower branch of frequency $\omega_{cyc}^I$ with rotation rate $\Omega$ for stars with different rotation periods.	83
4.3	Power law exponent $s$ for magnetic activity with age $t$ of stars $\in [1.066, 4]Gyrs$	87



# Chapter 1

## Introduction

Since the ancient times, researchers and scientists from around the world have been intrigued and fascinated by the study of the Sun and stars in the universe. With the technological advancements in computational power and high resolution observations, researchers have consistently made an effort to understand the detailed complexities of the origin of magnetic activity inside the Sun. The magnetic field inside the Sun is far from static and is responsible for all phenomena occurring in the solar interior and its atmosphere, such as solar flares, coronal mass ejections, solar winds etc. Sunspots are the most visible manifestation of magnetic activity occurring in the Sun. These are cool dark patches on the surface of the Sun and some of them are large enough to be seen by naked eye. The first evidence of sunspots was recorded around 325 B.C. by Theophrastus of Athens, one of Aristotle's students. Written evidences of non-telescopic, yet systematic, observations of sunspots are credited to Chinese observers around 165 BC. In the seventeenth century, with the invention of telescope, new and more accurate observations were made by Galileo which were a breakthrough in the development of observing and recording data connected to sunspots. For more than a hundred years observers carried on to simply document the presence of sunspots until the German astronomer called Heinrich Schwabe (1798-1875) discovered various

properties of sunspots. In 1843, he announced his discovery of the variation of sunspots on the solar surface with a possible period of 10 years which is known as solar cycle (presently known as a period of 11 years (Thomas and Weiss, 2008)). Followed by Schwabe's discovery, Richard Carrington (1826 - 1875) found the relation between the appearance of sunspots at certain latitude and the phase of the solar cycle. He mentioned that at the beginning of the solar cycle, spots appear on the surface of the Sun at the latitude of  $\pm 40^\circ$ . The preferred latitude of sunspot emergence drifts towards the equator with the progress of the solar cycle and finally vanishes in the next minimum. Through his observations, he also found that the rapid rotation of sunspots decreases with increasing latitude, indicating that the Sun rotates differentially - a discovery that is considered to be a landmark in the solar dynamo theory.

Many theories were proposed for the existence of sunspots but the major breakthrough in the understanding of sunspots was reported in the beginning of twentieth century when the existence of sunspots was linked to the solar magnetic field. Hale (1908a) observed a strong magnetic field of strength 3000 G (Gauss) in the sunspot by measuring the Zeeman splitting of spectral lines, and at the same time, he also detected the polarization of split component of these lines (Hale, 1908b). With the detection of extraterrestrial magnetic field, new direction was given to the research of magnetic fields in other stars and astronomical bodies. Further systematic observations revealed the magnetic polarity reversals of sunspot cycle with a period of 22 years of solar magnetic activity which is thought to be a manifestation of a strong toroidal magnetic field generated in the solar interior.

## **1.1 Magnetism in other stars**

During the extensive study of other stars it was revealed that the Sun is not the only body that exhibits magnetic activity but there are other stars across the Hertzsprung-Russell (H-R) diagram that exhibit similar phenomena. It is

now widely accepted that the rotation rate and stellar magnetism are inextricably connected to each other and are responsible for the stellar magnetic activity. Observations of nearby main sequence stars indicate a wide range of magnetic activity (Vaughan and Preston, 1980; Soderblom et al., 1991; Henry et al., 1996; Wright et al., 2004). In the stars of same spectral type and with deep convective envelopes, the chromospheric activity increases with increasing rotation rate and eventually becomes constant for very high rotation rates (see Fig.(1.1)-(1.2))(Noyes et al., 1984; Delfosse et al., 1998; Pizzolato et al., 2003; Wright et al., 2011).

Observations of lower-mass main sequence stars such as K- and M-type stars

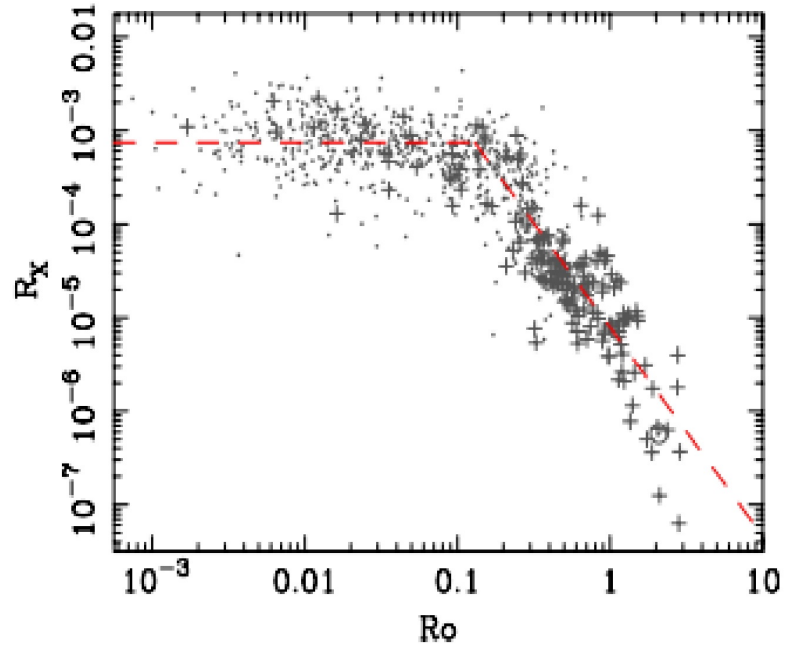


Figure 1.1: X-ray to bolometric luminosity ratio plotted against the Rossby number,  $Ro = \frac{P_{rot}}{\tau_c}$ , for all stars in a sample of 824 solar and late-type stars with X-ray luminosities and photometric rotation periods by Wright et al. (2011). The best-fitting saturated and non-saturated activity–rotation relations are shown as a dashed red line.

with convection zones and tachoclines display presence of global scale magnetic activity. Observations of fully convective stars (M-dwarfs  $\leq 0.35$  solar mass)

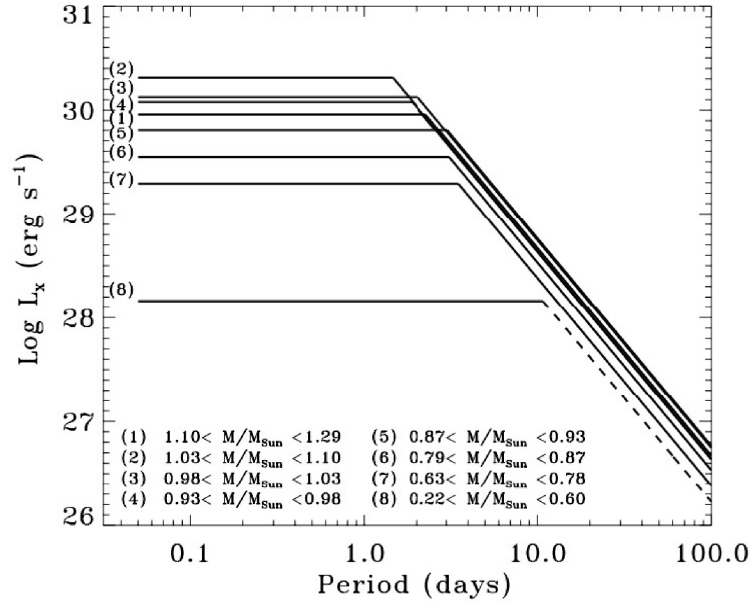


Figure 1.2: Magnetic activity of stars with different spectral type as a function of rotation period as shown by Pizzolato et al. (2003). For G-, K-, and M- type stars, the growth of activity is almost similar.

with no tachoclines have shown signatures of stronger magnetic activity. Since these stars do not have tachoclines, a distinct stellar dynamo than the Sun is believed to work in them.

Rotation rate and stellar magnetism are the main ingredients for the stellar spindown. Rapidly rotating star generates a strong magnetic field and is believed to produce an outward transport of angular momentum via stellar winds which eventually help in spindown of the star (MacGregor and Brenner, 1991; Keppens et al., 1995; Allain, 1998; Leprovost and Kim, 2010; Spada et al., 2011; Reiners and Mohanty, 2012; Gallet and Bouvier, 2013). Spindown of stars also depends upon the age and mass of stars. It is observed that the solar-type stars slowdown less rapidly as compared to low mass G- and K-type stars, but tend to lose most of their angular momentum by the age of  $10^9$  years. The observations of solar wind and angular momentum loss demonstrate that spindown time scales range from  $10^7 - 10^9$  years. Through the study of angular momentum loss and stellar

spindown as a function of age/mass provides a direct connection between stellar magnetism and rotation rate.

Nowadays, the main challenge in dynamo theory is to explain the observations theoretically. Therefore, a detailed analysis of stellar magnetism and rotation rate is required to establish a theoretical understanding of rotation-activity relationship and spindown of stars. To explain this a detailed analysis of idealized models is required to probe the effect of rotation rate, differential rotation (shear) and nonlinear transport on the working of stellar dynamo in the framework of dynamo theory. This establishes the basis of Chapters (2-4) in this thesis.

## 1.2 Fundamentals of dynamo theory

It is believed that solar (and stellar) magnetic activity is the result of a dynamo process which maintains a magnetic field by a rotating, convecting and electrically conducting fluid. Substantial research has been carried out in this field and various theories have been proposed to comprehend the complex nature of the dynamo process. It was Sir Joseph Larmor (1919) who, for the first time, proposed a tentative dynamo process for the maintenance of the solar magnetic field when he raised an important question “*How could a rotating body such as the Sun become a magnet?*”. The aim of the dynamo theory is to understand how an inductive motion of electrically conducting fluid induces the electric current that maintains the magnetic field. This mechanism is explained step by step as follows (Tobias, 2002):

- i. an electric field  $\mathbf{u} \times \mathbf{B}$  is induced by motion  $\mathbf{u}$  of electrically conducting fluid across a magnetic field  $\mathbf{B}$ .
- ii. electric field is also related to the rate of change of flux using Faraday’s equation  $\frac{\partial \mathbf{B}}{\partial t} = -\nabla \times \mathbf{E}$ .
- iii. a current  $\mathbf{j}$  is generated by this electric field that is related to current using

Ohm's Law in a moving medium  $\mathbf{j} = \sigma(\mathbf{E} + \mathbf{u} \times \mathbf{B})$ , where  $\sigma$  denotes the electrical conductivity.

- iv. a magnetic field is then generated by electric current by using Ampere's law in the absence of displacement currents given by  $\nabla \times \mathbf{B} = \mu \mathbf{j}$ , where  $\mu$  is the magnetic permeability.
- v. a Lorentz force  $\mathbf{j} \times \mathbf{B}$  is produced by the interaction of magnetic fields and current that back reacts on the motion of electrically conducting fluid.

The induction equation is obtained by eliminating  $\mathbf{E}$  from i.-iv. and is given as:

$$\frac{\partial \mathbf{B}}{\partial t} = \nabla \times (\mathbf{u} \times \mathbf{B}) - \nabla \times (\eta \nabla \times \mathbf{B}), \quad (1.1)$$

$$\nabla \cdot \mathbf{B} = 0, \quad (1.2)$$

where  $\eta = (\mu\sigma)^{-1}$  is the magnetic diffusivity,  $\nabla \times (\mathbf{u} \times \mathbf{B})$  is the induction term and  $\nabla \times (\eta \nabla \times \mathbf{B})$  is the diffusion term. If  $U$  and  $L$  are the typical velocity and length scales, then the advective (convective) time scale and diffusion time scale are defined as  $\tau_c = \frac{L}{U}$  and  $\tau_d = \frac{L^2}{\eta}$ , respectively. The ratio of diffusion time scale to advective time scale is known as magnetic Reynolds number and is given by  $R_m = \frac{\tau_d}{\tau_c} = UL/\eta$ . If  $R_m \gg 1$ , induction dominates over diffusion, whereas when  $R_m \ll 1$ , diffusion dominates over induction.

In the incompressible limit, the flows satisfy the momentum equation in the presence of Lorentz force and other body forces  $\mathbf{F}$ , and it can be written as

$$\frac{\partial \mathbf{u}}{\partial t} + \mathbf{u} \cdot \nabla \mathbf{u} = -\frac{1}{\rho} \nabla p + \frac{1}{\rho} \mathbf{F} + \frac{1}{\mu\rho} (\nabla \times \mathbf{B}) \times \mathbf{B} + \nu \nabla^2 \mathbf{u}, \quad (1.3)$$

$$\nabla \cdot \mathbf{u} = 0, \quad (1.4)$$

where,  $\rho$  is the density,  $p$  is the pressure,  $\mathbf{u}$  is the velocity of fluid,  $\mathbf{B}$  is the magnetic field and  $\nu$  is the diffusivity. In simple words, the induction equation describes the evolution of magnetic field, whereas the effect of  $\mathbf{B}$  on flow is

included in the Navier-Stokes equations by

$$\mathbf{j} \times \mathbf{B} = \frac{1}{\mu}(\nabla \times \mathbf{B}) \times \mathbf{B} = \frac{1}{\mu}(-\nabla(\frac{1}{2}|\mathbf{B}|^2) + (\mathbf{B} \cdot \nabla \mathbf{B})). \quad (1.5)$$

Equation (1.5) shows that the force can be divided into magnetic pressure, which reduces the gas pressure in strong field regions, and a magnetic tension, acting to straighten the magnetic field lines.

For more complex systems such as stellar interiors, apart from induction equation and momentum equation, other equations such as energy and continuity are also required.

## 1.3 Classification of Dynamos

After introducing the basic mechanism of a dynamo process and various equations, here we explain how and when a dynamo is considered to be linear or nonlinear in the traditional dynamo theory.

### 1.3.1 Kinematic versus dynamical dynamos

Theoretically, the dynamo process is classified into two categories: linear and nonlinear. In linear regime the induction equation is solved in the presence of prescribed velocity field in the limit when the magnetic field is very small as compared to velocity field and does not alter the flow. Dynamos studied in this framework are known as “kinematic dynamos”. The exponentially growing solutions can be obtained in this case for some values of  $R_m$  as magnetic field is amplified by the prescribed velocity field. However, the kinematic theory is no longer valid if the magnetic field becomes strong enough to alter the velocity field, i.e., the fluid motions are affected by the Lorentz force term which inhibits the growth of the magnetic field, and the system then becomes nonlinear. These types of dynamos are known as “non-linear dynamos”. Due to being computationally expensive in time, the induction equation is often solved in the framework of

kinematic dynamo theory.

### 1.3.2 Fast versus slow dynamos

For a prescribed velocity field, the growth rate of magnetic field,  $\sigma(\epsilon)$ , depends upon magnetic Reynolds number,  $R_m$  and a distinction between fast or slow dynamos can be made by studying the behavior of  $\sigma(\epsilon)$  with  $R_m$ , where  $R_m$  is related to  $\epsilon$  as  $R_m = \frac{1}{\epsilon}$ . If  $\sigma(\epsilon)$  is positive and bounded away from zero for  $R_m \rightarrow \infty$  or  $\epsilon \rightarrow 0$  then the dynamo is considered to be a “fast dynamo” (Childress and Gilbert, 1995). The rate at which the magnetic field grows is comparable to convective timescale of the flow. Therefore, a fast dynamo is defined by

$$\sigma_0 = \lim_{\epsilon \rightarrow 0} \sigma(\epsilon) > 0,$$

where  $\sigma_0$  is the growth rate for fast dynamo. For sufficiently small  $\epsilon$ , if the growth rate is not bounded above zero, that is,  $\sigma_0 \leq 0$  then the dynamo is considered to be a “slow dynamo”. This distinction is only applicable if the flow is prescribed. Various observations reveal that the stellar magnetic fields vary on a timescale faster than the diffusive timescale, e.g., the evolution of the magnetic field of the solar convection zone varies on convective timescale of months (sunspots) to years (solar cycle).

The mechanism responsible for fast dynamo action was proposed by Vainshtein and Zel’dovich (1972) and is known as ‘Stretch - Twist - Fold’ mechanism illustrated in Fig. (1.3). The magnetic field strength is increased by stretching while dissipative effects of magnetic diffusion are minimised by constructive folding.

### 1.3.3 Large scale versus small scale dynamos

Depending upon the nature of flow, the dynamos are categorised as large scale and small scale dynamos. For large scale dynamos, magnetic fields grow on large

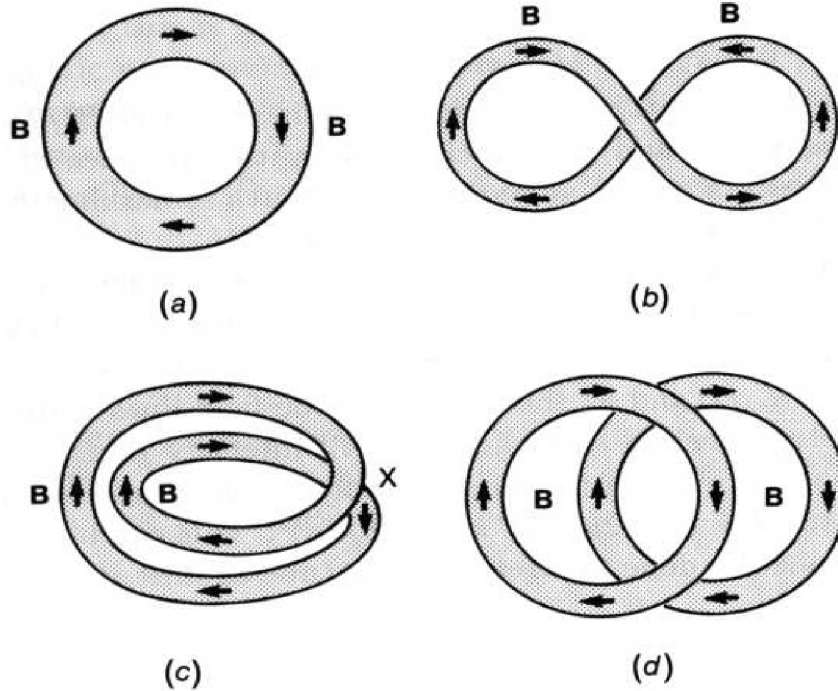


Figure 1.3: The schematic diagram of stretch-twist-fold mechanism taken from Roberts (1994).

scale, that is, fields are evolving on large scale by averaging and considering the mean part of the governing equations, specifically the induction equation, and are known as mean field dynamos. To study small scale dynamos the flows are chosen to be on small scale, which may be realised under fully isotropic conditions. Small scale or fluctuating dynamos play a crucial role in understanding the fundamental physical processes in astrophysical bodies as these are common random flows in conducting fluid (Brandenburg and Subramanian, 2005).

## 1.4 Mean Field Theory

Physical phenomena which are observed on large spatial or temporal scales are believed to be manifestations of processes happening on much smaller scales. To compute and resolve the dynamics on all relevant scales is computationally unfeasible. In the case of the Sun, the dynamical ranges being so large, it is virtually

impossible to apply this approach. To overcome this problem, the dynamo theory is studied in the framework of mean field electrodynamics (Steenback et al., 1966; Moffatt, 1978). In this approach, a physical quantity is expressed as the sum of mean and fluctuating parts as

$$F = \langle F \rangle + F',$$

where  $F'$  is the fluctuating part;  $\langle F' \rangle = 0$ . Here  $\langle ; \rangle$  represents the average. The Reynolds averaging rules that are required to solve the MHD equations are given as:

$$\begin{aligned} \langle \langle F \rangle \rangle &= \langle F \rangle, \\ \langle F' \rangle &= 0, \\ \langle F + G \rangle &= \langle F \rangle + \langle G \rangle, \\ \langle \langle F \rangle + \langle G \rangle \rangle &= \langle F \rangle + \langle G \rangle, \\ \langle \langle F \rangle G' \rangle &= 0. \end{aligned}$$

Splitting velocity  $\mathbf{u}$  and magnetic field  $\mathbf{B}$  into its mean and fluctuating parts, we have

$$\mathbf{u} = \langle \mathbf{u} \rangle + \mathbf{u}', \tag{1.6}$$

$$\mathbf{B} = \langle \mathbf{B} \rangle + \mathbf{B}', \tag{1.7}$$

Using Eqs. (1.4) and (1.5), the mean and fluctuating parts of the induction Eq. (1.1) can be written as:

$$\frac{\partial \langle \mathbf{B} \rangle}{\partial t} = \nabla \times (\mathbf{E} + \langle \mathbf{u} \rangle \times \langle \mathbf{B} \rangle) - \nabla \times (\eta \nabla \times \langle \mathbf{B} \rangle), \tag{1.8}$$

$$\frac{\partial \mathbf{B}'}{\partial t} = \nabla \times (\langle \mathbf{u} \rangle \times \mathbf{B}' + \mathbf{u}' \times \langle \mathbf{B} \rangle + \mathbf{G}) - \nabla \times (\eta \nabla \times \mathbf{B}'). \tag{1.9}$$

where  $\mathbf{E} = \langle \mathbf{u}' \times \mathbf{B}' \rangle$  and  $\mathbf{G} = \mathbf{u}' \times \mathbf{B}' - \langle \mathbf{u}' \times \mathbf{B}' \rangle$ . In Eq. (1.9),  $\mathbf{E}$  is electromotive force arising from the interactions of the turbulent motion and field which can be determined from Eq. (1.7). Here  $\langle \mathbf{u} \rangle$  is neglected. Introducing first order smoothing,  $\mathbf{G}$ , can be neglected and  $\mathbf{u}'$  acts on the mean  $\langle \mathbf{B} \rangle$  causing the generation of the turbulent field  $\mathbf{B}'$ . Therefore, we can write

$$E_i = \alpha_{ij} \langle B_j \rangle + \beta_{ijk} \frac{\partial \langle B_j \rangle}{\partial x_k}, \quad (1.10)$$

where the tensors  $\alpha_{ij}$  and  $\beta_{ijk}$  depend upon the local structure of velocity field i.e.  $\mathbf{u}'$  and  $\langle \mathbf{u} \rangle$ . Assuming that the field is isotropic, then  $\alpha_{ij} = \alpha \delta_{ij}$ ,  $\beta_{ijk} = \beta \varepsilon_{ijk}$  and  $\mathbf{E} = \alpha \langle \mathbf{B} \rangle - \beta \nabla \times \langle \mathbf{B} \rangle$ . If  $\tau_c$  is very small compared to  $\tau_d$ ,  $\alpha$  is found to be  $\alpha = -\frac{\tau_c}{3} \langle \mathbf{u} \cdot (\nabla \times \mathbf{u}) \rangle$ . The quantity  $\langle \mathbf{u} \cdot (\nabla \times \mathbf{u}) \rangle$  is a measure of flow helicity and is thought to be important in the mean field dynamo theory (Moffatt, 1978).

## 1.5 Kinematic Dynamo

The generation of large scale magnetic fields in solar/stellar interior and their maintenance against the turbulent motions is much researched area in the astrophysics. The results obtained from high resolution observations inspire the community to develop a better understanding of these observations from a theoretical point of view. Despite being investigated for almost a century, the understanding of stellar magnetism and rotation rate is still incomplete. Various models have been developed to investigate the dynamo process but the most dominant model in this field is the  $\alpha\Omega$  dynamo model in which the poloidal magnetic field is produced from toroidal magnetic field via  $\alpha$ -effect while differential rotation ( $\Omega$ -effect) is thought to generate toroidal magnetic field through poloidal magnetic field and closes the dynamo loop. The magnetic field lines are twisted due to Sun's rotation and cyclonic motions inside the convection zone. This twisting of magnetic field lines is shown in Fig. (1.4a) and is known as  $\alpha$ -effect. The stretching and wrapping of magnetic field lines around the Sun due

to differential rotation is called  $\Omega$ - effect (See Fig. (1.4b); courtesy of NASA, <http://solarscience.msfc.nasa.gov/dynamo.shtml>).

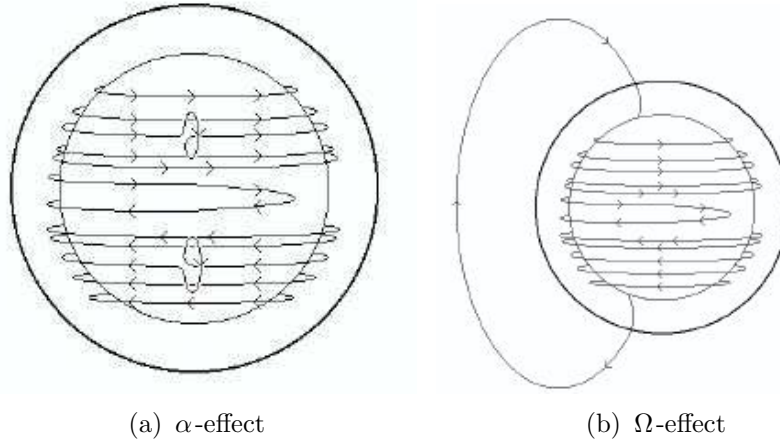
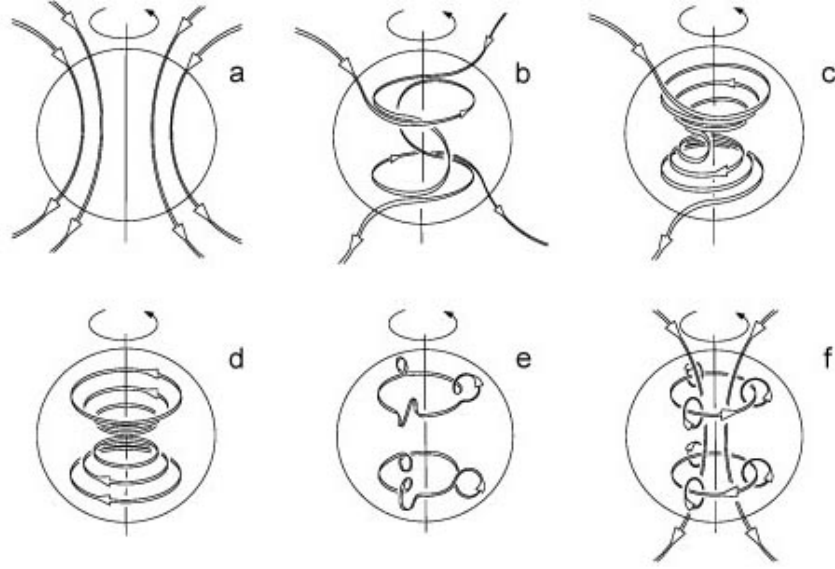


Figure 1.4: Twisting of magnetic field lines due to cyclonic convection and stretching due to solar differential rotation is shown in (a) and (b), respectively.

The magnetic field amplification of a dynamo cycle is explained with the help of a diagram taken from Love (1999). In Fig. 1.5, panel *a* shows the poloidal magnetic field lines which are wrapped by the differential rotation (panels *b* and *c*) inside the stellar interior which gives rise to toroidal field (panel *d*). The toroidal field lines are distorted by the helical motions (panels *e* and *f*), thus producing the poloidal field lines and completing the dynamo loop.

Therefore, in the dynamo process, the stellar rotation rate plays an important role. Mean helicity produces the  $\alpha$ -effect due to rotation rate (Moffatt, 1978; Parker, 1979) and is defined by a parameter  $\alpha = -\frac{\tau_c}{3} \langle \mathbf{u} \cdot (\nabla \times \mathbf{u}) \rangle$ , where  $\mathbf{u}$  is the convective velocity with magnitude  $U$  and  $\tau_c = L/U$  is the convective turnover time on characteristic length scale  $L$ . The quantity  $D_\alpha = \alpha L/\eta$  is a non-dimensional parameter which measures the  $\alpha$ -effect, where  $\eta = L^2/\tau_c$  is turbulent magnetic diffusivity. The differential rotation (shear) is responsible for the generation of toroidal magnetic field and is measured by a magnetic Reynolds number  $D_\Omega = \Omega' L^3/\eta$ , where  $\Omega' \propto \Omega/L$  is the gradient of rotation rate,  $\Omega$ . The dynamo action is controlled by a dimensionless parameter known as dynamo number,  $D$ ,



Love, J. J., 1999. *Astronomy & Geophysics*, 40, 6.14-6.19.

Figure 1.5: Dynamo cycle in an  $\alpha\Omega$  dynamo model

which is given by

$$D = D_\alpha D_\Omega = \frac{\alpha L}{\eta} \cdot \frac{\Omega' L^3}{\eta}. \quad (1.11)$$

In mean field dynamo theory,  $\alpha$  is often considered to be proportional to rotation rate and dynamo number  $D$  is given by

$$D \propto \Omega^2. \quad (1.12)$$

For stars with same spectral type, the power law dependence of cycle period  $P_{cyc}$  of the magnetic field on rotation rate  $\Omega$  is given as  $P_{cyc} \propto D^{-\frac{1}{2}} \propto \Omega^{-1}$  in case of kinematic dynamo theory. Further, the frequency of magnetic fields is related to  $\Omega$  as  $\omega \propto P_{cyc}^{-1} \propto \Omega$ , that is, as rotation rate increases, the period of the magnetic field decreases and this relationship is compatible with observations. However, in

case of nonlinear dynamo, the dynamo saturation inhibits the growth of magnetic fields, and questions the validity of linear relationship of frequency and rotation rate.

## 1.6 Stellar dynamo saturation mechanisms

In nonlinear dynamo theory, the Lorentz force acts back on the magnetic field and leads to dynamo saturation by inhibiting the infinite growth of magnetic field strength. In the present thesis, we have incorporated the following saturation mechanisms for the better understanding of the solar/stellar dynamo (Sood and Kim, 2013)

- i. Quenching is the source of generation of magnetic field (e.g.  $\alpha$ -quenching): the total helicity reduced by the large scale magnetic field can cause the saturation of the growth of the mean field.
- ii.  $\Omega$ -quenching (shear quenching): the reduction in  $\Omega$ -effect is caused by the tension in magnetic field lines due to Lorentz force that opposes the mean differential rotation, for example, the presence of torsional oscillations observed in the Sun (Labonte and Howard, 1982)
- iii. magnetic flux loss: magnetic field can be lost by the magnetic flux which is eliminated from the areas where dynamo functions. For example, magnetised fluid is lighter as compared to the unmagnetised plasma, leading to a reduction in magnetic pressure and density inside the magnetic flux tube. These flux tubes move upwards against the gravity, escaping from the regions where the dynamo operates.

## 1.7 Stellar magnetic activity and dynamical systems

The interaction of flows and magnetic fields inside the stellar interior constitutes a complex dynamical system. It is useful to utilise low order models to understand the behavior of a system and other complicated processes such as self-organisation of magnetic fields inside the Sun and stars. These low order models are basically dynamical systems which describe the evolution of important variables in time. Mathematically, a dynamical system is defined as a set of ordinary differential equations (ODE) with dependent variables as function of time (Ott, 1993) and is given as

$$\begin{aligned}\frac{dx_1}{dt} &= F_1(x_1, x_2, \dots, x_n), \\ \frac{dx_2}{dt} &= F_2(x_1, x_2, \dots, x_n), \\ &\vdots = \vdots \\ \frac{dx_n}{dt} &= F_n(x_1, x_2, \dots, x_n),\end{aligned}\tag{1.13}$$

which can be written in vector form as

$$\frac{d\mathbf{x}}{dt} = F[\mathbf{x}(t)],\tag{1.14}$$

where  $\mathbf{x}$  is the  $n$ -dimensional vector. Equation (1.14) can be solved by taking initial state  $x(0)$  to obtain the solution of the system  $x(t)$ .

Previously, in dynamo theory, low order models are used to explain the cyclic behavior of magnetic activity (Ruzmaikin, 1981; Ostriakov and Usoskin, 1990; Serre and Nesme-Ribes, 2000; Popova and Potemina, 2013). Low order models used to explain the features of solar dynamo are constructed by truncating the partial differential equations (PDE) of mean field electrodynamics and form a set

of ordinary differential equations. This method is advantageous as the truncated system of ODE provides an equivalent physical interpretation of each term derived from corresponding system of PDE. However, this procedure has the disadvantage of being sensitive to the level of truncation and could be responsible for losing some of the information. There is another method of constructing low order models which uses the nonlinear dynamics by applying symmetry argument or bifurcation theory (Tobias et al., 1995a; Knobloch and Landsberg, 1996; Knobloch et al., 1998). Though dynamics obtained in these models is robust yet physical interpretation of low order equations is not much clear as the terms in such a system do not provide any physical analogue for the given terms.

## 1.8 Summary

The present thesis is divided into six chapters. In Chapter 2-4, the role of nonlinear transport coefficients as well as mean/fluctuating shear is investigated to understand the working of stellar dynamo and self-organisation process. This work is further extended to model the spindown of stellar interior. In Chapter 5, the induction equation is solved numerically to understand the effect of large scale shear in the quenching of a dynamo. A brief synopsis of individual chapters is as follows:

- Chapter 1 is the introduction which provides the brief background to the present work.
- Chapter 2 proposes a minimum rotation and dynamo model which reproduces the observations such as linear increase of cycle frequency with rotation rate and saturation of magnetic activity for rapidly rotating stars. This work is published in *Astronomy and Astrophysics* (Sood, A. & Kim, E. 2013, *A&A*, 555, A(22)).

- In Chapter 3, we investigate how nonlinear transport coefficients help in the self-regulation of a stellar dynamo by studying the system for different limits of mean/fluctuating differential rotation. This work is published in *Astronomy and Astrophysics* (Sood, A. & Kim, E. 2014, A&A, 563, A(100)).
- In Chapter 4, the model for spindown of solar type stars is proposed in the presence of equation of evolution for magnetic field and rotation rate. For the first time, angular momentum loss is prescribed dynamically instead of kinematically to model the spindown of fast rotating and slow rotating stars. To this end, we evolve the stellar rotation and magnetic field simultaneously over stellar evolution time by extending our work in Chapter 2-3 on dynamo model which incorporates the nonlinear feedback mechanisms on rotation and magnetic fields. We show that our extended model reproduces key observations and is capable of explaining the presence of the two branches of (fast and slow rotating) stars which have different relations between rotation rate ( $\Omega$ ) - time ( $t$ ), magnetic field strength ( $|B|$ )-rotation rate and frequency of magnetic field ( $\omega_{cyc}$ ) - rotation rate (Sood, A., Hollerbach, R. & Kim, E., 2015, ApJ, under review).
- Chapter 5 studies the effects of large scale shear on kinematic dynamo where the velocity field is considered to be small scale. The results suggest the quenching of dynamo in the presence of shear. This work is done in collaboration with Prof. Rainer Hollerbach, University of Leeds, UK.
- Chapter 6 summarises the results and concludes the thesis.

## Chapter 2

# Consistent model of dynamo: activity and rotation

In order to understand the data obtained through observations, we investigate a dynamic model of dynamo and rotation which consistently reproduces the dependence of magnetic activity and differential rotation,  $\Delta\Omega$ , on stellar rotation rate,  $\Omega$ . In particular, a minimal seventh-order nonlinear dynamical system is presented by incorporating the effects of generation and destruction of magnetic fields through quenching of  $\alpha$ -effect, magnetic flux losses and differential rotation. We investigate different combinations of  $\alpha$ -quenching and flux losses to study how frequency of magnetic fields,  $\omega$ , magnetic field strength,  $|B|$ , and the differential rotation,  $\Delta\Omega$ , vary with the rotation rate,  $\Omega$ . We investigate three different cases:  $\alpha$ -quenching and no flux loss; flux loss and no  $\alpha$ -quenching;  $\alpha$ -quenching and flux loss. We find that results are in best agreement with observations for the last case where we have  $\alpha$ -quenching as well as poloidal/toroidal flux loss in equal amounts. The localized frequency of maximum intensity of magnetic fields depends upon  $\Omega$  as  $\omega \propto \Omega^{0.80}$ , which is consistent with the observations. Magnetic activity and mean differential rotation tend to saturate for higher rotation.



## 2.1 Introduction

In the realms of astrophysics it is established that the stellar magnetic activity is the result of dynamo action, which generates and sustains the magnetic fields by inductive motion of conducting fluid. Various models have been proposed and investigated to interpret the origin of magnetic activity occurring inside the stellar interior. In 1955, for the first time, Parker successfully proposed a dynamo model to explain the generation of toroidal field from poloidal field and a poloidal field from toroidal field, respectively, by considering the co-action of non-uniform rotation and cyclonic convection. Subsequently, over the years, several other models have been presented to explain the magnetic activity and its features such as butterfly diagrams, and sunspots by imposing several necessary conditions on the boundaries of the stellar surface. Stellar rotation rate is the key characteristic which is strongly correlated with the strength of observed magnetic field. Further, the two main components for mean field theory namely  $\alpha$ -effect and differential rotation are thought to increase linearly with rotation rate while the rotation rate depends upon a dimensionless parameter known as dynamo number  $D$ . Previously, the behaviour of nonlinear dynamos with varying  $D$  was investigated by Gilman (1983a,b) by numerical simulations of 3D MHD equations. On the other hand, Cattaneo et al. (1983) and Weiss et al. (1984) investigated nonlinear dynamos by using low-order models. Noyes et al. (1984), in their historic paper, showed that in lower main sequence, the chromospheric activity and magnetic activity of stars rely on the the inverse Rossby number  $\sigma = \tau_c/P_{rot}$ , with  $\tau_c$  as the convective turnover time and  $P_{rot}$  as the stellar rotation period at the base of the convection zone. By examining the behavior of magnetic activity and dynamo number,  $D$ , they obtained the dependence of cycle period  $P_{cyc}$  on stellar rotation period  $P_{rot}$  as  $P_{cyc} \propto P_{rot}^\beta$  for stars of same spectral type, where  $\beta$  is the value  $1.25 \pm 0.5$ . It has been revealed through detailed and organised investigation of different types of stars that there are two branches of stars with

different scaling exponents,  $\beta = 0.8$  for active branch for all the young and fast rotating stars, and  $\beta = 1.15$  for inactive branch containing all the old and slow rotating stars (Saar and Brandenburg, 1999; Saar, 2002).

In the  $\alpha - \Omega$  dynamo, the differential rotation is considered to be a crucial ingredient and is observed in stars due to the variation of stellar rotation rate with latitude. Differential rotation plays an important role in understanding the various activities occurring inside the stellar interior. The most visible manifestation of the differential rotation rate is starspots. Stellar rotation rate is observed to decrease with increasing latitude. However, it is still uncertain how differential rotation depends on stellar rotation, and this makes it an interesting subject for further investigations. Observationally, it has been revealed that stellar angular rotation,  $\Omega$ , depends upon its latitudinal difference,  $\Delta\Omega$ , with power law dependence  $\Delta\Omega \propto \Omega^n$ , where  $n$  takes a variable range of values as  $0 < n < 1$  (Arlt and Fröhlich, 2012; Hotta and Yokoyama, 2011; Donahue et al., 1996; Reiners and Schmitt, 2003; Barnes et al., 2005), which indicates the increase in velocity difference,  $\Delta\Omega$ , while decrease in the relative difference,  $\Delta\Omega/\Omega$ , with increasing stellar rotation rate,  $\Omega$ . For example, two different results were shown by Barnes et al. (2005) and Saar (2011), respectively. While the former suggested that in the cool stars differential rotation is not virtually dependent on rotation rate as,  $\Delta\Omega \propto \Omega^{0.15}$ , the latter demonstrated a very different dependence of differential rotation and rotation rate as  $\Delta\Omega \propto \Omega^{0.68}$ . Results obtained by Saar (2011) are almost similar to results obtained by Donahue et al. (1996), i.e.,  $\Delta\Omega \propto \Omega^{0.70}$ . Variation in differential rotation with time has also been shown recently by, e.g., Fröhlich et al. (2009); Hotta and Yokoyama (2011).

In the traditional  $\alpha - \Omega$  mean field dynamo theory, the efficiency of working of a dynamo is governed by a dynamo number,  $D$ , which scales with rotation rate as  $D \propto \Omega^2$ , where the  $\alpha$ -effect is proportional to  $\Omega$ . In linear dynamo theory, the dependence of cycle period  $P_{cyc}$  of stars with the same internal structures on dynamo number is given by a relationship of the form  $P_{cyc} \propto D^{-\frac{1}{2}}$

which further relates to rotation rate as  $P_{cyc} \propto \Omega^{-1}$ , i.e., cycle period of star decreases with increasing rotation rate. Although this linear dependence is compatible with observations in case of kinematic dynamo theory, yet in the case of nonlinear dynamo theory the validity of this relationship is but questionable, as the amplification of magnetic field is inhibited by back reaction from Lorentz force, as well as various saturation mechanisms. In particular, we have considered  $\alpha$ -quenching,  $\Omega$ -quenching and magnetic flux losses which act as dynamo saturation mechanisms in case of nonlinear dynamo. Previous results where the growth of magnetic field is controlled by the quenching of  $\alpha$ -effect or differential rotation (Jepps, 1975; Ivanova and Ruzmaikin, 1977; Yoshimura, 1978) were inconsistent with observations of rotation rate and activity cycle period. The advection-dominated dynamo (e.g., Dikpati and Charbonneau (1999)) is one of the most widely used and popular model for describing the various features of solar activity cycle. With no consensus on a precise form of the solar/stellar dynamo at present, one of the fundamental question in any dynamo theory is how stellar magnetic fields apparently manage to maintain almost the same dependence of their frequency on rotation rate as in a linear dynamo theory.

The purpose of this Chapter is to explain how the frequency of magnetic field and its strength (inferred from magnetic activity) and differential rotation depend on stellar rotation rate by using the aforementioned observational data. To accomplish this, a minimal dynamical model for magnetic fields and differential rotation is proposed. A detailed analysis is carried out by varying various parameters to reproduce the results consistent with observational data of  $\omega = \Omega^\beta$ , where  $\beta = 1.25 \pm 0.5$  (Noyes et al., 1984) and  $\Delta\Omega \propto \Omega^{0.70}$  (Donahue et al., 1996), the strength of magnetic field increases with rotation rate  $\Omega$  before saturation, as previously noted. Specifically, we investigate a low order model comprising of seven coupled equations for magnetic field and differential rotation by taking  $\alpha$ -quenching, magnetic flux loss, and the Lorentz force on mean and fluctuating differential rotations into account and comparing the outcome with observations.

The remainder of the Chapter 2 is organized as follows. In section 2.2, we present our extended dynamo model. Section 2.3 mentions the results obtained from the seventh-order system. In section 2.4 we investigate the system in the limit where fluctuating differential rotation is dominated by mean differential rotation, while the system is studied in the opposite limit in section 2.5. The basic property of the seventh-order system mentioned in Section 2.2 is discussed in detail in section 2.6, in particular, we investigate a more general seventh-order system to check parameter dependencies by taking the balance among various nonlinearities into account. In section 2.7, we discuss and conclude our results.

## 2.2 Model Construction<sup>1</sup>

A simple parameterized dynamo model is constructed by considering the dynamical interactions between the magnetic fields and differential rotation. The model is based upon  $\alpha$ - $\Omega$  dynamo constructed by Cattaneo et al. (1983). We consider plane wave solutions propagating in  $x$ -direction (Parker, 1979), in the presence of azimuthal velocity  $\mathbf{v} = (V(z) + W(x, z, t))\hat{\mathbf{y}}$ , where rotation velocity is represented by  $V = \Omega z$  (where  $z$  is the radial coordinate) while  $W(x, z, t)$  represents the differential rotation due to back reaction. Here, the local cartesian co-ordinates  $x$ ,  $y$  and  $z$  point northward, westward and radially outward, respectively (Weiss et al., 1984). The magnetic field  $\mathbf{B}$  in  $k$ -mode is given as  $\mathbf{B} = (0, B(t)e^{ikx}, ikA(t)e^{ikx})$  by assuming the periodic boundary conditions in terms of fourier mode. Lorentz force is quadratic in  $\mathbf{B}$  (details can be seen in Appendix A) and hence differential rotation takes the form  $\frac{\partial W}{\partial z} = w_0(t) + w(t)\exp(2ikx)$ , where  $w_0(t)$  and  $w(t)$  are the mean and fluctuating differential rotation which leads to a low-order dynamo model provided by seven first-order coupled differential equations in the following

---

<sup>1</sup>The dimensionless model represented by a set of Eqs. (2.1)-(2.4) in the absence of nonlinear transport coefficients is originally obtained by Cattaneo et al. (1983) and Weiss et al. (1984). A detailed derivation of these Eqs. is provided in the Appendix A as noted in Weiss et al. (1984). In present thesis, the model is extended by adding nonlinear transport coefficients represented by a system of Eqs. (2.5) - (2.8) and forms the basis of Chapters 2, 3 & 4, respectively.

dimensionless forms (Cattaneo et al., 1983):

$$\dot{A} = 2DB - A, \quad (2.1)$$

$$\dot{B} = i(1 + w_0)A - \frac{1}{2}iA^*w - B, \quad (2.2)$$

$$\dot{w}_0 = \frac{1}{2}i(A^*B - AB^*) - \nu_0w_0, \quad (2.3)$$

$$\dot{w} = -iAB - \nu w. \quad (2.4)$$

Here, notation dot ( $\dot{\cdot}$ ) represents the ordinary derivative with respect to time,  $t$ . The poloidal magnetic field,  $A$ , the toroidal magnetic field,  $B$ , and fluctuating differential rotation,  $w$ , are complex whereas mean differential rotation,  $w_0$ , is real. We note that  $w_0$  and  $w$  have zero and twice the frequency of  $A$  and  $B$ , respectively. The complex conjugates of  $A$  and  $B$  are denoted by  $A^*$  and  $B^*$ , respectively. We also note that poloidal magnetic field,  $A$ , is generated by the toroidal magnetic field,  $B$ , (e.g.  $\alpha$ -effect through helicity) which is assumed to be proportional to rotation rate  $\Omega$  (see Eq. (2.1)). Equation (2.2) represents the toroidal magnetic field,  $B$ , and is generated by the poloidal magnetic field,  $A$ , where the quenching of  $\Omega$ -effect is incorporated by total shear  $1 + w_0$ . The differential rotation is inhibited by the tension in the magnetic field lines via Lorentz force and causes the quenching of  $\Omega$ -effect. Due to back reaction of shear, the total shear is reduced from 1 to  $1 + w_0 < 1$  as  $w_0$  is always negative and is given by  $1 + w_0 = \frac{\Delta\Omega}{\Omega}$ . Generation of mean differential rotation  $w_0$  and fluctuating differential rotation  $w$  is represented by Eq. (2.3) and Eq. (2.4), respectively. The constant parameters  $\nu$  and  $\nu_0$  represent viscosity of mean and fluctuating differential rotations, respectively, and  $D$  is the dynamo number (Sood and Kim, 2013). The linear dispersion relation  $\omega = k^2[-1 \pm (1 + i)D^{1/2}]$  is obtained for Eqs. (2.1)-(2.4) and is similar to the results by Weiss et al. (1984), which provides finite amplitude nonlinear solutions for  $D > 1$ . By taking into account  $\alpha$ -quenching and magnetic flux loss, we extend the above system (2.1)-

(2.4) as follows :

$$\dot{A} = \frac{2DB}{1 + \kappa_1(|B|^2)} - [1 + \lambda_1(|B|^2)]A, \quad (2.5)$$

$$\dot{B} = i(1 + w_0)A - \frac{1}{2}iA^*w - [1 + \lambda_2(|B|^2)]B, \quad (2.6)$$

$$\dot{w}_0 = \frac{1}{2}i(A^*B - AB^*) - \nu_0w_0. \quad (2.7)$$

$$\dot{w} = -iAB - \nu w. \quad (2.8)$$

Here,  $\lambda_1(|B|^2)$ ,  $\lambda_2(|B|^2)$ , and  $\kappa_1(|B|^2)$  are considered to be functions of  $|B|$  that incorporate the feedback of growing magnetic field onto itself: the effect on the generation of the magnetic field is represented by  $\lambda_1(|B|^2)$ , whereas the effects on the dissipation of magnetic field are captured by  $\lambda_2(|B|^2)$  and  $\kappa_1(|B|^2)$ . These terms are assumed to increase monotonically with  $|B|$  (Robinson and Durnery 1982, Weiss et al 1984) and are zero when  $|B| = 0$ . For our minimal model,  $\lambda_1(|B|^2) = \lambda_1|B|^2$ ,  $\lambda_2(|B|^2) = \lambda_2|B|^2$ , and  $\kappa_1(|B|^2) = \kappa_1|B|^2$  with constant coefficients of  $\lambda_1$ ,  $\lambda_2$ , and  $\kappa_1$ . Thus, quenching of nonlinear  $\alpha$ -effect is represented by non-zero  $\kappa_1$  while loss of poloidal and toroidal fields due to enhanced magnetic dissipation is depicted by non-zero  $\lambda_1$  and  $\lambda_2$ , respectively. In our extended model, the efficiency of the generation of poloidal magnetic field from toroidal field (for instance, by helicity) is governed by  $\alpha$  which is supposed to increase linearly with rotation rate. As noted in introduction,  $D \propto \alpha\Omega$ , where  $\alpha$  is linearly scaled with  $\Omega$ . Previously, Noyes et al. (1984) has used quadratic  $\alpha$ -quenching and flux loss to investigate fourth-order system without considering the feedback from Lorentz force.

## 2.3 Seventh-Order System

We investigate our extended model (2.5) to (2.8) for the following three cases by taking  $\nu = 1.0$  and  $\nu_0 = 35.0$  and by varying  $D$  from 1 to 400. We note that the seventh-order system can be reduced to fifth- and sixth-order systems

depending upon the values of  $\nu$  and  $\nu_0$ , respectively. The effects of fluctuating differential rotation become zero if  $\nu \rightarrow \infty$ ,  $w \rightarrow 0$  and the system behaves as fifth-order whereas mean differential rotation has no effect on the system if  $\nu_0 \rightarrow \infty$ ,  $w_0 \rightarrow 0$ , the system becomes sixth order (for more details see sections 2.4 and 2.5). Therefore, the values of  $\nu$  and  $\nu_0$  are chosen in such a way that the system includes the combined effect of mean and fluctuating differential rotations. We further note that dynamo number and rotation rate are related to each other as  $\Omega = D^{\frac{1}{2}}$ , with rotation rate of 30 for younger Sun, i.e., when the Sun was born it was rotating thirty times faster than the present solar rotation rate and hence, the maximum value of  $D = 400$ , i.e.,  $\Omega = 20$  in dimensionless units converts to 1.5 day rotation period.

**Case 1:**  $\alpha$ -quenching and no flux loss i.e.,  $\lambda_1 = \lambda_2 = 0$ ,  $\kappa_1 \neq 0$

**Case 2:** no  $\alpha$ -quenching and flux loss i.e.,  $\lambda_1 = \lambda_2$ ,  $\kappa_1 = 0$

**Case 3:**  $\alpha$ -quenching and flux loss i.e.,  $\lambda_1 = \lambda_2 = \kappa_1$

Equations (2.5) to (2.8) are solved numerically to investigate the behavior of frequency of magnetic activity,  $\omega$ , with dynamo number,  $D$ , and rotation rate,  $\Omega$ . Frequency of maximum intensity for the magnetic activity of each dynamo number is determined by obtaining a time series of  $B$ . Fast Fourier transforms are used to determine a Fourier series of  $B$  and power spectrum of frequency for each dynamo number is computed. After computing the power spectra for all dynamo numbers, the colors are assigned according to the color coding as depicted in the color bar next to the figure, where frequency of maximum intensity to low intensity is illustrated from bright yellow to dark colors. We further examine the variation of magnetic field strength  $|B|$  and differential rotation  $\Delta\Omega$  with rotation rate  $\Omega$ . The dependence of the total shear on rotation rate,  $\Omega$ , is given by a power law relationship as  $1 + w_0 = \Omega^\delta$ , where  $\delta$  is the scaling exponent. Normalized differential rotation is given as  $1 + w_0 = \Delta\Omega/\Omega$ . Using these values in  $1 + w_0 = \Omega^\delta$ , we obtain the scaling of differential rotation as  $\Delta\Omega = \Omega^{\delta+1} = \Omega^\xi$  ( $\xi = \delta + 1$ )(Sood and Kim, 2013).

**Case 1:**  $\alpha$ -quenching causes the saturation (i.e.,  $\lambda_1 = \lambda_2 = 0$ ,  $\kappa_1 = 2.5$ ). We investigate the variation in frequency, say  $\omega_M$ , of  $B$  of maximum intensity with  $\Omega$  by a power law relationship as  $\omega_M = \Omega^\beta$ , where  $\beta$  is the scaling exponent (cf. Fig. 2.1(a)). We then examine how magnetic field strength  $|B|$  behaves with change in rotation rate and total shear change with rotation rate while change in total shear with  $\Omega$  is investigated using power law  $\Delta\Omega = \Omega^\xi$ , where  $\xi$  is the power law index (Fig. 2.1(b), 2.1(c)). In Fig. 2.1(a), the frequency of  $B$  is plotted as a function of rotation rate, where high to low intensity of the frequency is represented by bright yellow to dark black colors. Interestingly, we find a gradual increase in  $\omega_M$ , represented by bright yellow, with rotation rate  $\Omega$ . The frequency of maximum intensity  $\omega_M$  depends on  $\Omega$  with a power law using  $\omega_M = \Omega^\beta$  where  $\beta$  is found to vary for slow and high rotation rate with two scaling exponents as  $\beta = 0.67$  for  $\Omega < 8.3$  depicted in purple color and 1.20 for  $\Omega \geq 8.3$  illustrated in red color in Fig. 2.1(d), respectively. These results are not in agreement with observation. The dispersion in the frequency is depicted by the band in red around  $\omega_M$ , and its width is slowly reduced with increasing  $\Omega$ . In Figure 2.1(b) the behavior of the strength of toroidal magnetic field  $|B|$  as a function of  $\Omega$  can be seen. Clearly,  $|B|$  is noticed to increase up to  $\Omega \sim 6$  with increasing  $\Omega$  beyond which it starts decreasing for  $\Omega \geq 10$ . The decreasing behavior of  $|B|$  for  $\Omega > 10$  is due to the quenching of mean differential rotation,  $w_0$ , which is caused by the Lorentz force of magnetic fields. This shear quenching can be seen in Fig. 2.1(c), by plotting total shear  $1 + w_0$  against  $\Omega$ . This total shear approaches very small value for high rotation and does not display a significant power-law scaling. In the power law scaling of  $\Delta\Omega = \Omega^\xi = \Omega^{\delta+1}$ , we find too much variation in  $\xi$  ( $\xi$  has values 0.88 ( $1 \leq \Omega \leq 2.23$ ), 0.51 ( $2.23 \leq \Omega \leq 5$ ), -0.33 ( $5 \leq \Omega \leq 10$ ), -1.09 ( $10 \leq \Omega \leq 20$ )).

**Case 2:** magnetic flux loss alone causes the saturation (i.e.,  $\lambda_1 = \lambda_2 = 2.5$ ,  $\kappa_1 = 0.0$ ). Again the frequency of maximum intensity  $\omega_M$ , the magnetic field strength  $|B|$ , and the total shear for different values of rotation rate are investigated

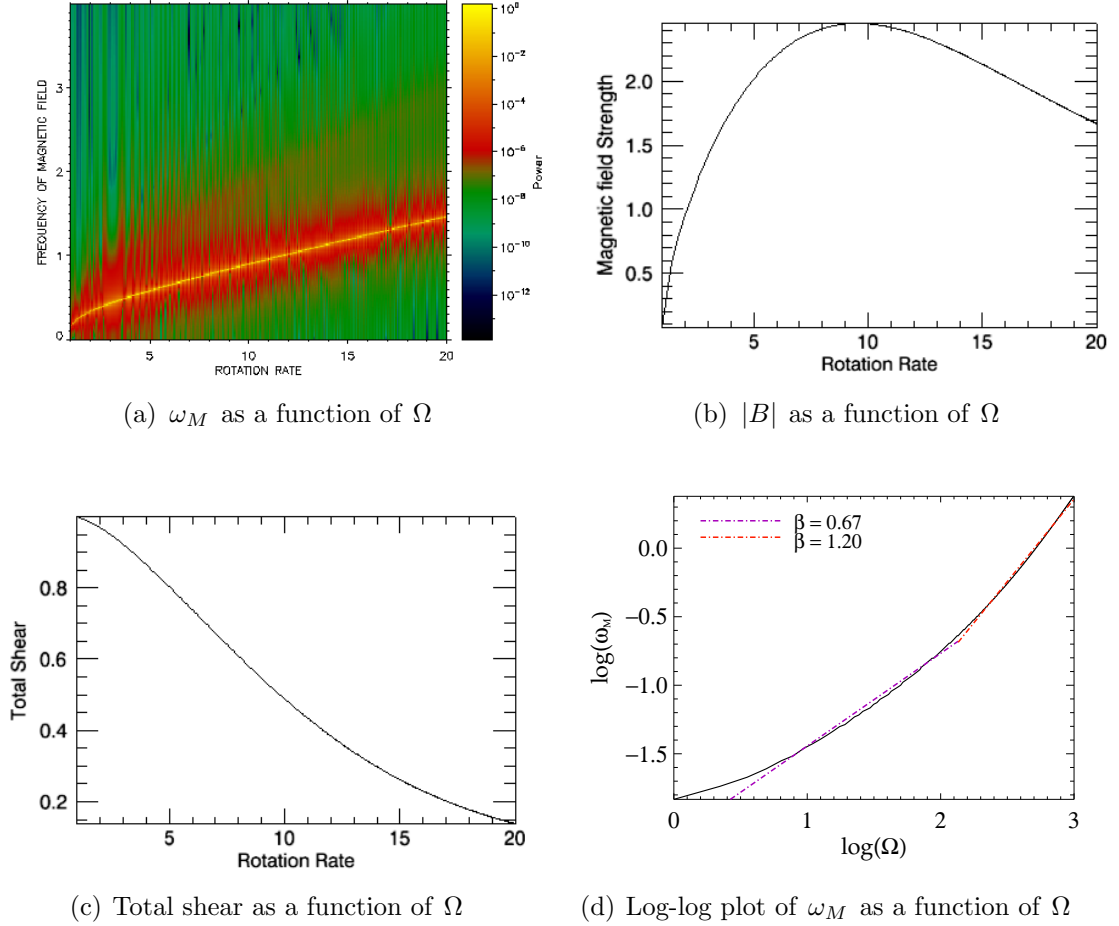


Figure 2.1: Frequency of maximum intensity  $\omega_M$ , magnetic field strength  $|B|$  and total shear are plotted as a function of  $\Omega$  for  $\kappa_1 = 2.5$ ,  $\lambda_1 = \lambda_2 = 0$  for Case 1 in the seventh-order system.

(cf. Fig. 2.2(a)- 2.2(c)). The frequency of  $B$  plotted as a function of rotation rate can be seen in Fig. 2.2(a). In Fig. 2.2(a) we study how frequency  $\omega_M$  of maximum intensity varies with rotation rate. Interestingly, we notice two branches of frequency in this case: a main branch of frequency  $\omega_M$  of maximum intensity followed by a second branch of frequency of localized intensity. The main branch of frequency illustrated in yellow increases with rotation rate  $\Omega$  with faster rate as compared to the rate observed in Fig. 2.1(a). In this case we find that power law exponent  $\beta$  decreases its value from slow to high rotation rate, that is,  $\beta = 1.08$  for  $\Omega \leq 7$ ,  $\beta = 0.87$  for  $7 < \Omega < 10$  and  $\beta = 0.73$  for

$\Omega > 10$ , represented by purple, green and red colors, respectively in Fig. 2.2(d). For slow rotation rate, that is,  $\Omega \leq 10$ , the values of  $\beta$  are within the observed range of  $\beta \sim 0.80$  to  $\beta \sim 1.15$  while for high rotation rate, that is, for  $\Omega > 10$ ,  $\beta = 0.73$  is near the observed value of  $\beta \sim 0.80$  for active branch. The dispersion in frequency around  $\omega_M$ , depicted in red, increases its width with increase in  $\Omega$ . Surprisingly, the second branch of frequency, depicted in red, is noticed above the main branch, increases very fast as rotation rate increases and is caused by the fluctuating differential rotation. Further, we find that the toroidal magnetic field strength  $|B|$  increases initially for  $\Omega \leq 6$  but starts declining for  $\Omega \geq 6$ . This decrease in  $|B|$  is slower than in Case 2.1 (cf. Fig. 2.1(b)). Here again, the decreasing behavior of  $|B|$  for  $\Omega > 6$ , which is shown in Fig. 2.2(c), is caused by mean differential rotation,  $w_0$ , due to the Lorentz force. Using the power law,  $\Delta\Omega = \Omega^\xi$ , we examine the value of  $\xi$  ( $\xi$  has values 0.96 ( $1 \leq \Omega \leq 2.23$ ), 0.54 ( $3 \leq \Omega \leq 6$ ), -0.43 ( $6 \leq \Omega \leq 10$ ), -1.06 ( $10 \leq \Omega \leq 20$ )) which in this case also varies too much with rotation rate.

**Case 3:** Saturation is due to the combined action of  $\alpha$ -quenching and loss due to magnetic flux (i.e.  $\lambda_1 = \lambda_2 = \kappa_1 = 2.5$ ). Figure 2.3(a) shows that frequency of maximum intensity  $\omega_M$  is increasing very slowly with rotation rate for which the power law scaling is obtained  $\beta \sim 0.80$  for active stars. The red band which depicts the dispersion in frequency around the well-defined frequency is found to increase reasonably and is broader than what is noticed in Case 1 and Case 2. The magnetic field strength is found to increase with rotation rate and attains the asymptotic value of 1.25 in Fig. 2.3(b). It is worth noting here that for given parameters, the magnetic field strength will decrease if rotation rate is increased further, i.e., for  $\Omega > 20$ . Fig. 2.3(c) shows the shear quenching and we find a decrease in total shear with rotation rate. This decreasing behaviour is slower than the decline observed in Fig. 2.1(c) and Fig. 2.2(c). We find the dependence of differential rotation on rotation rate in Fig. 2.3(d) to be a power law  $\Delta\Omega = \Omega^\xi$  with  $\xi = 0.70$  for certain range of  $\Omega$  ( $7 < \Omega < 10$ ). This

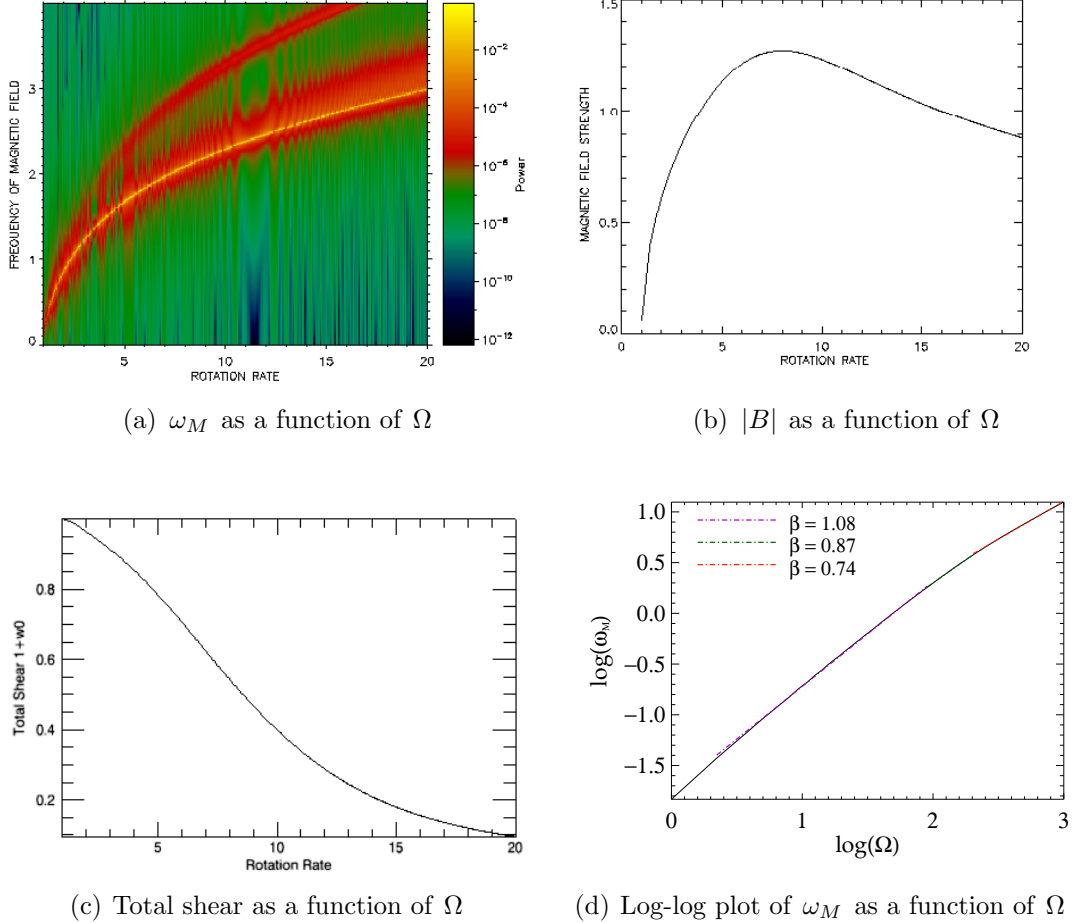


Figure 2.2: Frequency of maximum intensity  $\omega_M$ , magnetic field strength  $|B|$ , and total shear are plotted as a function of  $\Omega$  for  $\kappa_1 = 0.0, \lambda_1 = \lambda_2 = 2.5$  for Case 2 in the seventh-order system.

power law no longer holds for stars with rotation rate  $\Omega \leq 7.3$  (approximately) and  $\Omega \geq 9.6$  (approximately). Variation in  $\xi$  outside this range is noted as 0.98 ( $1 \leq \Omega \leq 2.23$ ), 0.93 ( $3 \leq \Omega \leq 5$ ), 0.84 ( $5 \leq \Omega \leq 7$ ), 0.44 ( $10 \leq \Omega \leq 14$ ), -0.03 ( $14 \leq \Omega \leq 17$ ) and -0.62 ( $17 \leq \Omega \leq 20$ ).

The comparison of all the three cases investigated above shows that Case 1 and Case 2 are not in agreement with observations. In these cases the magnetic field reduces the total shear by the back reaction from the Lorentz force. Therefore, the dynamo action is less efficient in the presence of either  $\alpha$ -quenching or both flux losses. We find our results from Case 3 are in agreement with observations

which shows an equal amount of  $\alpha$ -quenching and both flux losses. In particular, in this case the scaling of well localized frequency with rotation rate is  $\omega_M \propto \Omega^{0.80}$ , whereas, the magnetic field strength and mean differential rotation tend to saturate for high rotation. It is clear from these results that the generation and destruction of magnetic fields are balanced effectively to gain saturated behaviour of magnetic fields and high rotation which is explained in detail in Section 2.6.

## 2.4 Reduced Fifth-Order System

In the previous section, we notice that a very strong mean differential rotation is responsible for inefficient dynamo action. To understand the role of mean differential rotation,  $w_0$ , in a mean field dynamo, a much weaker fluctuating differential rotation,  $w$ , than mean differential rotation,  $w_0$ , is considered, that is, as  $\nu \rightarrow \infty$  is  $w \rightarrow 0$  and equations (2.5) to (2.8) can be written in the form

$$\dot{A} = \frac{2DB}{1 + \kappa_1(|B|^2)} - [1 + \lambda_1(|B|^2)]A, \quad (2.9)$$

$$\dot{B} = i(1 + w_0)A - [1 + \lambda_2(|B|^2)]B, \quad (2.10)$$

$$\dot{w}_0 = \frac{1}{2}i(A^*B - AB^*) - \nu_0 w_0. \quad (2.11)$$

We examine this fifth-order system with  $\nu_0 = 35.0$  by varying  $D$  for the following different three cases;

**Case 1:**  $\kappa_1 \neq 0$ ,  $\lambda_1 = \lambda_2 = 0$ ,

**Case 2:**  $\kappa_1 = 0$ ,  $\lambda_1 = \lambda_2 \neq 0$ ,

**Case 3:**  $\kappa_1 = \lambda_1 = \lambda_2 \neq 0$ .

**Case 1:** Saturation occurs through quenching of  $\alpha$ -effect only (i.e.,  $\lambda_1 = \lambda_2 = 0$ ,  $\kappa_1 = 1.0$ ). The behavior of frequency of the magnetic field,  $\omega_M$ , the magnetic field strength,  $|B|$ , (Fig. 2.4(a), 2.4(b)) and the total shear (Fig. 2.4(c)) as a function of rotation rate  $\Omega$  is investigated. The investigations of localized frequency of maximum intensity  $\omega_M$  with rotation rate reveal the presence of

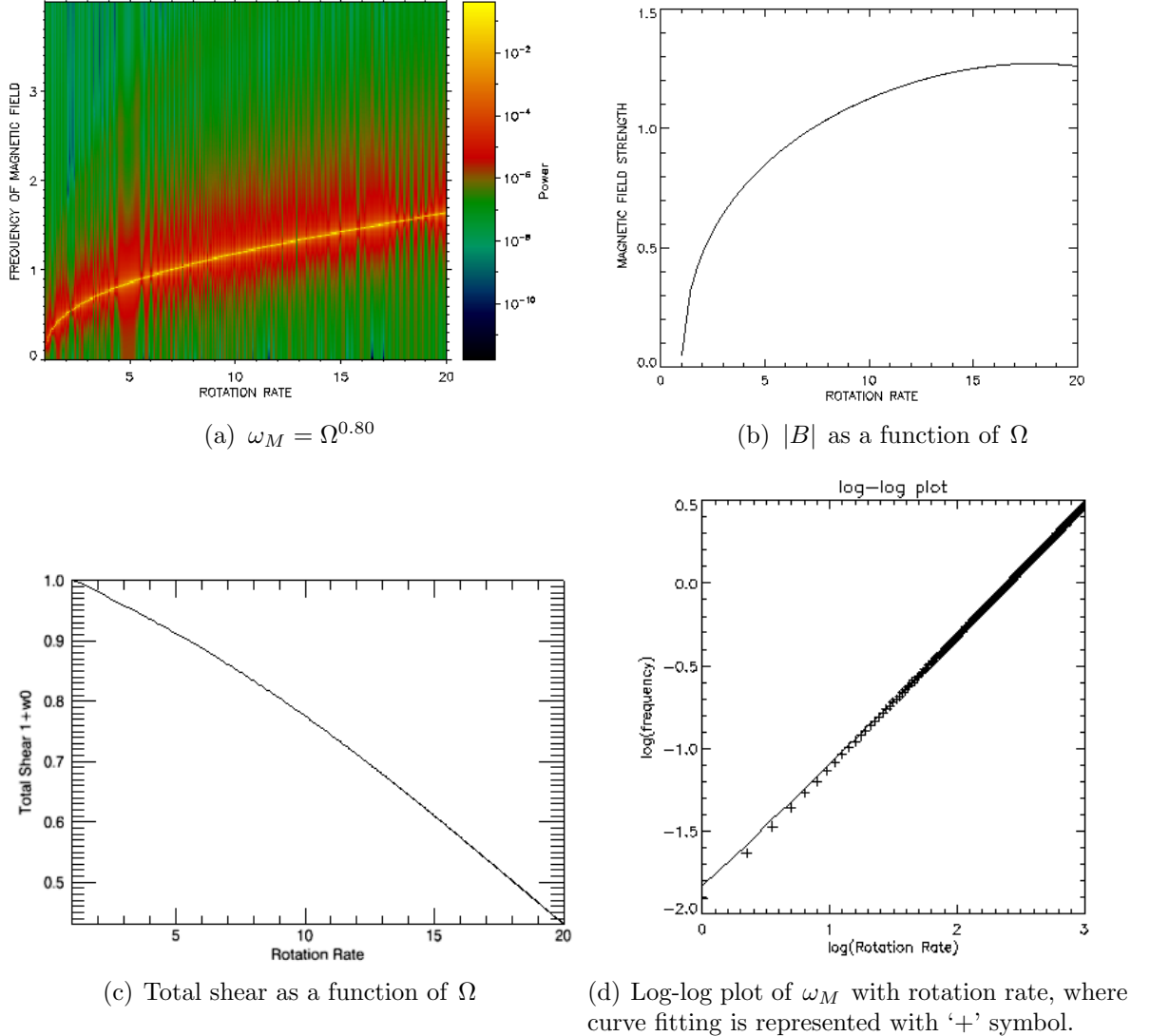


Figure 2.3: Frequency of maximum intensity  $\omega_M$ , magnetic field strength  $|B|$ , and total shear are plotted as a function of  $\Omega$  for  $\kappa_1 = \lambda_1 = \lambda_2 = 2.5$  for Case 3 in the seventh-order system.

finite amplitude wave with a fixed frequency of maximum intensity depicted in yellow colour in Fig. 2.4(a) which is contrary to the observations. The behavior of magnetic field can be seen in Fig. 2.4(b) where the toroidal magnetic field strength  $|B|$  is shown to increase initially with rotation rate up to  $\Omega \sim 6$  but starts decreasing for  $\Omega \geq 6$  which is due to the severe quenching in  $\alpha$ -effect and  $\Omega$ -effect. Also, total shear is noticed to decrease very rapidly up to  $\Omega \sim 10$  past

which it becomes almost zero (see Fig. 2.4(c)). This type of severe quenching of differential rotation was also seen in full MHD simulations of a flux transport dynamo model (Rempel, 2006).

**Case 2:** Dynamo action is ceased by loss due to magnetic flux only (i.e.,

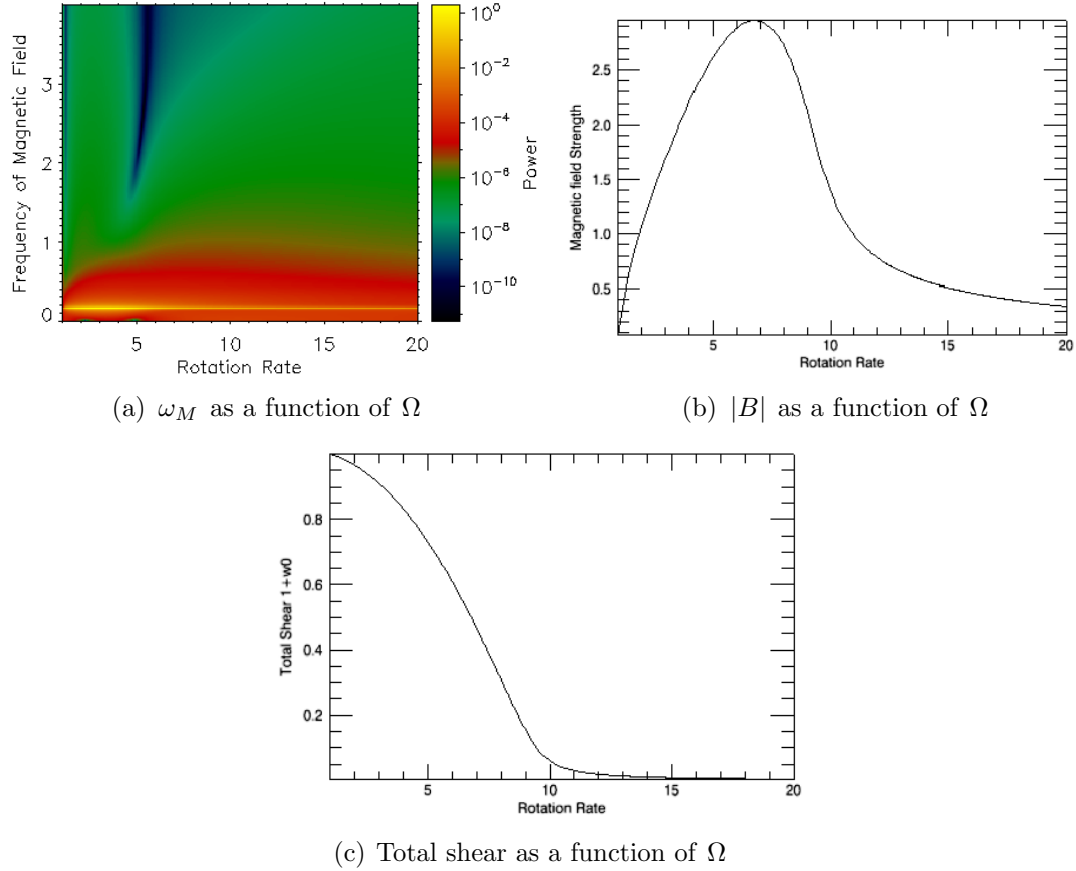


Figure 2.4:  $\omega_M$ ,  $|B|$ , and total shear are plotted as a function of  $\Omega$  for  $\lambda_1 = \lambda_2 = 0$ ,  $\kappa_1 = 1.0$  for Case 1 in the fifth-order system.

$\lambda_1 = \lambda_2 \neq 0, \kappa_1 = 0$ ). The behavior of  $\omega_M$ ,  $|B|$ , and total shear with  $\Omega$  is examined (cf. Fig. 2.5(a), 2.5(b), 2.5(c)). In Fig. 2.5(a), the frequency of maximum intensity  $\omega_M$  is noticed to change with rotation rate in this case unlike Case 1. Interestingly, the power law exponent  $\beta$  is obtained to be 0.91 for  $1 \leq \Omega \leq 5$  which lies in the observed range of 0.80 to 1.15. However, this relationship breaks down for  $\Omega \geq 5$ , that is,  $\omega_M$  decreases in a range  $5 \leq \Omega \leq 10$  and changes very

slightly with  $\Omega$  for  $\Omega \geq 10$ . Fig. 2.5(b) shows the behavior of magnetic field strength  $|B|$  with rotation rate. Clearly,  $|B|$  is found to decrease for  $\Omega \geq 8$  after attaining a maximum value of 1.25 approximately around  $\Omega = 7$ . This decreasing behaviour of  $|B|$  is due to quenching of mean differential rotation which is illustrated in Fig. 2.5(c). The decrease in shear is not as fast as noted in Fig. 2.4(c) and it approaches zero for  $\Omega \geq 12$ .

**Case 3:** Now the saturation of dynamo action is caused by the equal combi-

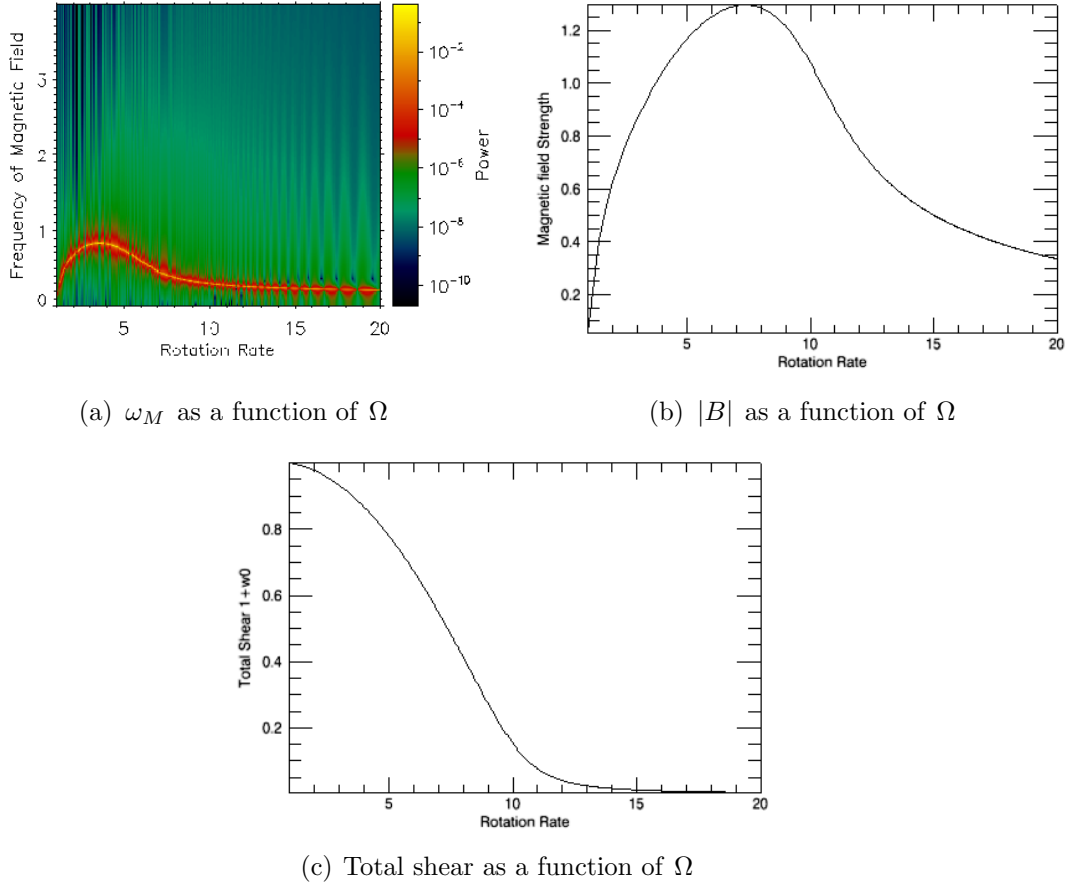


Figure 2.5:  $\omega_M$ ,  $|B|$ , and total shear are plotted as a function of  $\Omega$  for  $\lambda_1 = \lambda_2 = 2.5$ ,  $\kappa_1 = 0.0$  for Case 2 in the fifth-order system.

nation of  $\alpha$ -quenching and magnetic flux loss (i.e.,  $\kappa_1 = \lambda_1 = \lambda_2 = 3.5$ ). Figure 2.6(a) shows the behaviour of frequency spectrum of magnetic field,  $|B|$ , against rotation rate. A slow increase in  $\omega_M$  with rotation rate  $\Omega$  with two power law

scalings can be seen in Fig. 2.6(d) where purple color represents  $\beta = 0.63$  for  $\Omega \leq 10$  and red color depicts  $\beta = 0.45$  for  $\Omega > 10$  which are not consistent with observations. The dispersion in frequency depicted in red band around  $\omega_M$  is noticed to widen slowly with increasing  $\Omega$ . Also, the strength of magnetic field  $|B|$  can be seen increasing slowly with  $\Omega$  in Fig. 2.6(b) which is again in disagreement with observations. The behaviour of total shear as a function of  $\Omega$  is examined in Fig. 2.6(c) and a rapid decrease in total shear is observed for higher  $\Omega$ .

It is very clear from all the cases of fifth order system that the results are not compatible with observations for frequency and magnetic field strength. Therefore, it is imperative to investigate the role of fluctuating differential rotation, which is investigated in the following section.

## 2.5 Reduced Sixth-Order System

To examine the effects of fluctuating differential rotation the system (2.5)-(2.8) is studied by taking  $\nu_0 \rightarrow \infty$  and  $w_0 \rightarrow 0$ . Therefore, the reduced sixth order system in the presence of  $\alpha$ -quenching and both flux losses takes the following form

$$\dot{A} = \frac{2DB}{1 + \kappa_1(|B|^2)} - [1 + \lambda_1(|B|^2)]A, \quad (2.12)$$

$$\dot{B} = \frac{iA}{1 + \kappa_2(|B|^2)} - \frac{1}{2}iA^*w - [1 + \lambda_2(|B|^2)]B, \quad (2.13)$$

$$\dot{w} = -iAB - \nu w. \quad (2.14)$$

In this sixth order system, the reduction of  $\Omega$ -effect via shear-quenching is incorporated by including  $1 + \kappa_2|B|^2$  in Eq. (2.8). The system (2.12)-(2.14) is investigated for the following cases by taking  $\nu = 1.0$  and varying D.

**Case 1:**  $\lambda_1 = \lambda_2 = \kappa_1 = \kappa_2 \neq 0$ ,

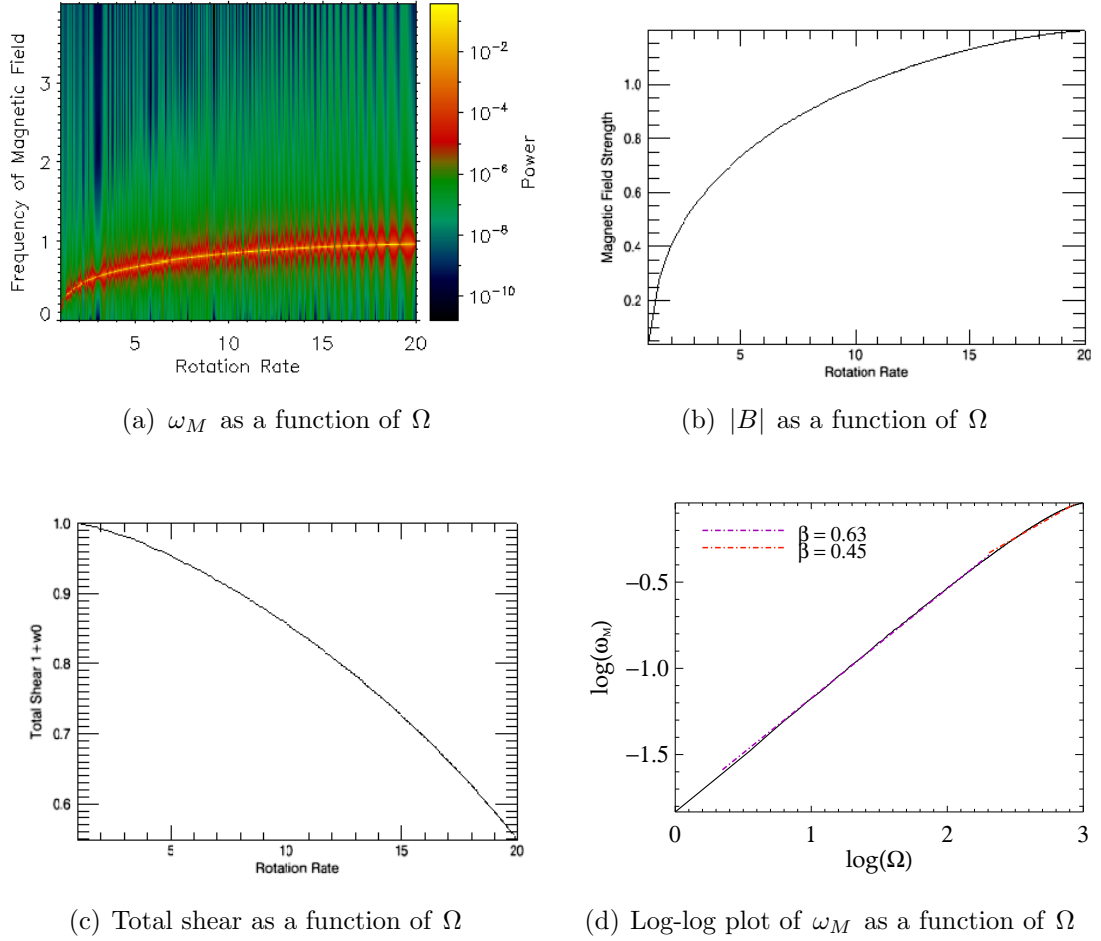


Figure 2.6:  $\omega_M$ ,  $|B|$ , and total shear are plotted as a function of  $\Omega$  for  $\kappa_1 = \lambda_1 = \lambda_2 = 3.5$  for Case 3 in the fifth-order system.

**Case 2:**  $\kappa_1 = 0, \kappa_2 = \lambda_1 = \lambda_2 \neq 0$ .

We note that Eqs. (2.12) to (2.14) are reduced to Weiss model (1984) when  $\lambda_1 = \lambda_2 = \kappa_1 = \kappa_2 = 0$ .

**Case 1:** Now this dynamo action is saturated by an equal combination of  $\alpha$ -quenching, shear quenching, and loss due to magnetic flux (i.e., for  $\lambda_1 = \lambda_2 = \kappa_1 = \kappa_2 = 0.5$ ). Frequency of magnetic field  $B$  and magnetic field strength,  $|B|$ , are plotted as a function of rotation in Fig. 2.7 (a-b). A well-defined frequency of maximum intensity  $\omega_M$ , illustrated in yellow is observed to increase with  $\Omega$  for which the power law exponent is  $\beta = 0.90$ . This value of  $\beta$  is within the

observed range of  $\beta = 0.80$  and  $\beta = 1.15$ . A red band of localized frequencies around  $\omega_M$  thickens with increasing  $\Omega$ . The magnetic field strength  $|B|$  can be seen increasing with  $\Omega$  in Fig. 2.7(b). Almost similar results have been obtained by considering  $\lambda_1 = 0, \lambda_2 = \kappa_1 = \kappa_2 \neq 0$ ,  $\lambda_2 = 0, \lambda_1 = \kappa_1 = \kappa_2 \neq 0$ ,  $\lambda_1 = \lambda_2 = 0, \kappa_1 = \kappa_2 \neq 0$  and  $\kappa_2 = 0, \lambda_1 = 0, \lambda_2 = \kappa_1 \neq 0$ .

**Case 2:** We investigate the dynamo action in the presence of shear-quenching

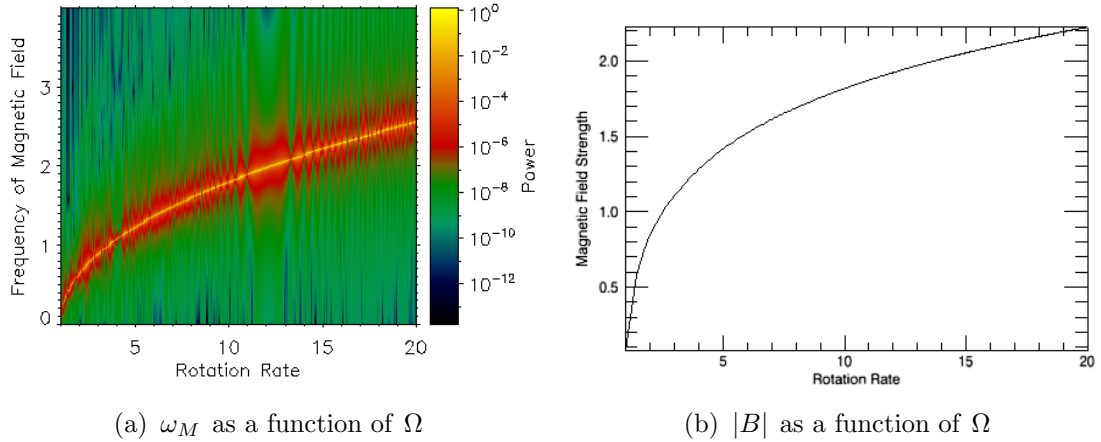


Figure 2.7: Frequency of maximum intensity  $\omega_M$  and strength of magnetic field  $|B|$  as a function of rotation rate  $\Omega$  for  $\kappa_1 = \kappa_2 = \lambda_1 = \lambda_2 = 0.5$  for Case 1 in the sixth-order system.

and both magnetic flux losses in the absence of  $\alpha$ -quenching (i.e.,  $\kappa_1 = 0, \kappa_2 = \lambda_1 = \lambda_2 = 0.5$ ). Again, the frequency of maximum intensity  $\omega_M$  is found to increase with rotation rate  $\Omega$  in Fig. 2.8(a) with power law exponent  $\beta = 1.25 \pm 0.5$  (Noyes et al. 1984). Dispersion in frequency depicted in red colour around  $\omega_M$  is found to expand gradually with rotation rate. Also, there is a second branch of localized frequency which is noticed above the main branch. This second branch is due to the effects of fluctuating differential rotation. In Fig. 2.8(b) the magnetic field strength  $|B|$  is shown to increase very rapidly with  $\Omega$ . The rate at which  $|B|$  increases is almost double of what we observed in previous case. Similar results are obtained for  $\lambda_1 = \lambda_2 \neq 0, \kappa_1 = \kappa_2 = 0$ .

The results obtained from different cases of sixth-order system suggest that the

absence of mean differential rotation leads to infinite growth of magnetic field strength with  $\Omega$ . This also illustrates that the severe quenching of dynamo and total shear in fifth-order system is balanced by fluctuating differential rotation which further emphasises the role of both differential rotations in the working of stellar dynamo.

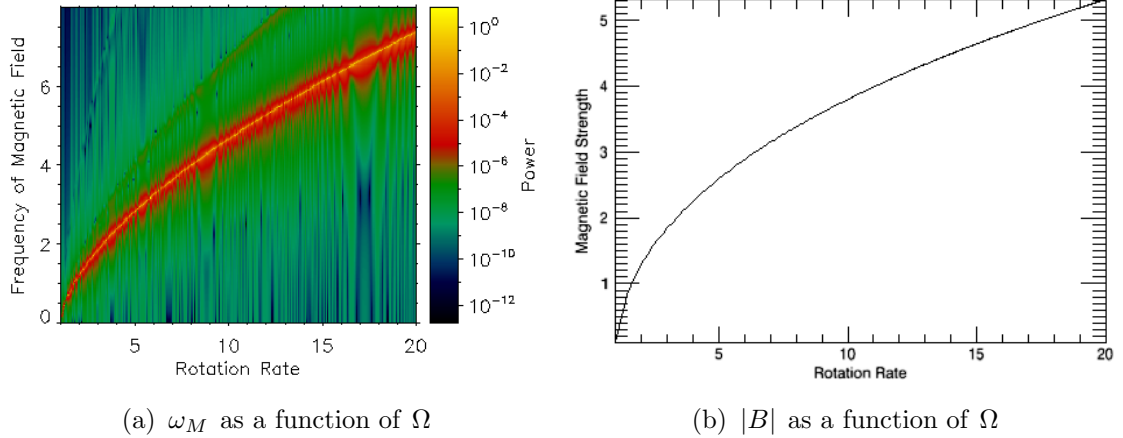


Figure 2.8: Frequency of maximum intensity  $\omega_M$  and  $|B|$  as a function of rotation rate  $\Omega$  for  $\kappa_1 = 0, \kappa_2 = \lambda_1 = \lambda_2 = 0.5$  for Case 2 in the sixth-order system.

## 2.6 Minimal Dynamical Model: parameter dependencies

From previous investigations, it is clear that Case 3 of seventh-order system reproduces the results which are in best agreement with observations. In this case  $\alpha$ -source term and flux losses are considered in equal amount with coefficient of order one. Case 3 is successful in reproducing observations due to its ability to keep a dynamical balance not only in generation and destruction of magnetic fields but also in mean and fluctuating differential rotations. This balance determines the working of dynamo near the dynamo instability, which eventually leads to almost linear increase in frequency, flattening of magnetic energy for high rotation

and rapid decrease in total shear, in agreement with observations. Now, we highlight how the seventh-order system is ‘minimal’ and how various parameters are necessary, by probing a more general seventh-order system which integrates various nonlinear power-law dependence of  $\alpha$  quenching and flux loss on  $|B|$  in equations (2.5) and (2.6) and by exploring parameter dependencies. Generalized equations are written as:

$$\dot{A} = \frac{2DB}{1 + \kappa_1(|B|^m)} - [1 + \lambda_1(|B|^n)]A, \quad (2.15)$$

$$\dot{B} = i(1 + w_0)A - \frac{1}{2}iA^*w - [1 + \lambda_2(|B|^n)]B, \quad (2.16)$$

$$\dot{w}_0 = \frac{1}{2}i(A^*B - AB^*) - \nu_0w_0, \quad (2.17)$$

$$\dot{w} = -iAB - \nu w, \quad (2.18)$$

where  $m$  and  $n$  represent the power-law index of the  $\alpha$ -quenching term and the flux-loss terms, respectively. By investigating about 35 cases where the values of  $m$ ,  $n$ ,  $\kappa_1$ ,  $\lambda_1$  and  $\lambda_2$  are varied systematically and by comparing the generation and dissipation terms on right and left hand sides of Eqs. (2.15) and (2.16), we conclude that our model can reproduce the observations only if the  $\alpha$ -source term and magnetic dissipation are balanced in Eq. (2.15) while the generation of  $A$  by shear and dissipation are balanced in Eq. (2.16). From this detailed and extensive analysis, it is found that there should be a quadratic increase in the  $\alpha$ -quenching power law and magnetic dissipation ( $m \geq 2$ ,  $n \geq 2$ ) for the coefficient of order 1 (i.e.,  $0.5 < \kappa_1, \lambda_1, \lambda_2 < 2.5$ ). Among these cases, we present results for the following four cases as examples:

**Case 1:**  $m = n = 1$  &  $\kappa_1 = \lambda_1 = \lambda_2 = 2.5$ ,

**Case 2:**  $m = n = 3$  &  $\kappa_1 = \lambda_1 = \lambda_2 = 2.5$ ,

**Case 1:** The saturation of dynamo occurs through weaker  $\alpha$ -quenching and flux loss due to magnetic field (i.e.,  $m = n = 1$  &  $\kappa_1 = \lambda_1 = \lambda_2 = 2.5$ ). The frequency of maximum intensity,  $\omega_M$ , as a function of rotation rate can be seen in Fig 2.9(a),

where high to low intensity of frequency is depicted via yellow to dark black colors. A slow increase in frequency of maximum intensity with rotation rate is noticed along with a band of lower frequency of maximum intensity that widens gradually with rotation. The power law scaling exponent  $\beta$  is obtained to be variable in this case with two values  $\beta \sim 0.80$  (purple) for  $\Omega \leq 10$ ,  $\beta \sim 0.91$  (red) for  $\Omega < 10$  which are within the observed range of  $\beta \sim 0.80$  and  $\beta \sim 1.15$  (See Fig. 2.9(d)). Whereas, the magnetic field strength shows an opposite behavior to the observations, that is,  $|B|$  is found to show a reducing behavior for high rotation after attaining a maximum value around  $\Omega \sim 15$  (See Fig. 2.9(b)). Shear quenching shown in Fig.2.9(c) causes this drop in  $|B|$ . Shear quenching is too small for high rotation and using power law  $\Delta\Omega = \Omega^\xi$ , the value of  $\xi$  is noticed to vary between 0.80 to -0.74 with rotation rate in this case. This variation of  $\xi$  for different ranges of  $\omega$  is noticed as 0.80 for  $\Omega(1 \leq \Omega \leq 4)$ , 0.87 for  $\Omega(4 \leq \Omega \leq 6)$ , 0.66 for  $\Omega(6 \leq \Omega \leq 9)$ , 0.36 for  $\Omega(9 \leq \Omega \leq 12)$ , -0.20 for  $\Omega(12 \leq \Omega \leq 15)$  and -0.74 for  $\Omega(15 \leq \Omega \leq 20)$ . The value of  $\xi$  is found to be closer to the observations only for  $\Omega(6 \leq \Omega \leq 9)$  with a value of  $\xi=0.66$ .

Thus, less efficient quenching of  $\alpha$  and flux losses generates a strong magnetic field which further reduces the total shear resulting in the drop of magnetic field strength,  $|B|$ . Almost similar results are noticed for weaker  $\alpha$ -quenching and stronger magnetic flux losses i.e.,  $m = 1$ ,  $n = 2$  &  $\kappa_1 = \lambda_1 = \lambda_2 = 2.5$ .

**Case 2:** The dynamo action is ceased by the action of stronger  $\alpha$ -quenching and flux loss due to the magnetic field (i.e.,  $m = n = 3$  &  $\kappa_1 = \lambda_1 = \lambda_2 = 2.5$ ). We find that stronger  $\alpha$ -quenching and flux losses slow down the growth of frequency of magnetic fields and  $|B|$  depicted in Fig. 2.10 (a-b). The frequency  $\omega_M$  is shown to increase at a slow rate with  $\Omega$  with power law exponent  $\beta \sim 0.75$ , closer to the observations. The width of red band around  $\omega_M$  is constant. The value of  $|B|$  does not saturate for high rotation but keeps on growing gradually which is associated with the slow decline in the total shear shown in Fig. 2.10(c). To study the differential rotation and rotation rate behavior we use power law  $\Delta\Omega = \Omega^\xi$ .

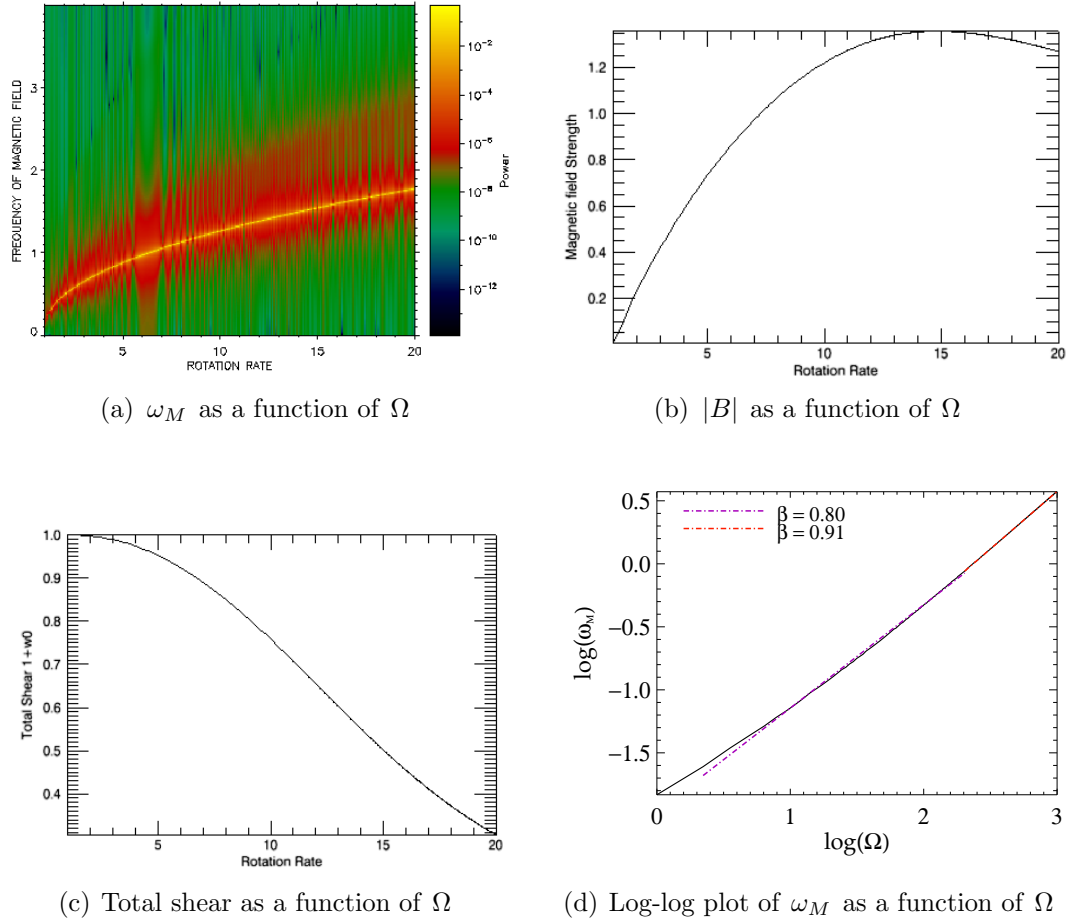
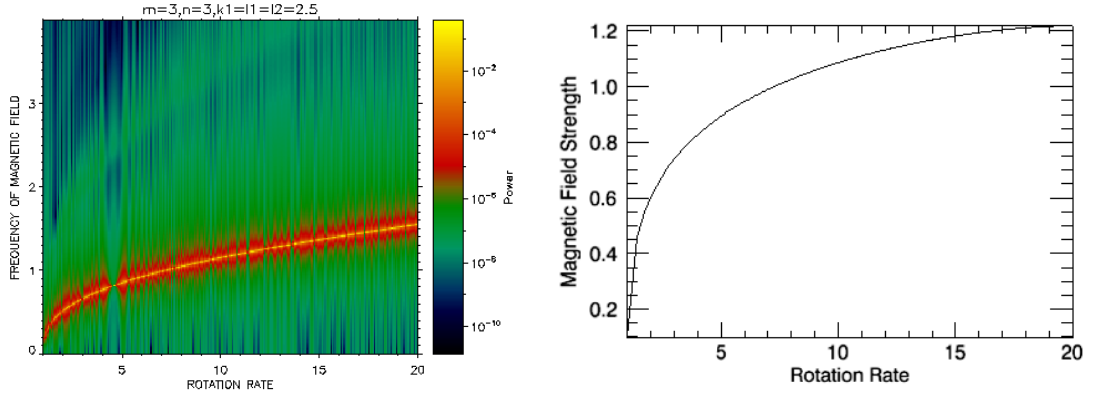


Figure 2.9: Case 1: Frequency of maximum intensity  $\omega_M$ , magnetic field strength  $|B|$ , and total shear are plotted as a function of  $\Omega$  for  $m=n=1$  and  $\kappa_1 = \lambda_1 = \lambda_2 = 2.5$ .

We find that  $\xi$  decreases its value from 0.95 to 0.60 as  $\Omega$  increases.

Further, the comparison of all nonlinear terms on RHS of Eqs. (2.15) and (2.16) shows an imbalance between not only the  $\alpha$ -source term and the magnetic dissipation in Eq. (2.15) but also between the generation of poloidal magnetic field by shear and dissipation in Eq. (2.16). We confirm that this imbalance in the nonlinear terms is responsible for the disagreement of results with observations. Therefore, we confirm that our model mentioned in section 2.2 is the minimal model that has the right balance between all nonlinear terms, their respective coefficients and is capable of reproducing the results consistent with observations.


 (a)  $\omega_M$  as a function of  $\Omega$ 

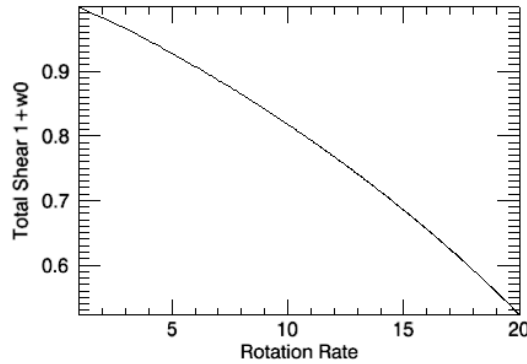
 (b)  $|B|$  as a function of  $\Omega$ 

 (c) Total shear as a function of  $\Omega$ 

Figure 2.10: Case 2: Frequency of maximum intensity  $\omega_M$ , magnetic field strength  $|B|$ , and total shear are plotted as a function of  $\Omega$  for  $m=n=3$  and  $\kappa_1 = \lambda_1 = \lambda_2 = 2.5$ .

## 2.7 Conclusions

We investigate a seventh-order nonlinear system by including the effects of  $\alpha$ -quenching, magnetic flux loss, and the Lorentz force on mean and fluctuating differential rotations. For different degrees of  $\alpha$ -quenching and magnetic flux losses we examine the behavior of magnetic field strength, frequency of magnetic field and total shear with rotation rate. Results obtained from the investigations such as linear increase in frequency, saturation of magnetic activity and quenching of shear with rotation rate are in good agreement with observations for the case where the combined effects of  $\alpha$ -quenching and flux losses with a quadratic

dependence on  $|B|$  are considered. Further, investigations of seventh-, fifth- and sixth-order system highlight that a proper balance between  $w_0$  and  $w$  is essential to reproduce the results that agree with observations. This indicates the importance of upward ( $w_0$ ) and downward ( $w$ ) scale coupling to the differential rotation for the working of a dynamo.

It is interesting to emphasize that this balance suggests an organized process in the stellar dynamo, which helps the working of a dynamo near marginal stability as a consequence of a balance among generation and destruction of magnetic field and between toroidal and poloidal magnetic fields as well as mean and fluctuating differential rotations. This indicates that self-organisation process could be responsible for the stellar dynamo where a long range correlation in stellar interiors and open boundary is important. Almost linear dependence of frequency of magnetic fields on rotation rate could be another signature of self-organisation. We highlight the importance of this balance in the self-regulation of stellar dynamo and rotation in subsequent chapter.

Our simple parameterised model has some limitations, such as, failing to capture the spatial evolution of stellar magnetic fields, yet it has the advantages of being less sensitive to the precise form of dynamo (Sood and Kim, 2013). Moreover, our model is able to provide an explanation to the observed frequency and strength of magnetic field and the differential rotation for stars with different rotation rates and serves as a full dynamo model. In next chapter, we explain how this dynamical model emphasizes the role of *nonlinear* generation and destruction of magnetic fields through  $\alpha$ -effect and flux losses in the self-regulation of a stellar dynamo. It is worth noting that signatures of self-organisation have been observed by using reduced dynamical model in shear flow dynamics (Newton et al., 2013) and stochastic dynamo (Newton and Kim, 2013).

## Chapter 3

# Signature of Self-regulation in a Nonlinear Dynamo

To understand the role of self-regulation in a dynamo via  $\alpha$ -quenching, flux losses and feedback by mean/fluctuating differential rotations, we investigate a nonlinear dynamical system analytically and numerically. Our detailed investigations reveal how the presence of these transport coefficients in the limit of very weak mean and/or fluctuating differential rotation effects the frequency,  $p$ , of magnetic field, phase,  $\varphi$ , and magnetic field strength,  $|B|$ . In the absence of back reaction due to fluctuating differential rotation,  $p$  and  $\varphi$  are found to be controlled by both flux losses with no  $\alpha$ -quenching. Similar effects of poloidal flux loss and toroidal flux loss on  $p$  and  $|B|$  are noticed when there is no back reaction from shear. However, in the presence of back reaction from shear their effects are observed to be different. From our detailed investigations it becomes clear that in the presence of fluctuating shear, poloidal flux loss is less effective than toroidal flux loss with or without  $\alpha$ -quenching. Moreover,  $\alpha$ -quenching is more effective when combined with toroidal flux loss which indicates that the presence of  $\alpha$ -quenching and flux loss helps in the self-regulation of dynamo. The importance of various nonlinear transport coefficients and both differential rotations (mean and fluctuating) in the self-regulation of dynamo is highlighted from our results.



### 3.1 Introduction

Self-organisation is a process of spontaneously emerging new structures without being imposed by an external agent and is an important phenomenon for all evolutionary systems. A system is known to be a self-organised, nonequilibrium system if it is, “*a distinguishable collection of matter, with recognizable boundaries, which has a flow of energy, and possibly matter, passing through it, while maintaining, for time scales long compared to the dynamical time scales of its internal processes, a stable configuration far from thermodynamic equilibrium. This configuration is maintained by the action of cycles involving the transport of matter and energy within the system and between the system and its exterior. Further, the system is stabilized against small perturbations by the existence of feedback loops which regulate the rates of flow of the cycles.*” (Simon, 1997, pg.51). Various examples of self-organisation such as crystallisation, snow-flakes, Benard convection, etc., can be seen in day to day life. In the area of astrophysics, the Sun is the most observed and investigated complex system as various processes occurring inside the solar interior emerge on their own without being triggered from the outside. The presence of well structured and organised small/large scale magnetic fields in the solar interior have been revealed through high-resolution observations available these days. Due to the interactions between these magnetic fields and rotation, the Sun displays a definite and significant intensity of self-organisation on large scales in terms of magnetic activity cycle, formation of sunspots, appearance of butterfly diagrams and polarity reversals, etc. To understand these observations, the behavior of magnetic field is studied by using nonlinear dynamo theory in which the magnetic field is amplified by inductive motion of conducting fluid. These structured and well organised magnetic fields owe their existence to the interplay among various nonlinear transport coefficients which provide a way in the working of solar/stellar dynamo.

To understand the complexity of self-regulated magnetic fields and dynamo pro-

cess, a dynamical system was first used in early 80's to explain the various features of solar magnetic field such as magnetic activity of 11 years (Weiss et al., 1984). Interestingly, they explained the change in system from regularity to chaos by varying a control parameter known as 'dynamo number'. Thereafter, dynamical systems and parameterized models have been used to reproduce various observations in Sun and sun-like stars (Tobias et al., 1995b; Mininni et al., 2001; Pontieri et al., 2003; Wilmot-Smith et al., 2005; Passos and Lopes, 2008; Lopes and Passos, 2009; Passos and Lopes, 2011). There is another dynamo model known as flux transport dynamo model which has gained popularity in recent years due to its capability of explaining various properties of solar cycle. This model deals with the transport of magnetic fields on global scale through meridional circulation and buoyant rise of magnetic field (Dikpati and Charbonneau, 1999; Rempel, 2006). Continuous efforts have been made to further develop dynamo models which are able to explain various features of solar magnetic activity and its differential rotation, revealed through high-resolution observational data (Yoshimura, 1975, 1978; Jepps, 1975; Ivanova and Ruzmaikin, 1977).

Furthermore, Sood and Kim (2014) emphasized the importance of simple parameterised models in explaining the observations of magnetic fields of Sun and other stars, "*A simple parameterised dynamo model can serve as a useful model to understand how various nonlinear transport coefficients influence the evolution of magnetic fields and rotation rate during the stellar spin-down. In fact, the observations of the evolution of magnetic fields and rotation of other stars of different ages with different rotation rates have been providing us with valuable information about the relation among rotation, differential rotation, and magnetic activity, which can be utilised to test a dynamo theory against observations for improvement. It can work not only for the Sun but also for other solar-type stars with different rotation rates. The exploration of the relation between magnetic activity and rotation for a broad range of rotation rates is, however, a very challenging problem and cannot be practically performed by full MHD simulations due*

to the required high computational demand (e.g., the resolution of a broad range of length and time scales, etc). An illustrative theoretical model for a minimal number of key quantities is, thus, valuable to gain an insight into this problem. This is particularly the case in view of the limitations inherent in any model (e.g., in parameterisations of transport coefficients in MHD simulations)” (Sood and Kim, 2014).

The main aim of this chapter is to provide detailed analysis of non-linear dynamo models by elucidating the effect/role of various non-linear interactions which are proposed previously, and thus to recognise the self-regulatory behavior in a feasible solar/stellar dynamo model which is capable of explaining the observations. To achieve this, the nonlinear effect through nonlinear transport coefficients such as  $\alpha$ -quenching and flux losses and feedback of differential rotation (mean and fluctuating) on frequency  $p$  of magnetic field and magnetic field strength  $|B|$  are examined. It is then signified that self-regulation by the “near” balance among the (nonlinear) generation and destruction of the magnetic fields is the most desired feature of a successful model. In particular, this self-regulatory behavior gives rise to “the almost linear increase in frequency with rotation rate and flattening of magnetic energy for high rotation, and quenching in total shear consistent with observations” (Sood and Kim, 2013, 2014).

The remainder of this chapter is organised as follows. In section 3.2, the model is introduced. In sections 3.3-3.5, we provide step by step detailed analysis of this model: nonlinear effects through transport coefficients are discussed in section 3.3; section 3.4 (3.5) focuses on nonlinear effects through mean (fluctuating) differential rotation. The implications of our results together with key observational data are provided in section 3.6. Section 3.7 discusses conclusions.

## 3.2 Model equations

Here we again investigate the dynamical system represented by equations (2.5)-(2.8) in Chapter 2, section 2.2 (Sood and Kim 2013; Weiss et al. 1984), consisting

of seven coupled ordinary differential equations (ODE) rewritten in the following dimensionless form

$$(\partial_t + F_2)A = 2DB, \text{ where } D = \frac{D_0}{F_1}, \quad (3.1)$$

$$(\partial_t + F_3)B = i(1 + w_0)A - \frac{1}{2}iA^*w, \quad (3.2)$$

$$(\partial_t + \nu_0)w_0 = \frac{1}{2}i(A^*B - AB^*), \quad (3.3)$$

$$(\partial_t + \nu)w = -iAB. \quad (3.4)$$

Here,  $A$ ,  $B$ ,  $w_0$  and  $w$  represent the poloidal magnetic field, toroidal magnetic field, mean and fluctuating differential rotations, respectively, where mean and fluctuating differential rotations are due to a nonlinear back reaction of  $A$  and  $B$  and have zero and double the frequency of  $A$  and  $B$ , respectively.  $A$ ,  $B$ ,  $w$  are complex, whereas  $w_0$  is real. The complex conjugate of  $A$  and  $B$  are represented by  $A^*$  and  $B^*$ , respectively. In dimensionless units,  $1 + w_0 = \frac{\Delta\Omega}{\Omega}$  gives the total mean differential rotation; thus, as a result of back reaction,  $w_0$  always possesses a negative sign to reduce the total shear from 1 to  $1 + w_0 < 1$ . This reduction in shear is caused by the tension in the magnetic field lines through Lorentz force which inhibits the differential rotation (i.e., causing the quenching of  $\Omega$ -effect.). The constant parameters  $\nu$  and  $\nu_0$  represent the viscosity of fluctuating and mean differential rotation, respectively.

The dynamo number  $D_0 \propto \alpha\Omega$  is the main control parameter, described in Eq. (3.1) while  $F_1$ ,  $F_2$ , and  $F_3$  are the ‘nonlinear’ transport coefficients, defined as

$$F_1 = 1 + \kappa_1|B|^2,$$

$$F_2 = 1 + \lambda_1|B|^2,$$

$$F_3 = 1 + \lambda_2|B|^2,$$

where  $\kappa_1$ ,  $\lambda_1$ , and  $\lambda_2$  are constant parameters; the  $\alpha$  source term (i.e., helicity by the magnetic field) due to the back reaction by magnetic field is represented by  $F_1$ , which was previously studied by Pouquet et al. (1976). Here,  $F_2$  and  $F_3$  represent the enhanced magnetic dissipation via the loss of toroidal and poloidal magnetic fluxes, respectively, which eliminates magnetic flux from the area where the dynamo works. It is worth noting that this is totally different from the supposition of depletion in magnetic dissipation used in some previous works. Based upon the traditional  $\alpha\Omega$  dynamo,  $\alpha$  is assumed to increase with rotation as  $\alpha \propto \Omega$  in our model and, therefore, our dynamo number  $D_0$  is scaled with rotation rate  $\Omega$  as  $D_0 \propto \Omega^2$  (Sood & Kim, 2013). In this chapter, we focus mainly on the dynamic balance through  $F_1 - F_3$ . We note that according to our non-dimensionalization, the physical poloidal magnetic field,  $A$ , is obtained by dividing our dimensionless poloidal magnetic flux  $A$  in Eqs. (3.1)-(3.4) by rotation rate,  $\Omega$ .

We expect that the self-regulatory behavior weakens chaos in our nonlinear dynamo model and thus propose the following finite-amplitude solution to Eqs. (3.1)-(3.4) as (Sood and Kim, 2014)

$$A = ae^{ipt}, B = be^{i(pt+\varphi)}, w = ca^2e^{2ipt}, w_0 = \text{real constant}, \quad (3.5)$$

where  $a > 0$  and  $b > 0$  are supposed to be positive and real constants;  $c$  is a complex constant;  $p$  is real angular frequency;  $w_0$  is a real constant which measures the amplitude of mean differential rotation generated as a result of back reaction of Lorentz force;  $\varphi$  represents the phase difference between toroidal  $b$  and poloidal  $a$  magnetic fields. We use finite amplitude solution of these forms in Eqs. (3.1)- (3.4) to obtain the following five relations among  $a$ ,  $b$ ,  $\varphi$ ,  $p$ , and

$w_0$

$$-p^2 + F_2 F_3 = \frac{-(2p^2 + F_2 \nu) \epsilon a^2}{2(4p^2 + \nu^2)}, \quad (3.6)$$

$$(F_2 + F_3)p = 2D - \frac{pa^2}{\nu_0} + \frac{(2F_2 - \nu)p\epsilon a^2}{2(4p^2 + \nu^2)}, \quad (3.7)$$

$$w_0 = \frac{-pa^2}{2\nu_0 D}, \quad (3.8)$$

$$a = \frac{2Db}{\sqrt{p^2 + F_2^2}}, \quad (3.9)$$

$$\tan \varphi = \frac{p}{F_2}, \quad (3.10)$$

where  $D = \frac{D_0}{F_1}$ ,  $F_1 = 1 + \kappa_1 b^2$ , and  $F_{2,3} = 1 + \lambda_{1,2} b^2$ . In the above equations, the presence of fluctuating shear,  $w$ , is tracked by a parameter,  $\epsilon$ , which is given by

$$\epsilon = \begin{cases} 1, & w \neq 0, \\ 0, & w = 0. \end{cases}$$

Therefore, in the absence of fluctuating shear ( $\epsilon = 0$ ), Eqs. (3.6)-(3.7) are simplified as

$$p = \pm \sqrt{F_2 F_3}, \quad (3.11)$$

$$\left\{ (F_2 + F_3) + \frac{4D_0^2 b^2}{\nu_0 F_1^2 F_2 (F_2 + F_3)} \right\} F_1 \sqrt{F_2 F_3} = 2D_0, \quad (3.12)$$

where Eqs. (3.11) and (3.9) were used in obtaining Eq. (3.12). We note that ignoring nonlinear terms in the above equations (i.e.,  $F_1 = F_2 = F_3 = 1$ ,  $w_0 = 0$ ) provides the linear dispersion relation for the onset of bifurcation as  $p = 1$  and  $\varphi = \pi/4$ .

It is interesting to note that the frequency,  $p$ , of the magnetic field is equal to the geometric mean of  $F_2$  and  $F_3$  represented by Eq. (3.11) and is determined by the dissipation of both magnetic fields. This results in an increase in  $p$  with  $b$  due to the enhanced magnetic dissipation represented by  $F_2 = 1 + \lambda_1 b^2$  or  $F_3 = 1 + \lambda_2 b^2$ .

However,  $\alpha$ -quenching ( $F_1$ ) does not influence  $p$  which shows different effects of  $\alpha$ -quenching and magnetic flux losses on  $p$ . The phase,  $\varphi$ , between  $b$  and  $a$  is determined by  $F_2$  and  $F_3$  as  $\varphi = \sqrt{F_3/F_2}$ ; that is, variation in the phase,  $\varphi$ , between  $b$  and  $a$  depends upon the fact that stronger (weaker) is toroidal flux loss  $F_2$  than poloidal flux loss  $F_3$ , i.e.,  $b$  is removed more (less) systematically than  $a$ , the more increase (decrease) is observed in the phase,  $\varphi$ , between  $b$  and  $a$ . It is clear from Eq. (3.8) that  $w_0$  is negative definite and always reduces the total mean differential rotation  $1 + w_0 < 1$ . Explicit examples of these can be seen in Sects. 3.4-3.5 where detailed investigations of finite amplitude solution are provided by considering the different limits of  $F_1$ ,  $F_2$ , and  $F_3$  as well as  $w_0, w \rightarrow 0$ . This emphasizes the role of nonlinear transport coefficients such as  $\alpha$ -quenching, flux losses as well as mean and fluctuating differential rotation to understand the self-regulatory behaviour of magnetic activity/cycle. We confirm our analytical predictions in Sects. 3.3-3.4 by numerical simulations. In particular, for the numerical parts, Eqs. (3.1)-(3.4) are solved by time-stepping for all variables  $A$ ,  $B$ ,  $w$ , and  $w_0$  using  $\nu = 0.5$ ,  $\nu_0 = 35.0$  for different values of  $D_0$  varied between 1 - 400 (see Sood and Kim, 2013, 2014 for more details). We also note that for numerical simulations, the values of parameters, i.e.,  $\kappa_1$ ,  $\lambda_1$ , and  $\lambda_2$  are assumed to have the same value, i.e.,  $\kappa_1 = \lambda_1 = \lambda_2 \equiv \lambda = 2.5$ .

### 3.3 Nonlinear effects through transport coefficients

Nonlinear transport processes such as  $\alpha$ -effect and flux losses play a very important and critical role in capturing the overall effects of small scale unresolved turbulence. These transport mechanisms are tailored by the feedback of growing magnetic fields and eventually depend upon magnetic fields. The self-consistent behavior of dynamo depends upon these nonlinear transport mechanisms as the unresolved turbulence helps in the working of a dynamo. In order to understand

the effects of nonlinear transport, it is important to further probe the behavior of the system in the limit of a very weak mean or fluctuating differential rotation by assuming  $w_0, w \rightarrow 0$  and Eqs. (3.11), (3.12) followed by Eqs. (3.8) to (3.9) are summarised as follows:

$$p = \pm \sqrt{F_2 F_3}, \quad (3.13)$$

$$(F_2 + F_3) F_1 \sqrt{F_2 F_3} = 2D_0, \quad (3.14)$$

$$a = \frac{2D_0 b}{F_1 \sqrt{p^2 + F_2^2}}, \quad (3.15)$$

$$\tan \varphi = \frac{p}{F_2}. \quad (3.16)$$

The behavior of  $p$ ,  $b$ , and  $a$  with rotation is examined for different cases of  $F_1$ ,  $F_2$ , and  $F_3$ .

1.  $F_1 = F = 1 + \lambda b^2, F_2 = F_3 = 1$ . In the presence of  $\alpha$ -quenching only with no flux loss, equations (3.13)-(3.16) are simplified as

$$p = 1, \quad (3.17)$$

$$2(1 + \lambda b^2) = 2D_0, \quad (3.18)$$

$$a = \frac{2D_0 b}{(1 + \lambda b^2)}, \quad (3.19)$$

$$\tan \varphi = 1. \quad (3.20)$$

Equation (3.17) clearly illustrates that though the growth rate of magnetic field is saturated by the nonlinear damping provided by the  $\alpha$ -quenching ( $F_1$ ), it does not effect the frequency  $p = 1$ , i.e., the value of the frequency remains constant with rotation rate. In addition, the phase,  $\varphi$ , maintains a linear value  $\frac{\pi}{4}$  without being altered by  $\alpha$ -quenching. For  $D_0 \gg 1$ , the scalings of  $a$  as  $a \sim \Omega$  and  $b$  as  $b \sim \Omega$  are obtained by using Eqs. (3.18)-(3.20)

These analytical results are further compared with numerical simulation of Eqs. (3.1)-(3.4). The analytical scalings are consistent with the results obtained from

numerical simulations, as shown in Fig. 3.1. The intensity of frequency spectrum for various values of rotation rate is depicted in Fig. 3.1a, where bright to dark colours represent high-to-low intensity. The frequency of maximum intensity illustrated by a yellow color strip, does not change with  $\Omega$  by keeping the same scaling ( $p = 1$ ) as estimated by analytical results. The quantities  $b$  and  $a$  as functions of  $\Omega$  are shown in Fig. 3.1(b-c), and scalings identical to the analytic values are obtained, which confirms the validity of our finite amplitude solutions.

2.  $F_1 = 1, F_2 = F_3 = F = 1 + \lambda b^2$ . Now, both flux losses are taken into

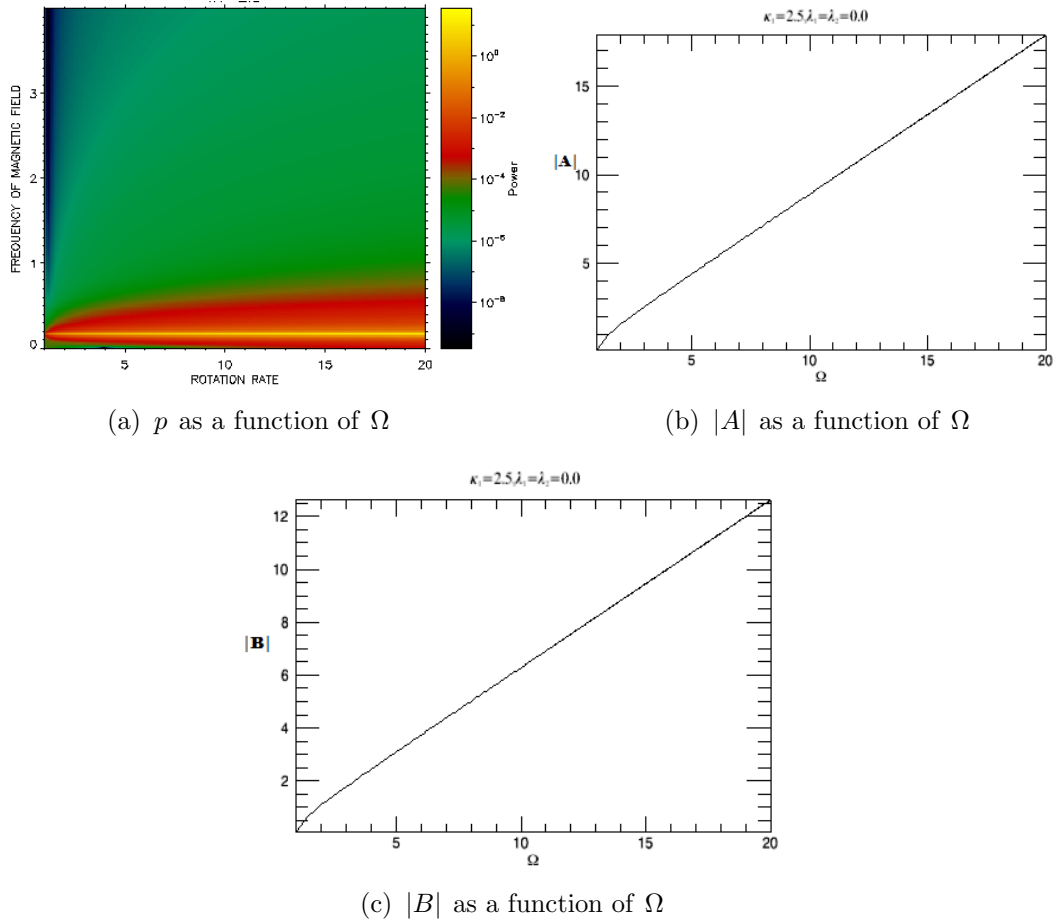


Figure 3.1: Frequency of maximum intensity  $p$ , poloidal magnetic field  $|A|$  and toroidal magnetic field  $|B|$  as a function of rotation rate  $\Omega$  for  $F_1 = F, F_2 = F_3 = 1.0$  for Case 1 in the fourth-order system.

account in the absence of  $\alpha$ -quenching and Eqs. (3.13)-(3.16) take a form of

$p \sim (1 + \lambda b^2)$ ,  $2D_0 = 2(1 + \lambda b^2)^2$ ,  $a \sim 2D_0/2^{1/2}(1 + \lambda b^2)^{3/2}$ , and  $\tan \varphi = 1$ . Clearly, the frequency  $p \sim (1 + \lambda_{1,2}b^2)$  increases with  $b$  in the presence of both flux losses, while cancelling their effects in the phase shift  $\varphi = \frac{\pi}{4}$ . In the limit of  $D_0 \gg 1$ , we obtain the scalings of  $p$ ,  $b$ , and  $a$  to be  $p \sim \Omega$ ,  $b \sim \Omega^{\frac{1}{2}}$ , and  $a \sim \Omega^{\frac{3}{2}}$  and we confirm them by numerical simulations (cf. Table (3.1)). The behavior of  $p$ ,  $|B|$  and  $|A|$  with respect to rotation rate can be seen in Fig. (3.2).

**3.**  $F_1 = F_2 = F_3 = F = 1 + \lambda b^2$ . Here,  $\alpha$ -quenching and enhanced flux

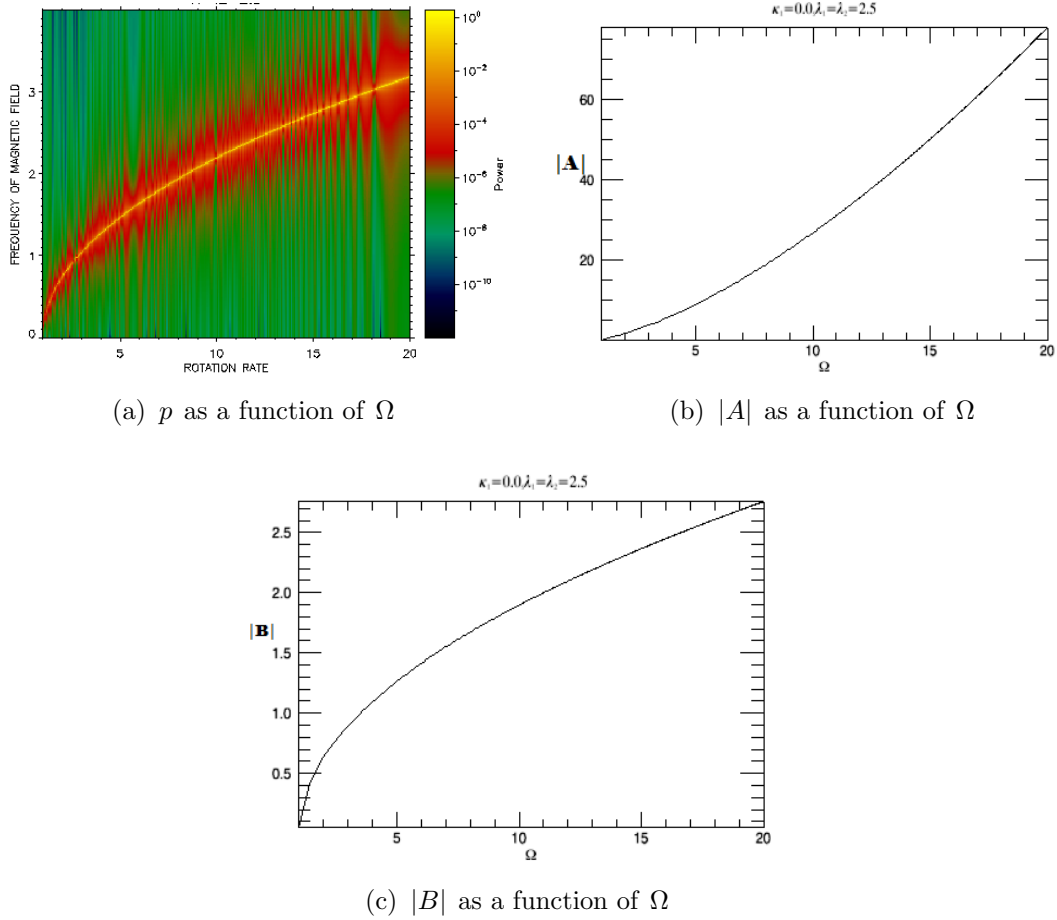


Figure 3.2: Frequency of maximum intensity  $p$ , poloidal magnetic field  $|A|$  and toroidal magnetic field  $|B|$  as a function of rotation rate  $\Omega$  for  $F_1 = 1.0, F_2 = F_3 = F$  for Case 2 in the fourth-order system.

losses due to poloidal magnetic field and toroidal magnetic field have equal input

towards magnetic fields saturation for large rotation rates. Equations (3.13)-(3.16) provide  $p \sim F \sim 1 + \lambda b^2$ ,  $D_0 = (1 + \lambda b^2)^3$ ,  $a = 2D_0 b / 2^{1/2} (1 + \lambda b^2)^3$ , and  $\tan \varphi = 1$ . Clearly, the maximum frequency,  $p$ , of the magnetic field is decided by both poloidal and toroidal flux losses, respectively;  $p$  is found to grow with  $\Omega$ . These results are similar to the case where the effect of both flux losses is taken into account. Further, both  $a$  and  $b$  are noticed to rise with rotation rate (cf. Fig. 3.3(a) to 3.3(c)). It is interesting to note that equal contribution of  $F_2$  and  $F_3$  does not alter the phase between  $a$  and  $b$ , with its value  $\varphi = \frac{\pi}{4}$ . In the limit of  $D_0 \gg 1$ , we obtain  $p \sim \Omega^{\frac{2}{3}}$ ,  $a \sim \Omega$ , and  $b \sim \Omega^{\frac{1}{3}}$ . The scalings obtained from numerical simulations are almost same for  $p$ ,  $b$  and  $a$  (cf. Table (3.1)). Therefore, the combined effect of  $\alpha$ -quenching, enhanced poloidal flux loss and toroidal flux loss with the equal contribution causes stronger quenching in magnetic field for a higher rotation rate, through which a strong dynamic balance can be provided towards the working of nonlinear dynamo.

**4.**  $F_1 = F_2 = F = 1 + \lambda b^2, F_3 = 1$ . The presence of only  $\alpha$ -quenching and enhanced poloidal magnetic flux loss, we simplify the various scalings to  $p \sim (1 + \lambda b^2)^{1/2}$ ,  $2D_0 = (2 + \lambda b^2)^2 (1 + \lambda b^2)^{1/2}$ ,  $a = 2D_0 b / (2 + \lambda b^2)^{1/2} (1 + \lambda b^2)^2$ ,  $\tan \varphi \sim 1 / (1 + \lambda b^2)^{1/2}$ . Thus,  $\varphi$  is obtained to decrease for large  $b$  (or large  $D_0$ ) as a result of which the phase shift between  $b$  and  $a$  is found to reduce to zero. Furthermore, in the limit of  $D_0 \gg 1$ , these provides us  $p \sim \Omega^{\frac{2}{5}}$ ,  $b \sim \Omega^{\frac{2}{5}}$ , and  $a \sim \Omega^{\frac{4}{5}}$ .

**5.**  $F_1 = F_3 = F = 1 + \lambda b^2, F_2 = 1$ . In this case the nonlinear effects through  $\alpha$ -quenching and flux loss due to toroidal magnetic field are considered; Eqs. (3.13) to (3.16) provide  $p \sim (1 + \lambda b^2)^{1/2}$ ,  $2D_0 = (1 + \lambda b^2)^{5/2}$ ,  $a = 2D_0 b / (2 + \lambda b^2)^{1/2} (1 + \lambda b^2)^2$ , and  $\tan \varphi = 1$ . Clearly, the frequency,  $p$ , of magnetic field is affected by the toroidal magnetic field,  $b$ , due to toroidal flux loss. The frequency of maximum intensity  $p$  increases at a very slow rate. The toroidal magnetic field,  $b$ , initially increases very fast but as  $\Omega$  increases, slower increase in  $b$  is noticed. In this case  $a$  increases rapidly as compared to the previous cases.  $\alpha$ -quenching

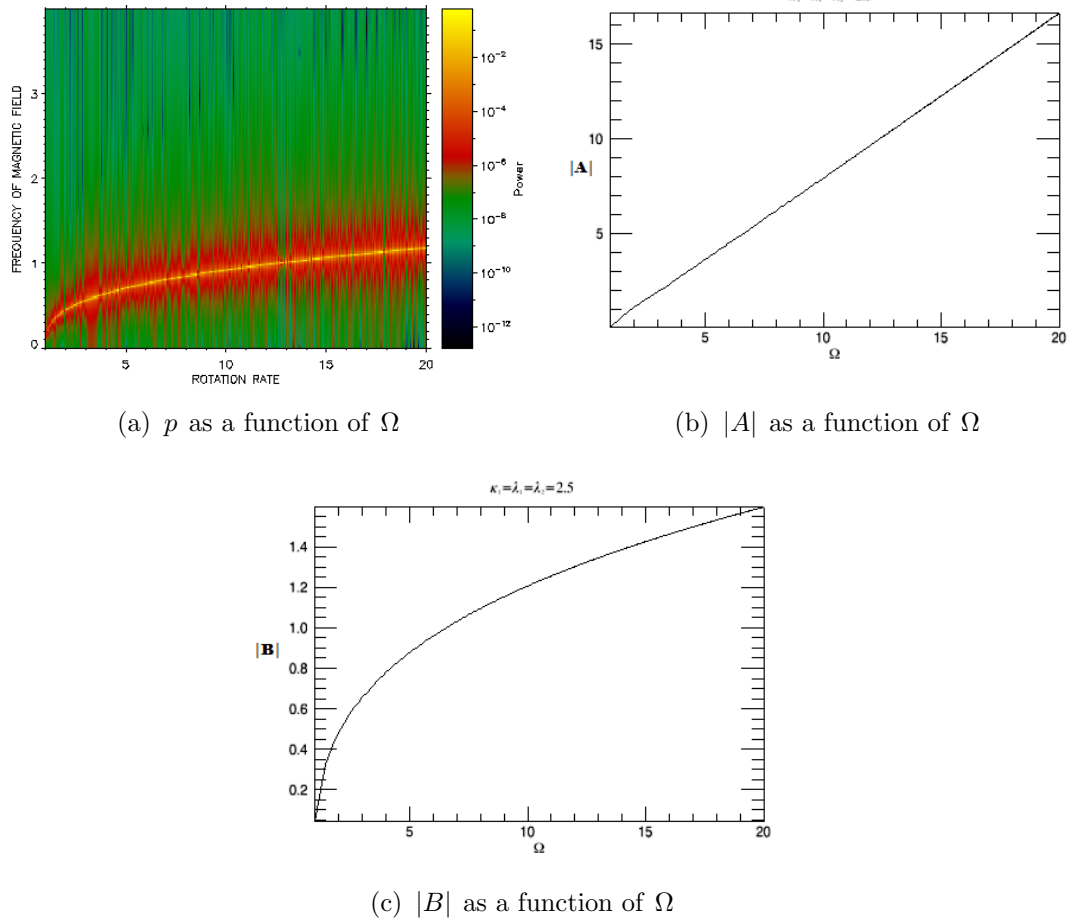


Figure 3.3: Frequency of maximum intensity  $p$ , poloidal magnetic field  $|A|$  and toroidal magnetic field  $|B|$  as a function of rotation rate  $\Omega$  for  $F_1 = F_2 = F_3 = F$  for Case 3 in the fourth-order system.

and flux loss due to  $b$  do not alter the phase shift between poloidal flux loss,  $a$ , and toroidal flux loss due to  $b$ , keeping the value of  $\varphi$  almost linear i.e.  $\frac{\pi}{4}$ . For  $D_0 \gg 1$ , the obtained scalings of  $p$ ,  $b$ , and  $a$  are  $p \sim \Omega^{\frac{2}{5}}$ ,  $b \sim \Omega^{\frac{2}{5}}$ , and  $a \sim \Omega^{\frac{6}{5}}$ . Clearly, change from toroidal to poloidal flux loss only impacts the scaling of  $a$  with  $\Omega$ .

**6.**  $F_3 = F = 1 + \lambda b^2$ ,  $F_1 = F_2 = 1$ . This is the case where flux loss due to toroidal magnetic field tracks the amplitude of  $b$  for large  $\Omega$ , by obtaining equations (3.13) - (3.16) into the form  $p = (1 + \lambda b^2)^{1/2}$ ,  $2D_0 = (2 + \lambda b^2)(1 + \lambda b^2)^{1/2}$ ,

$a = 2D_0b/(1 + \lambda b^2)^{1/2}$ , and  $\tan \varphi \sim (1 + \lambda b^2)^{1/2}$ . Hence, toroidal flux loss contributes to the growth of the frequency in fashion similar to the strength of  $b$ , which is prescribed dynamically. The phase,  $\varphi$ , between  $a$  and  $b$  increases with a value  $\frac{\pi}{2}$  as  $D_0 \gg 1$ . In the limit of  $D_0 \gg 1$ , power-law scalings are  $p \sim \Omega^{\frac{2}{3}}$ ,  $b \sim \Omega^{\frac{2}{3}}$ , and  $a \sim \Omega^2$ .

**7.**  $F_2 = F = 1 + \lambda b^2, F_1 = F_3 = 1$ . The frequency, toroidal magnetic field strength and poloidal magnetic field strength are determined by the poloidal flux loss by simplifying equations (3.13) - (3.16) as  $p = (1 + \lambda b^2)^{1/2}$ ,  $2D_0 = (2 + \lambda b^2)(1 + \lambda b^2)^{1/2}$ ,  $a = 2D_0b/(1 + \lambda b^2)(2 + \lambda b^2)^{1/2}$ ,  $\tan \varphi = (1 + \lambda b^2)^{-1/2}$ . For  $D_0 \gg 1$ , the scalings obtained are  $p \sim \Omega^{2/3}$ ,  $b \sim \Omega^{2/3}$  and  $a \sim \Omega^{4/3}$ ,  $\tan \varphi \sim \Omega^{-2/3}$ . Therefore, compared to case where toroidal flux loss is considered (i.e., Case 6), the scalings of  $a$  and  $\varphi$  are different here and we obtain reduced power law scalings for  $a$  and  $\varphi$  with  $\Omega$ .

It is clear from above studies, that  $\alpha$ -quenching,  $F_1$ , and flux losses,  $F_2$  and  $F_3$ , have different effects in the absence of mean and fluctuating shear. Here, flux losses,  $F_2$  and  $F_3$ , determine the behavior of  $p$ , which is not influenced by  $\alpha$ -quenching,  $F_1$ , i.e.,  $p$  remains constant with value 1 when  $\alpha$ -quenching is considered, whereas the increasing behavior of  $p$  is obtained due to flux losses. Similar effects of  $F_2$  and  $F_3$  are noticed which give same scalings for  $p$  and  $b$  with  $\Omega$ . The ratio of  $F_2$  and  $F_3$  determines the phase,  $\varphi$ . In all the above cases,  $b$  is noticed to increase with  $\Omega$  as  $b \propto \Omega^\beta$ , where  $\beta \in [1/3, 1]$ . The largest value of  $\beta = 1$  is obtained for the case where the dynamo is saturated through quenching of  $\alpha$ -effect, while the smallest value ( $\beta = 0.4$ ) is obtained for the combined effects of all nonlinear terms of the same magnitude. Thus, in the absence of mean and fluctuating shear,  $b$  continues to rise with  $\Omega$ , without being flattened for large  $\Omega$ . Table (3.1) summarizes the numerical and analytic values of scaling exponent for  $p$ ,  $b$  and  $a$ , respectively. We find that analytic and numerical values both agree with each other as the effects of mean and fluctuating differential rotations are not taken into account.

Transport coefficients	Numerical Scalings			Analytic Scalings		
	$\xi$	$\beta$	$\gamma$	$\xi$	$\beta$	$\gamma$
$F_1 = F, F_2 = F_3 = 1$	0	1.0	1.0	0	1	1
$F_1 = 1, F_2 = F_3 = F$	1.0	0.50	1.55	1	1/2	3/2
$F_1 = F_2 = F_3 = F$	0.66	0.41	1.08	2/3	1/3	1
$F_1 = F_2 = F, F_3 = 1$	0.41	0.47	0.84	2/5	2/5	4/5
$F_1 = F_3 = F, F_2 = 1$	0.41	0.47	1.55	2/5	2/5	6/5
$F_1 = F_2 = 1, F_3 = F$	0.67	0.69	2.03	2/3	2/3	2
$F_1 = F_3 = 1, F_2 = F$	0.67	0.69	1.35	2/3	2/3	4/3

Table 3.1: Scaling exponents for  $p$ ,  $|B|$ , and  $|A|$  for  $\Omega \geq 5$  in the cases of the fourth-order system where  $p = \Omega^\xi$ ,  $|B| = \Omega^\beta$ , and  $|A| = \Omega^\gamma$ .

### 3.4 Nonlinear effect through mean differential rotation

In the previous sections, nonlinear effect due to the modification of differential rotation by magnetic fields is incorporated and the role of mean differential rotation in self-regulatory behaviour of a dynamo is examined. Here, the main focus is to recognise the effect of mean differential rotation, therefore we do not consider the effects of fluctuating differential rotation. The effects of fluctuating differential rotation are discussed in the next section. The main equations are Eqs. (3.6)-(3.10) for  $w = 0$ , and for numerical simulations  $\nu_0$  is considered to be equal to 35.

1.  $F_1 = F_2 = F_3 = 1$ . In the absence of  $\alpha$ -quenching or any flux loss, the saturation of dynamo occurs through the back reaction of mean differential rotation,  $w_0$ , which confirms a finite-amplitude solution by reducing Eqs. (3.6)-(3.10) to

$$p = \pm 1, \quad (3.21)$$

$$b = D_0^{-1/2} \nu_0^{1/2} (1 - D_0^{-1})^{1/2}, \quad (3.22)$$

$$a = D_0^{1/2} \nu_0^{1/2} \sqrt{2(1 - D_0^{-1})}, \quad (3.23)$$

$$w_0 = -1 + \frac{1}{D_0}, \quad (3.24)$$

$$\tan \varphi = 1. \quad (3.25)$$

It is clear from Eq. (3.21) that the frequency of magnetic field does not depend upon the rotation rate, without being effected by  $w_0$ . For high rotation rate, i.e.,  $D_0 \gg 1$ , Eqs. (3.22)-(3.25) provide us with analytical scalings of  $b$ ,  $a$ , and total shear  $1 + w_0$  with  $\Omega$  as  $b \sim \Omega^{-1}$ ,  $a \sim \Omega$  and  $1 + w_0 \sim \Omega^{-2} \ll 1$  for  $\Omega \gg 1$ . The linear value of the phase angle between the poloidal magnetic field,  $a$ , and toroidal magnetic field,  $b$ , is maintained with a value  $\varphi = \frac{\pi}{4}$  (cf. Eq. (3.25)). A remarkable shear quenching is shown by power law relationship of the total shear on rotation rate  $\Omega^{-2}$ . Analytic results are verified by numerical simulations. A single dominant frequency,  $p \sim 1$  can be seen in Fig. 3.4(a) with almost no dependence on rotation. The localized frequency of maximum intensity is surrounded by a broad red band of weak intensity frequency whose width changes with increasing rotation rate. Initially, there is an increases in its width which is found to decline slowly for higher rotation. This behaviour is caused by the shear quenching due to Lorentz force which is too strong to significantly quench the magnetic field strength,  $b$ , for  $\Omega \gg 1$ . The poloidal magnetic field  $|A|$  is obtained to increase linearly with rotation rate  $\Omega$  in Fig. 3.4(b) while the toroidal magnetic field strength,  $|B|$ , is observed to initially increase with  $\Omega$  for slower rotation rate and is found to decrease as we increase the rotation rate  $\Omega$  (see Fig. 3.4(c)). Figure 3.4(d) shows the rapid decrease in total shear, which approaches zero for a higher rotation rate ( $\Omega \geq 12$ ), and illustrates the severe shear quenching due to the effect of magnetic fields on mean differential rotation. We find scalings of  $|B|$ ,  $|A|$  and total shear  $1 + w_0$  numerically for high rotation which are  $a \sim \Omega^{1.02}$ ,  $b \sim \Omega^{-0.98}$ ,  $1 + w_0 \sim \Omega^{-2.0} \sim D_0^{-1}$ , and are similar to analytic results.

**2.**  $F_1 = F = 1 + \lambda b^2, F_2 = F_3 = 1$ . This case studies the effect of  $\alpha$ -quenching alone without taking the flux losses into consideration, and, Eqs. (3.6) to (3.10)

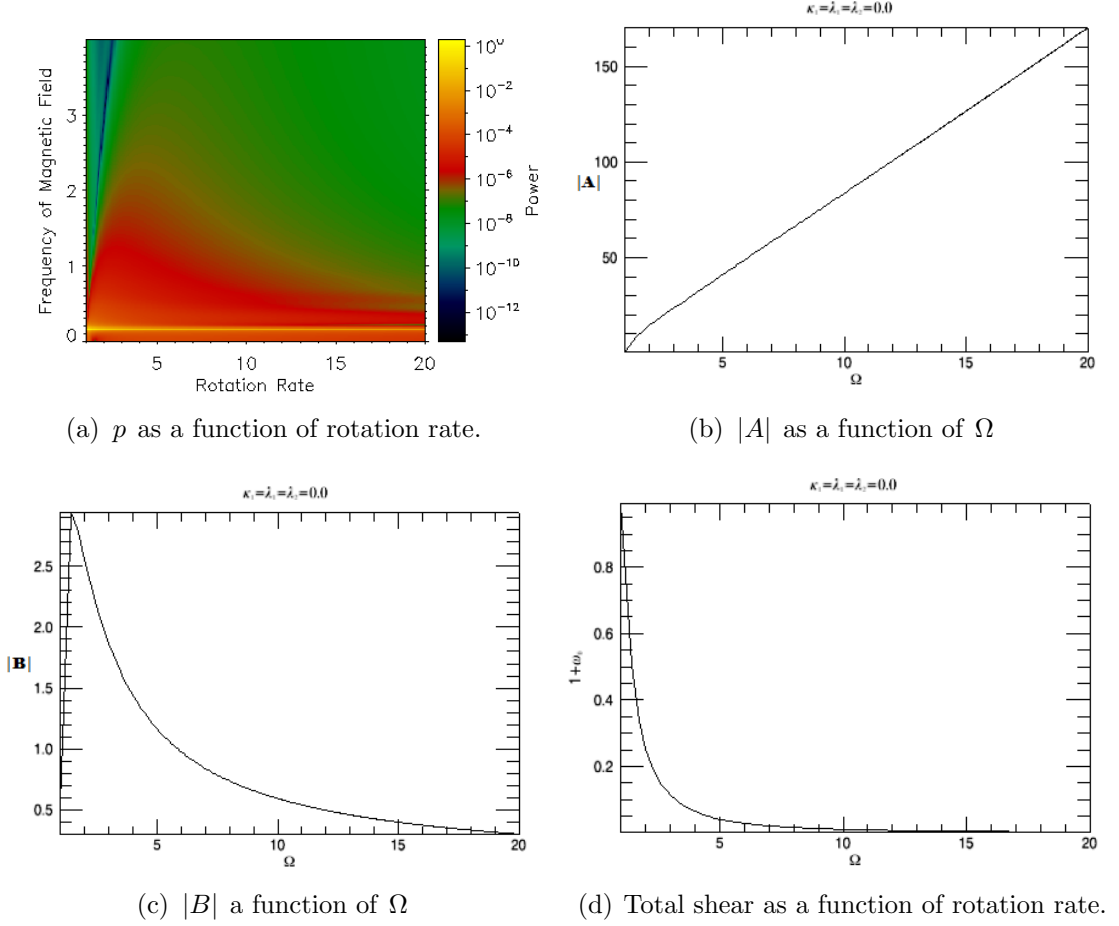


Figure 3.4: Frequency of maximum intensity  $p$ , poloidal magnetic field  $|A|$ , toroidal magnetic field  $|B|$  and total shear as a function of rotation rate  $\Omega$  for  $F_1 = F_2 = F_3 = 1$  for Case 1 in the fifth-order system.

become

$$p = \pm 1, \quad (3.26)$$

$$F^2 + \frac{D_0^2 b^2}{\nu_0} = D_0 F, \quad (3.27)$$

$$a = \frac{\sqrt{2} D_0 b}{F}, \quad (3.28)$$

$$w_0 = -\frac{D_0 b^2}{F \nu_0}, \quad (3.29)$$

$$\tan \varphi = 1. \quad (3.30)$$

Again, the rotation rate does not affect the frequency,  $p$ . The Eqs. (3.26)-(3.30) are used to obtain analytical scalings for the limit of high rotation rate. For high rotation rate,  $D_0 \gg 1$ , the scalings are found to be  $b \sim \Omega^{-1}$ ,  $a \sim \Omega$ , and  $(1 + w_0) \sim \Omega^{-2}$ . Thus, it is clear that a strong mean differential rotation  $w_0 < 0$  is generated by Lorentz force efficiently, which is responsible for the significant reduction in the magnetic field.

**3.**  $F_2 = F_3 = F = 1 + \lambda b^2$ ,  $F_1 = 1$ . In the presence of both flux losses, Eqs. (3.6) - (3.10) give us

$$p = \pm F, \quad (3.31)$$

$$F^4 + \frac{D_0^2 b^2}{\nu_0} = D_0 F^2, \quad (3.32)$$

$$a = \frac{\sqrt{2} D_0 b}{F^{3/2}}, \quad (3.33)$$

$$w_0 = -\frac{D_0 b^2}{F^2 \nu_0}, \quad (3.34)$$

$$\tan \varphi = 1. \quad (3.35)$$

Due to the effects of nonlinear flux losses,  $F_2$  and  $F_3$ , a change in  $p$  is noticed as  $b$  alters with  $\Omega$  (cf. Eq. (3.31)). In the limit of the high rotation rate,  $D_0 \gg 1$ , the scalings are  $b \sim \Omega^{-1} \ll 1$ ,  $1 + \lambda b^2 \sim 1$ ,  $a \sim \Omega$ , and  $1 + w_0 \sim \Omega^{-2}$ . The quenched behavior of toroidal magnetic field with  $\Omega$  is credited to the severe shear quenching present in the system. Further, due to the equal amounts of the toroidal and poloidal magnetic fluxes the phase shift between  $a$  and  $b$  remains unaltered as  $\frac{\pi}{4}$ .

**4.**  $F_1 = F_2 = F_3 = F = 1 + \lambda b^2$ . Equations (3.6)-(3.10) are simplified for the equal amount of  $\alpha$ -quenching and flux losses and are given by

$$p = \pm F, \quad (3.36)$$

$$F^6 + \frac{D_0 b^2}{\nu_0} = D_0 F^3, \quad (3.37)$$

$$a = \frac{\sqrt{2}D_0b}{F^{3/2}}, \quad (3.38)$$

$$w_0 = -\frac{D_0b^2}{F^2\nu_0}, \quad (3.39)$$

$$\tan \varphi = 1. \quad (3.40)$$

In the presence of  $F_1, F_2$ , and  $F_3$ , interesting behavior is obtained for large  $\Omega$ . A sudden change in  $p$ ,  $|B|$ ,  $|A|$ , and total shear for very high rotation rate is noticed (cf. Figs. 3.5(a)-3.5(d), i.e., the system's behaviour changes at  $\Omega = 19.7$  and further investigations of time series and frequency analysis reveal the damping behavior of the system beyond  $\Omega = 19.7$ . Figure 3.5(a) shows that well-defined, single, frequency,  $p$ , increases initially up to  $\Omega \sim 19.7$  and then  $p$  suddenly drops its value with increasing  $\Omega$ . In addition to this dominant frequency, a red band of lower frequencies with very weak intensity is also visible. Fig. 3.5(c) shows that  $b$  grows and attains a maximum value of  $|b| = 1.296$  at  $\Omega \sim 17$ ; For  $\Omega \geq 17$ , there is a decrease in  $b$  till  $\Omega = 19$ , and then there is a sudden drop in the value of  $b$ . The poloidal magnetic field,  $a$ , grows almost linearly with rotation rate  $\Omega$  for higher rotation rate till  $\Omega \sim 19$ , and there is a sharp increase in  $|a|$  near  $\omega = 19.7$  (Fig. 3.5(b)). The total shear is also observed to decrease very rapidly up to  $\Omega \sim 19$  whereas for  $\Omega = 19.7$ , there is a sudden drop in total shear before it reaches its minimum value (cf. Fig. 3.5(d)). For higher rotation rate, the scaling exponents for  $p$ ,  $b$ ,  $a$  and total shear vary with rotation rate which are very different from what we find analytically. These results suggest a possible change in the dynamo due to a strong mean shear.

**5.**  $F_1 = F_2 = F = 1 + \lambda b^2, F_3 = 1$ . In this case the Eqs. (3.6)-(3.10) reduce to

$$p = \pm\sqrt{F}, \quad (3.41)$$

$$b^2 = 2^{-1}D_0^{-1}F^6(1 + F^{-1})(F^{1/2} - 1 - F^{-1}), \quad (3.42)$$

$$a = \frac{2D_0b}{F^2\sqrt{F+1}}, \quad (3.43)$$

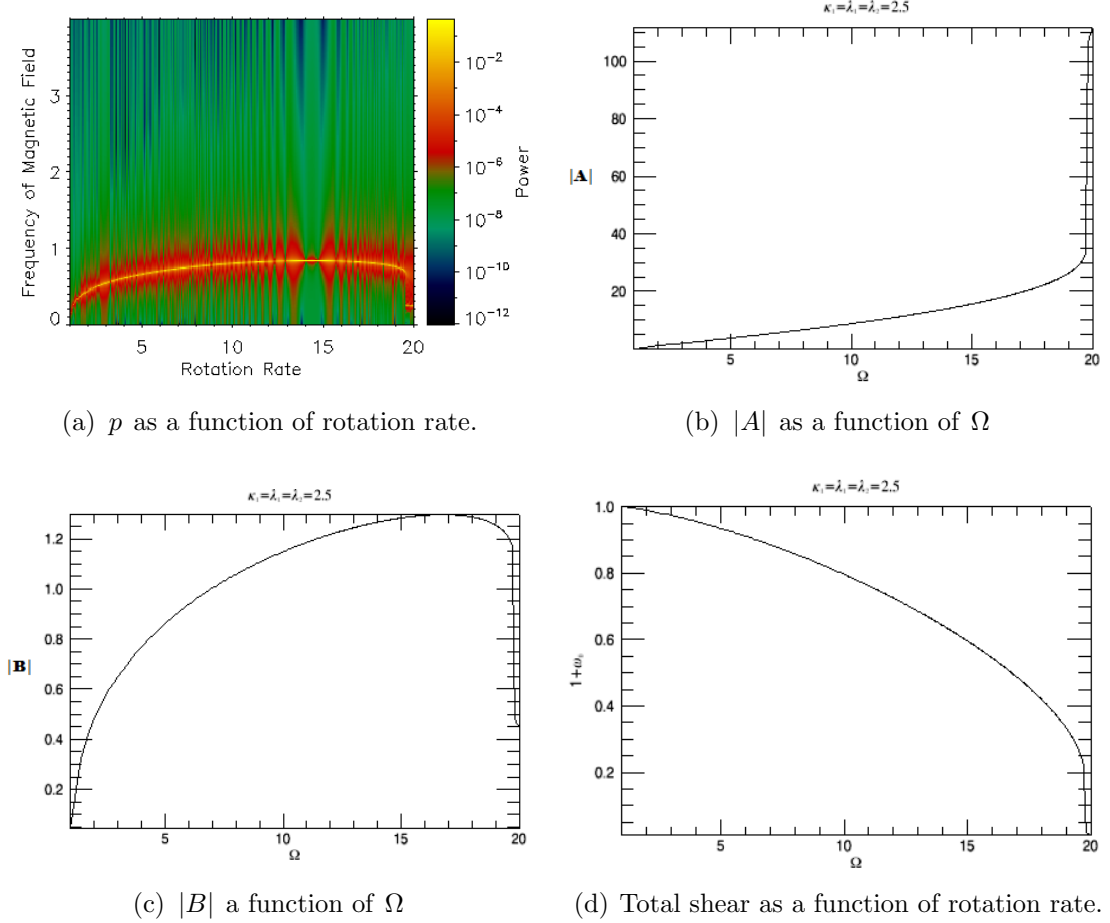


Figure 3.5: Frequency of maximum intensity  $p$ , poloidal magnetic field  $|A|$ , toroidal magnetic field  $|B|$  and total shear as a function of rotation rate  $\Omega$  for  $F_1 = F_2 = F_3 = F$  for Case 4 in the fifth-order system.

$$w_0 = \frac{-pa^2F}{2\nu_0D_0}, \quad (3.44)$$

$$\tan \varphi = F^{-1/2}. \quad (3.45)$$

Here,  $p$  is noted to be affected by  $b$  as  $p \sim b$  (cf. Eq. 3.41). Within the limit of a very high rotation rate, i.e.,  $D_0 \gg 1$ , the analytical scalings are obtained as  $p \sim \Omega^{2/5}$ ,  $b \sim \Omega^{2/5}$ ,  $a \sim \Omega^{4/5}$ , and  $(1+w_0) \sim \Omega^{-2}$ , while the phase shift between  $a$  and  $b$  is found to decrease with increasing rotation rate. These analytical results are very similar to numerically obtained results and also scalings for  $p$ ,  $|B|$ ,

Transport coefficients	Numerical Scalings				Analytic Scalings			
	$\xi$	$\beta$	$\gamma$	$\delta$	$\xi$	$\beta$	$\gamma$	$\delta$
$F_1 = F_2 = F_3 = 1$	0	-0.98	1.02	-2.0	0	-1	1	-2
$F_1 = F, F_2 = F_3 = 1$	0	-1.39	1.42	-3.46	0	-1	1	-2
$F_1 = 1, F_2 = F_3 = F$	-0.99	-1.56	1.30	-4.30	-1	-1	1	-2
$F_1 = F_2 = F_3 = F$	varies	varies	varies	varies	2/3	2/3	2/3	-2/3
$F_1 = F_2 = F, F_3 = 1$	0.39	0.45	0.93	-0.16	2/5	2/5	4/5	-2
$F_1 = F_3 = F, F_2 = 1$	-0.43	-1.45	1.66	-4.40	-1/2	-1/2	5/2	-7/2
$F_1 = F_2 = 1, F_3 = F$	-0.30	-1.02	1.20	-2.76	-3/2	-3/2	7/2	-5/2
$F_1 = F_3 = 1, F_2 = F$	-0.57	-1.62	1.30	-3.21	-3/2	-3/2	5/2	-7/2

Table 3.2: Scaling exponents for  $p$ ,  $|B|$ ,  $|A|$ , and  $1 + w_0$  for  $\Omega \geq 5$  in the cases of the fifth-order system where  $p = \Omega^\xi$ ,  $|B| = \Omega^\beta$ ,  $|A| = \Omega^\gamma$ , and  $1 + w_0 = \Omega^\delta$ .

and  $|A|$  match with the results obtained in the fourth-order system in the case of  $\alpha$ -quenching and flux loss. The behaviour of  $p$ ,  $|A|$ ,  $|B|$  and total shear with rotation rate,  $\Omega$ , can be seen in Fig. 3.6(a-d).

Almost similar results are found for different cases and are briefly discussed here. For  $F_1 = F_3 = F, F_2 = 1$ , and  $F_3 = F, F_1 = F_2 = 1$ , the frequency,  $p$ , and phase shift are influenced by  $b$ . For  $F_2 = F, F_1 = F_3 = 1$ ,  $p$  and phase shift are similar to what we obtain in Case 5. All the numerical and analytic results for high rotation,  $\Omega \geq 5$  are listed in Table (3.2). We find disagreement between numerical and analytic results which is caused by the strong shear quenching in the system.

The results obtained in this section are now compared with the results obtained from fourth-order system. We find that flux losses  $F_2$  and  $F_3$  control the frequency of magnetic field  $p$  and phase shift  $\varphi$  with no influence of  $\alpha$ -quenching, which are consistent with fourth order system. In the absence of all nonlinear transport coefficients ( $F_1 = F_2 = F_3 = 1$ ),  $p$  is independent of rotation rate. Interestingly, for  $F_1 = F, F_2 = F_3 = 1$ ,  $p$  again does not depend upon rotation rate which is similar to the Case 1 in Sect. (3.3). However,  $F_2$  and  $F_3$  no longer behave in similar fashion like in fourth-order system and this behavior is caused by the mean differential rotation. Also, scalings obtained from analytic results and numerical simulations are not consistent as in fourth-order system, with a

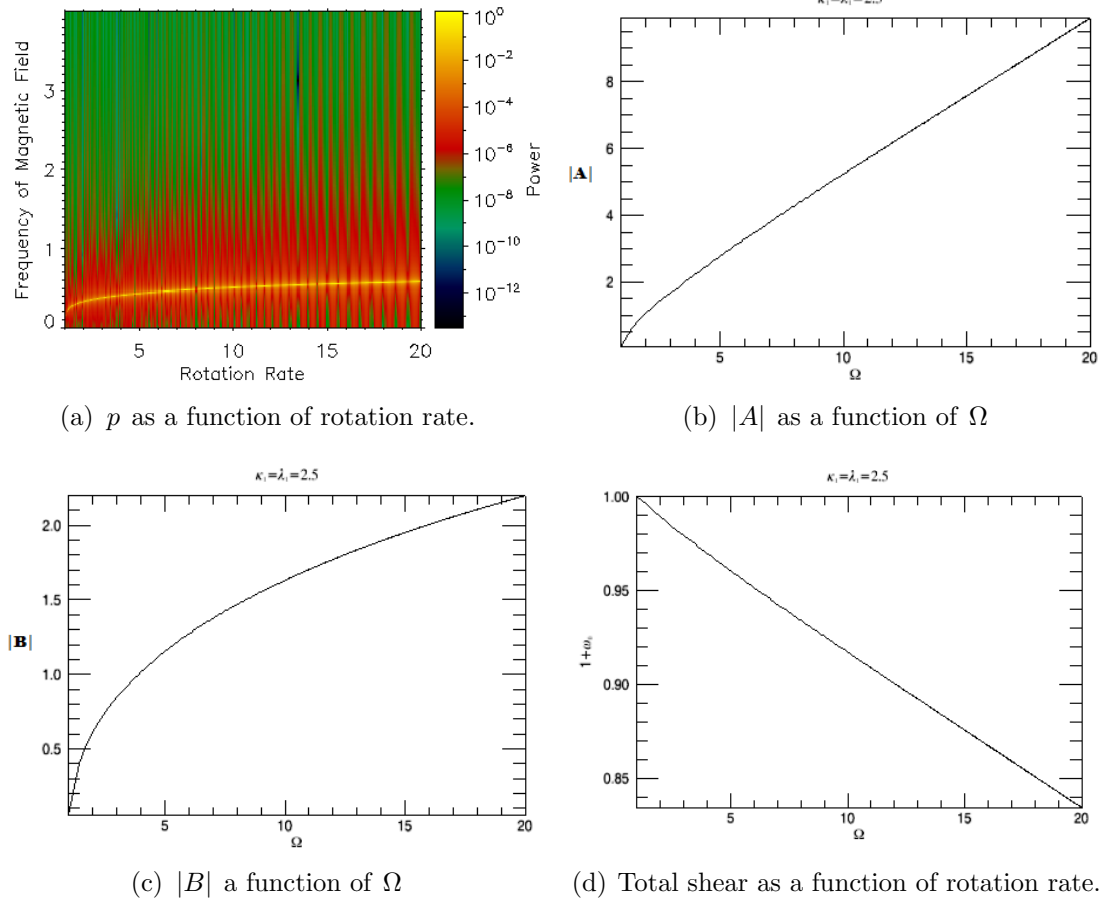


Figure 3.6: Frequency of maximum intensity  $p$ , poloidal magnetic field  $|A|$ , toroidal magnetic field  $|B|$  and total shear as a function of rotation rate  $\Omega$  for  $F_1 = F_2 = F, F_3 = 1$  for Case 5 in the fifth-order system.

close match for two cases only (e.g.,  $F_1 = F_2 = F_3 = 1$  and  $F_1 = F_2 = F, F_3 = 1$ ). Decreasing behavior of  $b$  and  $a$  for higher  $\Omega$  is observed for almost all cases except for  $F_1 = F_2 = F, F_3 = 1$ , that is,  $b$  and  $a$  are noticed to increase with rotation for  $F_1 = F_2 = F, F_3 = 1$ , which are consistent with Case 4 of Sect. (3.3). There are some cases where the presence of  $F_1, F_2$  and  $F_3$  in equal amounts is responsible for the fast growth of  $A/\Omega$  as compared to  $|B|$  for higher  $\Omega$ .

In summary, the dynamo action is inhibited by the severe quenching of magnetic field for large rotation rate owing to the mean differential rotation generated by the Lorentz force, i.e., in the absence of fluctuating differential rotation, quenching

in mean differential rotation is perhaps very strong and suppresses the dynamo for large  $\Omega$ . Therefore, this highlights the importance of fluctuating differential rotation to the self-regulatory behavior of differential rotation for the efficient working of dynamo. This will be discussed in detail in the next section.

### 3.5 Nonlinear effect through fluctuating differential rotation

The aim of this section is to recognize/grasp the effect of fluctuating differential rotation by assuming  $w_0 = 0$  in Eqs. (3.5)-(3.9). We solve the system numerically in order to investigate the behaviour of scalings of  $a$ ,  $b$ , and  $p$  with  $\Omega$  in different cases as analytical solutions do not provide specific insights. For numerical simulation  $\nu$  is chosen to be 0.5 and the effects of nonlinear terms are highlighted to show that the chaos is controlled in the presence of these terms.

**I.**  $F_1 = F_2 = F_3 = 1$ : In this case, the system is investigated in the absence of nonlinear transport coefficients. We find an increasing behaviour of frequency  $p$  with rotation rate. Fluctuations are observed in the rapidly growing behaviour of toroidal and poloidal magnetic fields with rotation rate. This behaviour owes to the fluctuating differential rotation because of Lorentz force and gives rise to chaotic behaviour for high rotation (cf Fig. 3.7(a-c)).

**II.** To understand the behaviour of  $p$ ,  $b$ , and  $a$  with respect to rotation rate in the presence of nonlinear transport coefficients, the local slopes  $\alpha$ ,  $\beta$ , and  $\gamma$  are investigated and the scalings are summarised in Table 3.3. For  $\alpha$ -quenching case, i.e.,  $F_1 = F, F_2 = F_3 = 1$ ,  $b$  is noted to grow very fast with  $\Omega$  as compared to the slow increase in frequency,  $p$ , and poloidal magnetic field. For equal magnitude of  $\alpha$ -quenching and toroidal flux loss there is a decrease in local slope of magnetic field strength,  $b$ , by approximately half of what is observed in the case of  $\alpha$ -quenching considered without the influence of flux losses. Furthermore, when equal amounts of poloidal flux loss are added to  $\alpha$ -quenching and toroidal

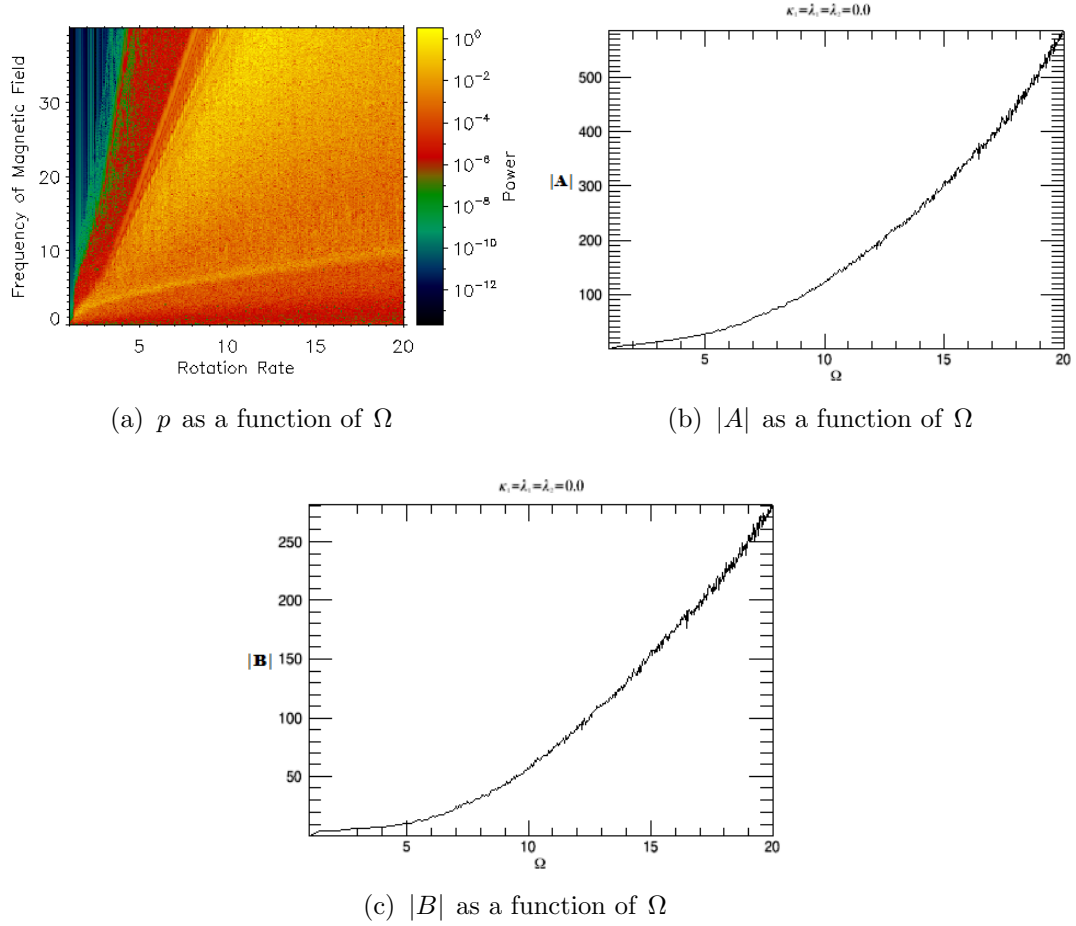


Figure 3.7: Frequency of maximum intensity  $p$ , poloidal magnetic field  $|A|$  and toroidal magnetic field  $|B|$  as a function of rotation rate  $\Omega$  for  $F_1 = F_2 = F_3 = 1$  for Case 1 in the sixth-order system.

flux loss, the magnetic field strength, frequency and poloidal magnetic field are shown to increase slowly indicating the role of poloidal flux loss and it is clear that there is almost no contribution of poloidal flux loss in controlling the growth of magnetic field strength.

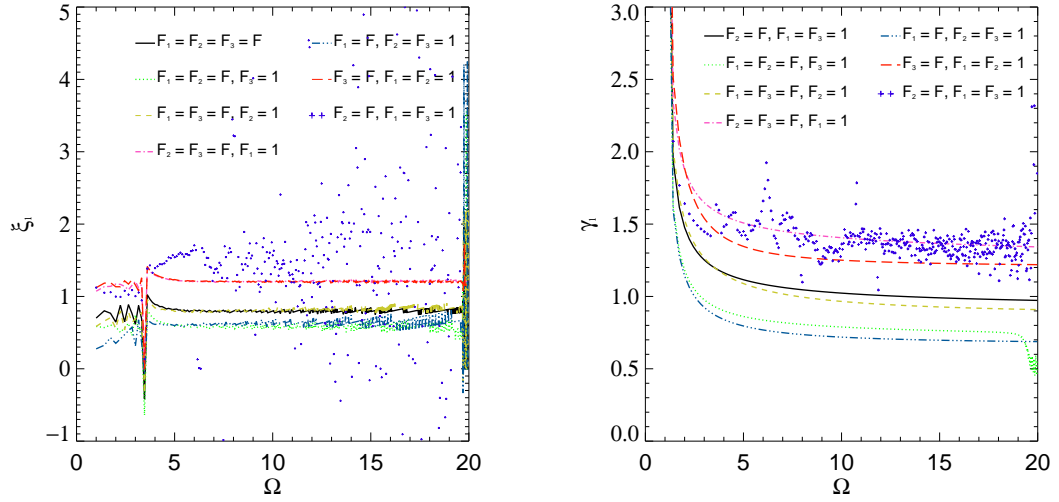
For  $F_2 = F_3 = F$ , i.e., in the presence of equal amounts of both toroidal and poloidal flux losses, a fast growth of toroidal magnetic and poloidal magnetic field is observed as compared to the case where only toroidal flux loss is considered. Interestingly, the scaling exponent,  $\alpha$ , is found to have the same value of  $\frac{6}{5}$  in

Transport coefficients	$\xi$	$\beta$	$\gamma$
$F_1 = F, F_2 = F_3 = 1$	0.63	0.73	0.71
$F_1 = F_2 = F, F_3 = 1$	0.57	0.50	0.78
$F_1 = F_2 = F_3 = F$	0.78	0.40	1.01
$F_1 = F_3 = F, F_2 = 1$	0.81	0.36	0.95
$F_1 = 1, F_2 = F_3 = F$	1.20	0.52	1.39
$F_1 = F_2 = 1, F_3 = F$	1.20	0.44	1.24
$F_1 = F_3 = 1, F_2 = F$	-	-	-

Table 3.3: Scaling exponents for  $p$ ,  $|B|$ , and  $|A|$  for  $\Omega \geq 5$  in the cases of the sixth-order system where  $p = \Omega^\xi$ ,  $|B| = \Omega^\beta$ , and  $|A| = \Omega^\gamma$ .

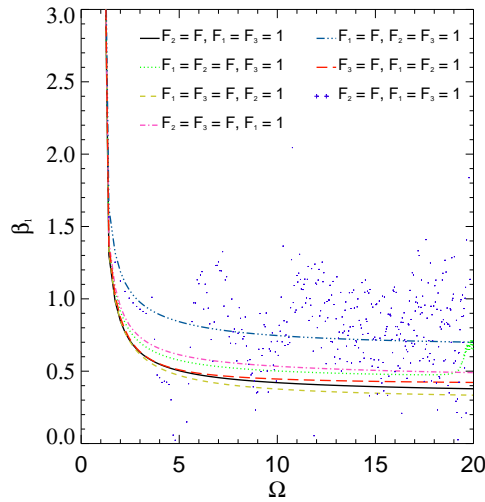
both the cases. The case of poloidal flux loss only, ( $F_2 = F, F_1 = F_3 = 1$ ) shows fluctuating behavior of  $p$ ,  $b$  and  $a$  for higher rotation which is depicted from the scattered behavior of local slopes of  $p$ ,  $b$  and  $a$  in Fig. 3.8(a-c). This indicates that the effects of fluctuating differential rotation are not reduced by poloidal flux loss efficiently.

It is very clear from the detailed investigations of different cases of nonlinear transport coefficients that fluctuating differential rotation is responsible for the infinite growth of magnetic field strength. The magnetic field strength is reduced by magnetic dissipation mechanisms such as  $\alpha$ -quenching and toroidal flux loss while poloidal flux loss helps generating the magnetic fields which can be seen in the results where its addition to  $\alpha$ -quenching and toroidal flux loss has helped increasing the growth of  $b$  and  $a$ . This further suggests that fluctuating differential rotation is necessary to balance the effects of shear-quenching caused by mean differential rotation. The scalings of  $p$ ,  $|B|$ , and  $|A|$  are found to be highly variable with  $\Omega$ , particularly for small  $\Omega$ . Therefore, we investigate the behavior of  $p$ ,  $|B|$ , and  $|A|$  as a function of  $\Omega$  by calculating the local scalings and by plotting them in Figs. 3.8(a-c). For different combinations of  $F_1$ ,  $F_2$ , and  $F_3$ , we plot the results using different colours/linestyles in Figs. 3.8(a-c). We denote the local scaling exponents of  $p$ ,  $|B|$ , and  $|A|$  as  $\xi_1$ ,  $\beta_1$ , and  $\gamma_1$ , respectively. Clearly, the change in local scalings of  $p$ ,  $|B|$ , and  $|A|$  becomes less variable for high-rotation  $\Omega \geq 5$  (cf. Figs. 3.8(a-c)).



(a)  $\xi_1$  as a function of  $\Omega$

(b)  $\gamma_1$  as a function of  $\Omega$

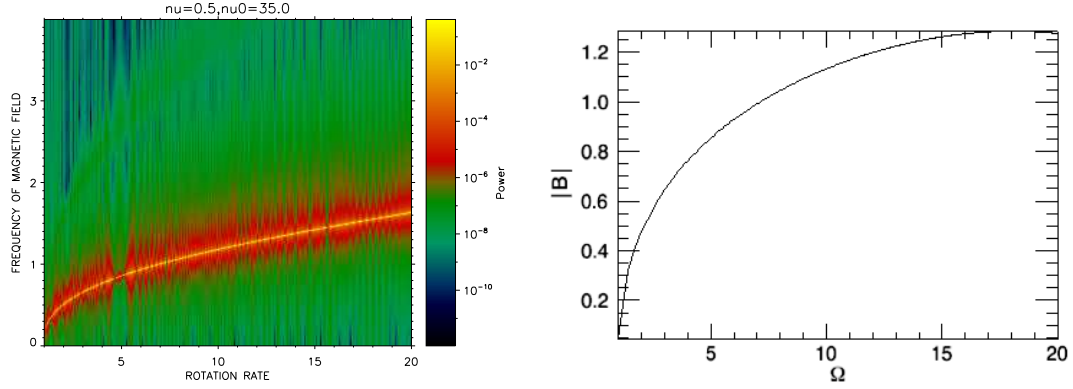


(c)  $\beta_1$  as a function of  $\Omega$

Figure 3.8: Local scalings  $\xi_1$  for  $p$ ,  $\gamma_1$  for  $|A|$ , and  $\beta_1$  for  $|B|$  are plotted as functions of rotation rate for different combinations of  $F_1$ ,  $F_2$ , and  $F_3$ , where for different combinations, different colours/linestyles are assigned as: for  $F_1 = F_2 = F_3 = F$  black/solid line,  $F_1 = F_2 = F, F_3 = 1$  green/dot,  $F_1 = F_3 = F, F_2 = 1$  gold/dash,  $F_1 = 1, F_2 = F, F_3 = F$  pink/dash dot,  $F_1 = F, F_2 = F_3 = 1$  turquoise/dash dot dot,  $F_1 = F_2 = 1, F_3 = F$  red/long dash,  $F_1 = F_3 = 1, F_2 = F$  turquoise/'+'.

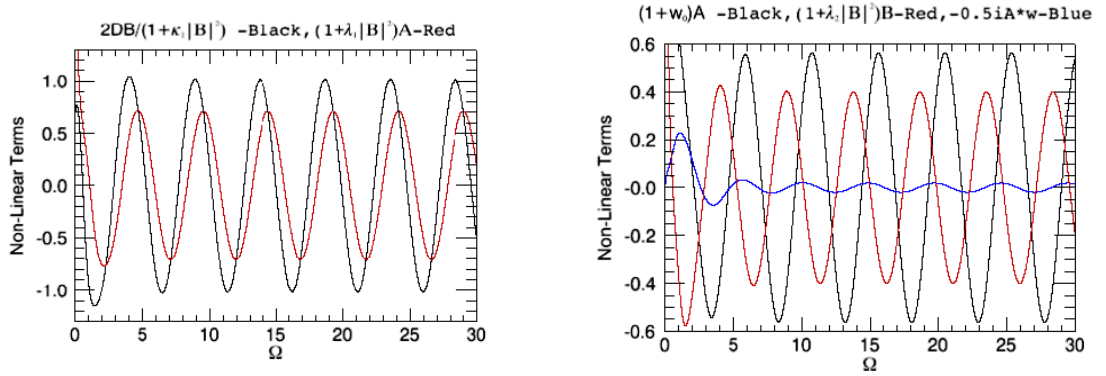
## 3.6 Self-regulatory behavior of seventh-order system

It is important to note that the cases considered in section 3.3-3.5 are not consistent with observations. In order to understand these observations, we have already numerically investigated seventh-order system represented by Eqs. (2.1)-(2.4) in Chapter 2. A thorough parameter study is performed by taking different choices of nonlinear transport coefficients as well as  $\nu = 1$  and  $\nu_0 = 35$ . The importance of dynamical balance among generation and destruction of magnetic fields is emphasised and dynamo is shown to work near marginal stability which leads to almost linear increase in frequency and flattening of magnetic field strength. It is also demonstrated that both mean and fluctuating differential rotation are necessary for the working of a dynamo and could be a manifestation of self-regulatory behaviour of magnetic fields and back reaction from Lorentz force. This regulatory behaviour of seventh-order system is demonstrated by investigating the balance among various effects of nonlinear transport coefficients and mean/fluctuating differential rotation by using  $\nu = 0.5$ . For the fixed value of  $D = 2$ , dynamical balance of nonlinear terms is depicted in Fig. 3.9(a-b). The balance between  $\alpha$ -quenching term and poloidal flux loss term (depicted in black and red color respectively) show that dissipation and generation of magnetic fields are balanced in this case. Further, the dissipation of magnetic fields is found to be double than the generation of magnetic fields for higher values of dynamo number. The toroidal flux loss (red color) is noticed to balance the poloidal magnetic field due to shear (black color). The detailed investigation of  $p$  and  $b$  as well as the dynamical balance among various terms thus highlight that mean and fluctuating differential rotations are required for the onset of dynamo near marginal stability.



(a)  $p$  as a function of rotation rate  $\Omega$ . (b) Magnetic field strength  $|B|$  as a function of rotation rate  $\Omega$ .

Figure 3.9: Frequency  $p$  of magnetic field and toroidal magnetic field  $|B|$  are plotted as a function of rotation rate  $\Omega$  for  $F_1 = F_2 = F_3 = F$  in case of the seventh-order system for  $\nu = 0.5$  and  $\nu_0 = 35.0$



(a) Dynamical balance between nonlinear terms on R.H.S. of Eq(1). (b) Dynamical balance between nonlinear terms on R.H.S. of Eq(2).

Figure 3.10: Time series of different nonlinear terms for  $F_1 = F_2 = F_3 = F$  in case of the seventh-order system for  $\nu = 0.5$  and  $\nu_0 = 35.0$

### 3.7 Conclusions

Upon conducting detailed study of nonlinear dynamo model in the presence of above mentioned limiting cases, it is found that in the absence of mean differential rotation and fluctuating differential rotation the system works near marginal stability. Linear growth of frequency, toroidal magnetic field and poloidal magnetic

field with respect to rotation rate agree with theoretical predictions of kinematic dynamo theory but shows no agreement with observations. Due to the back reaction of Lorentz force, there is a strong shear quenching in the presence of mean differential rotation which causes the shutting down of dynamo action even after adding the various nonlinear transport coefficients to the system. This further suggests that fluctuating differential rotation is required to diminish the effects of shear-quenching which is another indication of self-consistent behaviour of two differential rotations. Further, the indefinite growth of frequency, toroidal and poloidal magnetic field due to fluctuating differential rotation is slowed down without being saturated in the presence of various dynamo saturation mechanisms. These results highlight that a shear-quenching is required to balance the effect of fluctuating differential rotation. Thus we conclude from the results obtained for various combinations of nonlinear transport coefficients in the presence of mean and fluctuating differential rotations that the right amount of both differential rotations combined with different nonlinear transport coefficients is required for the working of a dynamo near marginal stability which itself is a signature of self-regulation of magnetic fields.

# Chapter 4

## Spindown of solar type stars

We propose a spin-down model where the loss of angular momentum by magnetic fields is dynamically treated, instead of being kinematically prescribed. To this end, we evolve stellar rotation and magnetic field simultaneously over the stellar evolution time by incorporating the nonlinear feedback mechanisms on rotation and magnetic fields and examine the behaviour of rotation rate,  $\Omega$ , with time,  $t$ , magnetic field strength,  $|B|$ , and frequency of magnetic field,  $\omega_{cyc}$ , with rotation rate,  $\Omega$ . Initially, rotation rate is found to decrease very rapidly with time until there is a sudden transition from fast to slow spin down of stars. The dependence of rotation rate on time illustrates exponential spin-down for rapid rotators and power law spin-down for slow rotators. For fast rotators, the strength,  $|B|$ , is found to saturate for large  $\Omega$  while for slow rotators,  $|B|$  increases almost linearly with  $\Omega$ . The analysis of the local frequency of magnetic fields reveals the existence of the two (active and inactive) branches of magnetic fields for stars with different frequencies  $\omega_{cyc}$  which have different scalings with rotation rate,  $\Omega$ : the active and inactive branches with power law scaling exponents 0.85 and 1.16, respectively. The transition from fast to slow rotators occurs very rapidly with the disappearance of the active branch. The Vaughan-Preston (V-P) gap is consistently explained in our model by the shortest spin-down timescale in this transition from fast to slow rotators. All these results successfully reproduce the key observations and capture the V-P gap in a self-contained model.



## 4.1 Introduction

Modelling the rotational evolution of stars is among the most difficult problems in astrophysics. Stellar angular momentum loss is assumed to play an important role in the spindown of stars but its origin and evolution is still an unresolved issue. With improved technical facilities over the years and availability of high resolution data, it is important to develop models which can provide an insight into the various observations such as rotation rate, magnetic activity and stellar spin-down etc. For the past few decades, a number of models have been developed to understand the rotational evolution of stars: double zone models (DZM)(MacGregor and Brenner, 1991; Keppens et al., 1995; Allain, 1998; Leprovost and Kim, 2010; Spada et al., 2011; Reiners and Mohanty, 2012; Gallet and Bouvier, 2013), symmetrical empirical model (SEM) (Barnes, 2010; Barnes and Kim, 2010) and metastable dynamo model (MDM)(Brown, 2014). Recently, Matt et al. (2015) proposed a stellar wind torque model which derives the dependence of stellar wind torque on the Rossby number.

Spindown of stars is a complex process as a star undergoes various internal changes since its birth, as a collapsing giant molecular cloud to pre-main sequence phase. We recall that during early pre-main sequence evolutionary stage, the young stars are fully convective and experience changes in their internal structure. When the star is in early protostar evolutionary phase, a thick stellar core is developed as a result of adiabatic contraction. This stellar core leads to the formation of radiative core due to various changes in the star. This radiative core rotates faster than convective envelope, and as a result, of strong coupling between core and envelope, rotation of convective envelope increases. In the whole process, there is a loss of angular momentum via stellar wind which gradually stops the spin up of convective envelope and a fast spin down starts as the star reaches the main sequence. It has been thought that the loss in angular momentum slows down the surface layers and a differential rotation is produced beneath

the outer convective zone. When this differential rotation is unstable, it can lead to turbulence which transports angular momentum between the interior and the convection zone.

Depending on the spindown process the stars are divided into two groups of Active (A) and Inactive (I) based upon a power law relationship between the cycle periods  $P_{cyc}$  of magnetic fields and rotation period  $P_{rot}$  of the stars (Brandenburg et al., 1998; Saar, 2002; Barnes, 2003). The power law dependence of cycle period on rotation period was first established by Noyes et al. (1984) as  $P_{cyc} \propto P_{rot}^n$  with a power law index  $n = 1.25 \pm 0.5$ . Further, Brandenburg et al. (1998) and Saar (2002) explained the existence of two branches, namely active and inactive with active branch consisting of rapidly rotating young stars with  $P_{cyc} \propto P_{rot}^{0.80}$  and inactive branch comprising of slow rotating old stars with  $P_{cyc} \propto P_{rot}^{1.15}$ . It is observed that magnetic activity is saturated for fast rotating young stars while it increases linearly with rotation for slow rotating old stars (Saar, 2002; Barnes, 2003; Pizzolato et al., 2003; Wright et al., 2011). The relationship of  $\Omega$  with  $t$  is also different for fast rotators and slow rotators. For fast rotators, there is an exponential dependence of  $\Omega$  on  $t$  as  $\Omega \propto e^{mt}$  where  $m$  is a negative constant. For slow rotators, a power law dependence of  $\Omega$  on  $t$  is observed, for instance, as  $\Omega \propto t^{-0.50}$  (Skumanich, 1972). The gap between active and inactive branch is known as Vaughan-Preston (V-P) gap which was first observed by Vaughan and Preston in 1980 in Mount Wilson Observatory (MWO). Various reasons have been proposed for the presence of this gap such as the possibility of different dynamos for two sequences, a change in morphology of magnetic field, change in character of convection, absence of radiative core causing the change in magnetic field generation, etc. (Durney et al., 1981; Scholz, 2009; Böhm-Vitense, 2007). Barnes (2003, 2010) has done notable work explaining the reasons for this gap between active and inactive branches and why the spindown timescale for the stars in the gap is much shorter than the time scale for stars in active sequence which itself is shorter than the time scale in case of inactive sequence.

In this Chapter we propose a new dynamical model of spindown by treating the evolution of magnetic fields and rotation on the same footing and successfully reproducing the key observations noted above. The remainder of this Chapter is organised as follows. We discuss our model in Section 4.2, results in section 4.3 and conclusions are summarised in section 4.4.

## 4.2 Model

We propose a dynamical model for the evolution of rotation rate and magnetic field in spindown by extending our nonlinear system mentioned in Chapter 2 by replacing  $D$  with time dependent  $\Omega^2$  in Eq. (2.5) (see Chapter 2, Section 2.2) and adding the equation of evolution for rotation rate in the system (2.5)-(2.8). Specifically, this extended model takes the following dimensionless form

$$\dot{A} = \frac{2\Omega^2 B}{1 + \kappa(|B|^2)} - [1 + \lambda_1(|B|^2)]A, \quad (4.1)$$

$$\dot{B} = i(1 + w_0)A - \frac{1}{2}iA^*w - [1 + \lambda_2(|B|^2)]B, \quad (4.2)$$

$$\dot{w}_0 = \frac{1}{2}i(A^*B - AB^*) - \nu_0 w_0, \quad (4.3)$$

$$\dot{w} = -iAB - \nu w, \quad (4.4)$$

$$\dot{\Omega} = -\varepsilon_1 |B|^2 \Omega - \varepsilon_2 \frac{|A|^2}{\Omega^2} \Omega. \quad (4.5)$$

Equations (4.1)-(4.4) are same as Eqs. (2.5) -(2.8) and are explained in detail in Section 2.2. Equation 4.5 represents the spindown of stars due to loss of angular momentum by magnetic field. The constant parameters  $\varepsilon_1$  and  $\varepsilon_2$  represent the efficiency of angular momentum loss<sup>1</sup> via toroidal and poloidal magnetic fields, respectively, as a result of magnetised stellar winds (Keppens et al. 1995). Here,  $|B|$  represents the strength of toroidal magnetic field and  $\frac{|A|}{\Omega}$  (the second term on R.H.S of Eq. 4.5) is the strength of poloidal magnetic field in physical units

<sup>1</sup>Effectively, the value of  $\varepsilon_1$  and  $\varepsilon_2$  determines the required total computation time to slow down the younger Sun rotating 30 times faster to the present solar rotation. We have confirmed that the values of these two constants have no effect on our results.

due to our non-dimensionalisation (see Sood & Kim 2013).

## 4.3 Results

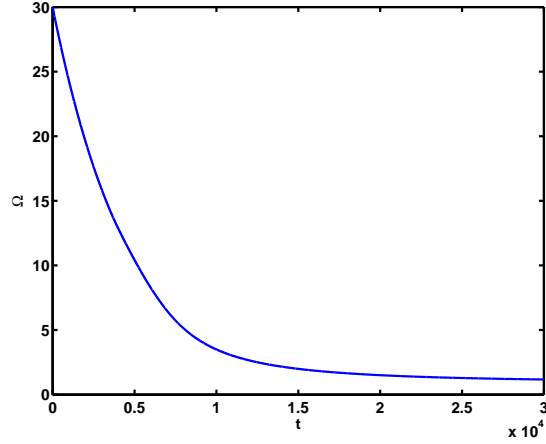
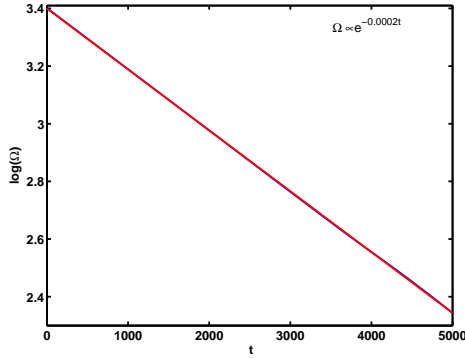
The system is investigated by taking  $\nu = 0.5$ ,  $\nu_0 = 35.0$ ,  $\kappa = 0.025$ ,  $\lambda_{1,2} = 1.125$  and  $\varepsilon_{1,2} = 0.000035$ . To model spindown, we take initial value of  $\Omega$  to be 30, which corresponds to the thirty times solar rotation ( $\Omega = 1$  at present in our non-dimensionalisation)

### 4.3.1 The $\Omega - t$ relationship

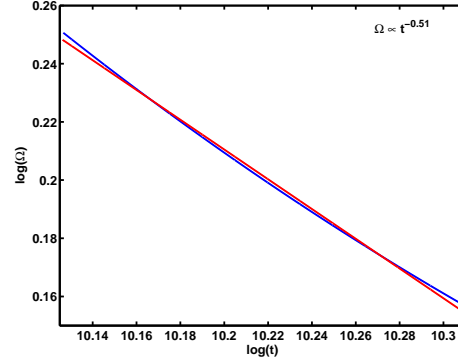
Figure 4.1(a-c) show the relationship between  $\Omega$  and  $t$ . A sharp decrease in  $\Omega$  can be seen for smaller time which slows down as time starts increasing (Fig. 4.1(a)). We fit this  $\Omega - t$  curve using exponential law, i.e.,  $\Omega \propto e^{mt}$ , where  $m$  is a negative exponential scaling exponent and power law, i.e.,  $\Omega \propto t^n$ , where  $n$  is the power law exponent. In Fig. 4.1(b), for smaller time (very high rotation rate) we obtain exponential fitting with scaling exponent  $m = -0.0002$  for rapidly rotating stars with rotation periods  $3 < P_{rot} \leq 1$ . For larger time we obtain power law scaling which varies for different rotation rates and decreases from -1.73 to -0.51. For larger time (slow rotation rate), the power law exponent  $n$  is found to be -0.51 for slow rotating stars with rotation periods in the range  $25.6 \leq P_{rot} < 23$  (see Fig 4.1(c)). For different rotation rates we summarise the scalings in Table (4.1).

Table 4.1: Power law exponent  $n$  for stars with different rotation period in days

$n$	$\Omega$	$P_{rot}(days)$
-1.73	$\Omega \in [5.8, 3.5]$	5.17 - 8.57
-1.38	$\Omega \in [3.5, 1.99]$	8.57- 15
-0.97	$\Omega \in [1.99, 1.50]$	15 - 20
-0.70	$\Omega \in [1.50, 1.28]$	20 - 23.4
-0.51	$\Omega \in [1.28, 1.17]$	23.4 - 25.6

(a)  $\Omega$  as a function of time

(b) exponential spindown



(c) power law spindown

Figure 4.1: Behaviour of rotation rate  $\Omega$  is shown as function of time.

### 4.3.2 The $|B| - \Omega$ relationship

The magnetic field strength,  $|B|$ , is shown as a function of rotation rate in Fig. 4.2(a-b). We note that  $|B|$  behaves differently for two different rotation rate regimes. For slow rotation rate regime, we can clearly see the increasing behavior of  $|B|$  with rotation rate which attains a maximum value at  $\Omega \approx 5.8$ . Interestingly, there is decrease in  $|B|$  which continues up to  $\Omega \simeq 12.5$ . For  $\Omega \geq 12.5$ , i.e., for very high rotation rate regime, we find a fluctuating behaviour (doubly periodic) of  $|B|$  for which time averaged value of maximum and minimum, depicted in red color, is noticed to become independent of rotation rate. These

fluctuations in  $|B|$  are due to the presence of two modes of  $|B|$  with different frequencies. The fluctuating behaviour of  $|B|$  with  $\Omega$  can be seen in Fig. 4.2(b) for a small cut of  $\Omega \in [23.30, 23.31]$  and clearly fluctuations are observed to be more rounded at the top while narrow at the bottom. That is, for rapid rotation  $|B|$  spends more time near the top as compared to near the bottom and therefore, the time averaged value of  $|B|$  is a bit higher than the average value of maximum and minimum (see Fig. 4.2(a)). Furthermore, we notice a gap between the two different rotation rate regimes in the region  $\Omega \in [5.8, 12.5]$ .

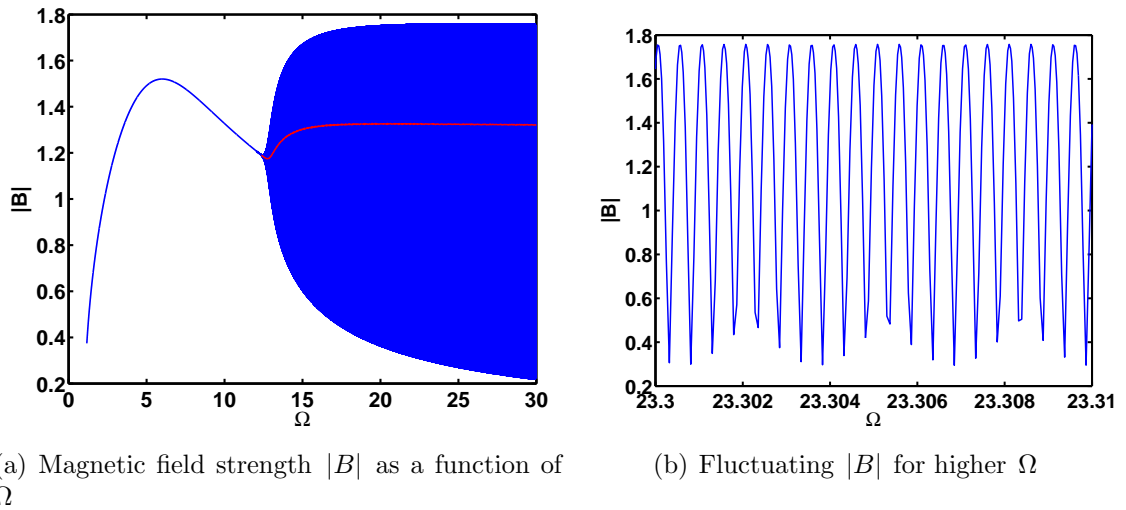


Figure 4.2: Magnetic field strength  $|B|$  is shown as a function of  $\Omega$ . Also, fluctuating behavior  $|B|$  for high rotation rate regime is shown for  $\Omega \in [23.30, 23.31]$

### 4.3.3 The Power spectra of $B$ and the $\omega_{cyc} - \Omega$ relationship

We use fast Fourier transforms (FFT) to analyse the time series of  $B$ . We divide the data in equal number of bins of size 150000 and use FFT for further investigations where time is computed using bin-size and time step. The power spectra of  $B$  is noted in Fig. 4.3(a-d) from high to slow rotation rate. Note that the plots in each subfigure are plotted in four rows and two columns and they must be seen in rows. The number written at the top of each plot represents the time for which power spectrum is obtained. In Fig 4.3(a), for the first row, there are

two subplots. We can clearly see that in case of smaller time there are two peaks of frequency followed by localised frequencies for the first subplot and the subsequent plot in the same row. Almost similar behavior can be seen for all subplots in second, third and fourth row of Fig. 4.3(a), respectively. We find that peaks gradually shift towards lower frequency as time increases. Figure 4.3(b-c) show the gradual shift of peaks towards lower frequency with increasing time. This behavior continues until we reach approximately 4200, beyond which the multiple peaks of frequency are found to diminish. For time  $\in [4200, 30000]$ , we find only a single peak of frequency (see Fig. 4.3(d)) which depicts time  $\in [4200, 4800]$ . The behavior of power spectra of  $B$  clearly shows that the second peak of frequency vanishes as time increases, that is, the rotation rate decreases.

We further use an advanced method to find FFT of the system using short time Fourier transforms (STFT) to show the behavior of localised frequency of maximum intensity with time and rotation rate, respectively. In the STFT technique, again, the magnetic field data is divided into equal chunks of 150000 and these chunks are overlapped to find the maximum intensity frequency of the magnetic field. We observe two branches of frequency of maximum intensity  $\omega_{cyc}$  (depicted in red color) with time (Fig. 4.4(a)). The upper line has larger amplitude of frequency (say  $\omega_{cyc}^A$ ) than the lower line (say  $\omega_{cyc}^I$ ), where the upper and the lower lines correspond to active and inactive branches of stars, respectively. We find a decreasing behavior of both branches of frequency of maximum intensity with time. It is interesting to see that the upper branch,  $\omega_{cyc}^A$ , vanishes near the time  $\simeq 4200$  and we are left with only the lower branch of frequency,  $\omega_{cyc}^I$ , which slowly decreases with time. Figure 4.4(b) depicts the behavior of frequency of maximum intensity,  $\omega_{cyc}$ , with rotation rate,  $\Omega$ . Again, we notice that for high rotation rate we have two branches of frequency whereas, for slow rotation rate we only have one branch of frequencies. We use the power law relationship, i.e.,  $\omega_{cyc}^A \propto \Omega^r$ , where  $r$  is the power law exponent for upper branch of frequency of maximum intensity and  $\omega_{cyc}^I \propto \Omega^q$ , where  $q$  is the scaling exponent for lower

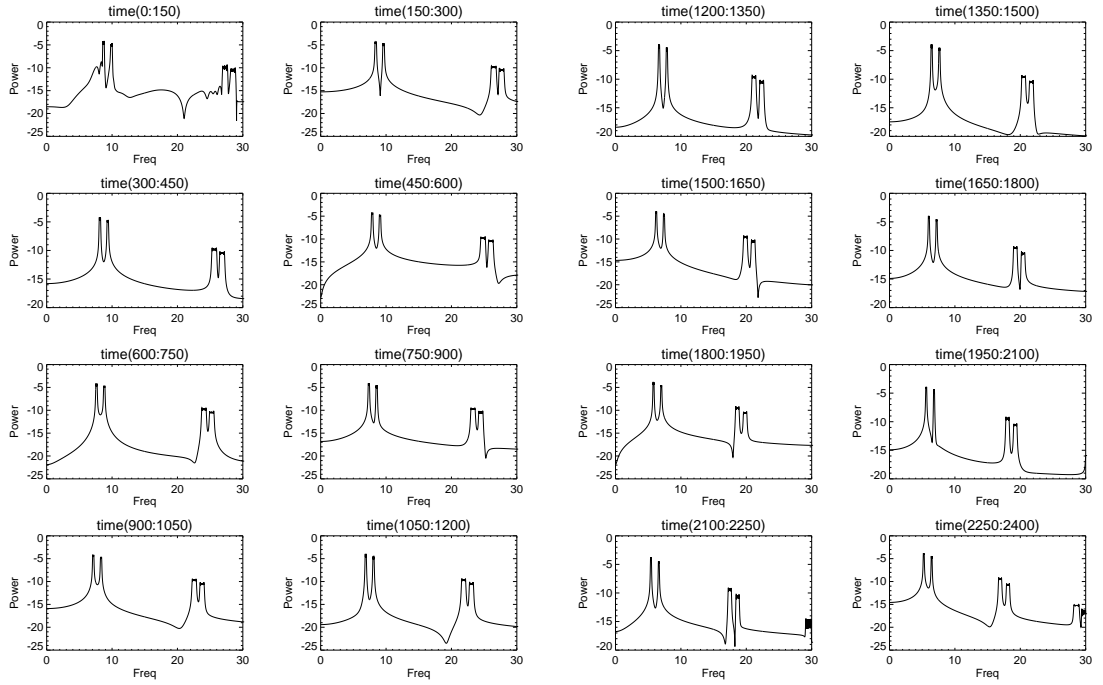
branch of frequency. We find the value of  $r = 0.85$  for stars with rotation periods  $1 \leq P_{rot} \leq 2$ , which is very close to the scaling exponent for stars in the active branch. It is noticed that the scaling exponent  $q$  of lower branch varies with rotation rate. It takes a value of 1.16 for Sun-like stars with rotation periods in the range [8.75, 25.6], which is in good agreement with observed scaling exponent for old Sun-like stars lying on the inactive branch. For different rotation rates we summarise the scalings for lower branch of frequency of maximum intensity in Fig. 4.4(b) with rotation rate  $\Omega$ , that is,  $\omega_{cyc}^I \propto \Omega^q$  in Table (4.2).

Table 4.2: Power law exponent  $q$  for lower branch of frequency  $\omega_{cyc}^I$  with rotation rate  $\Omega$  for stars with different rotation periods.

$q$	$\Omega$	$P_{rot}(days)$
1.16	$\Omega \in [1.17, 3.5]$	25.6 - 8.7
0.98	$\Omega \in [3.5, 6]$	8.7 - 5
0.80	$\Omega \in [6, 13]$	5 - 2.30
1.06	$\Omega \in [16, 30]$	1.88 - 1

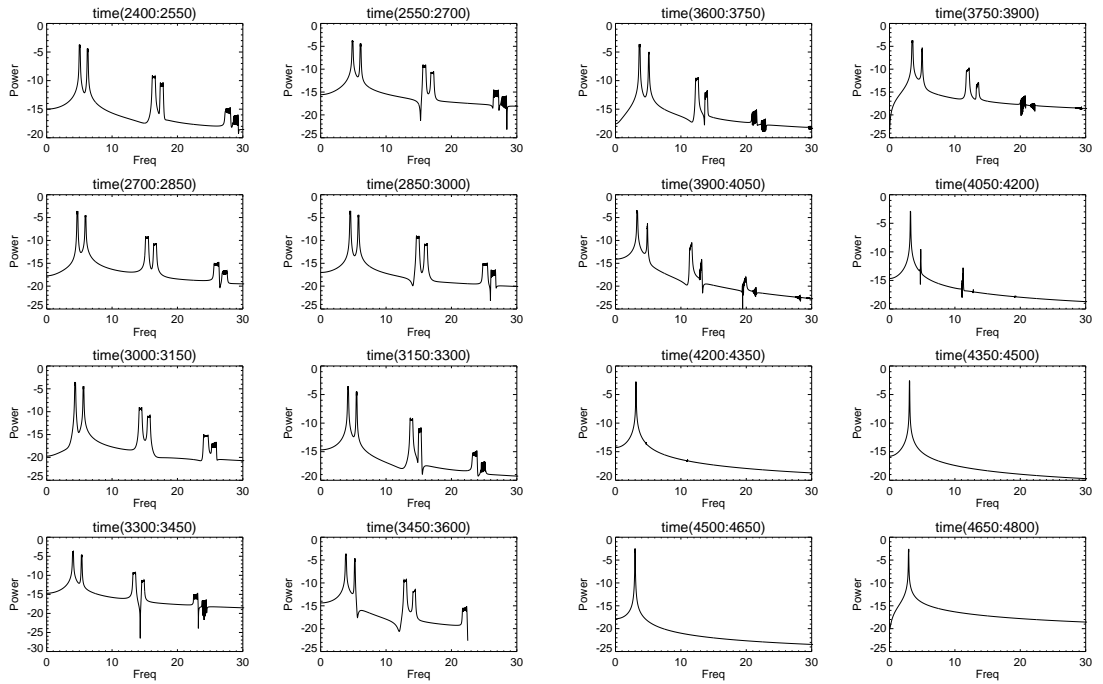
#### 4.3.4 The total shear - $\Omega$ relationship

In our dimensionless unit, the total shear is given by  $1 + w_0$ . We present how this quantity changes with rotation rate  $\Omega$  in Fig. 4.5. As  $\Omega$  increases from  $\Omega = 1$ , the total shear is seen to decrease by 90% from 1 to 0.1 with increasing  $\Omega$ . This reduction in total shear results from the effect of magnetic back-reaction on the shear. The saturation of the total shear for high rotation indicates that the dynamo efficiency is not saturated beyond certain rotation rate. After taking the minimum value around  $\Omega = 12.5$ , the total shear increases with  $\Omega$  in a small interval  $\Omega \in [12.5, 17]$  and then remains almost constant for high rotation rate  $\Omega \geq 17$ . It is important to note that the apparently broad band of the total shear for  $\Omega \geq 12.5$  in Fig. 4.5 is due to the two different modes with different frequencies existing in this interval. The inset in Fig. 4.5 shows the total shear for a small range of  $\Omega \in [29.82, 29.84]$  to highlight the fluctuation in total shear due to the two modes. Finally, the  $\Omega = 12.5$  value where the total shear takes its



(a)

(b)



(c)

(d)

Figure 4.3: Power spectra of magnetic field  $B$  is shown as a function of frequency.

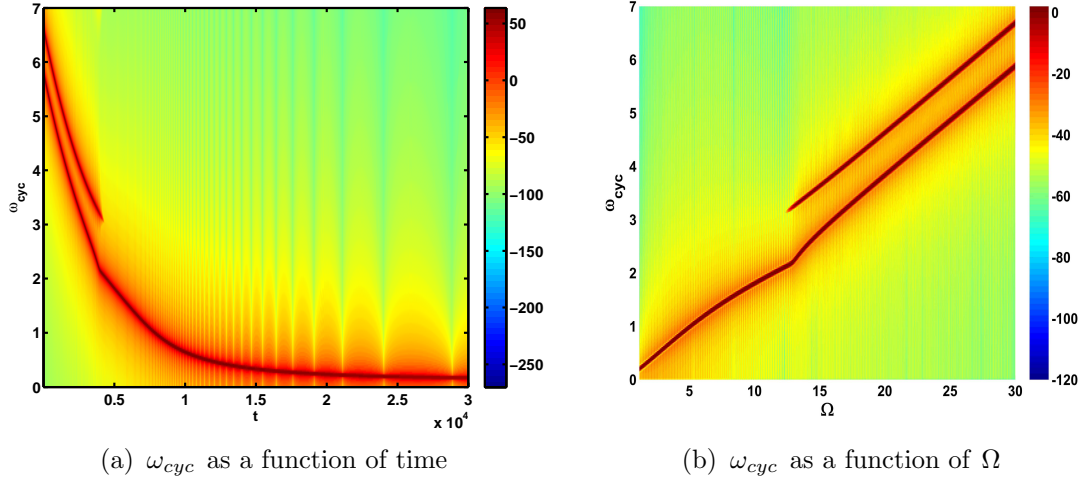


Figure 4.4: Frequency of maximum intensity  $\omega_{cyc}$ , as a function of time and rotation rate, respectively.

minimum value and is related to a very rapid transition in rotational evolution and is related to the V-P gap as shall be discussed later.

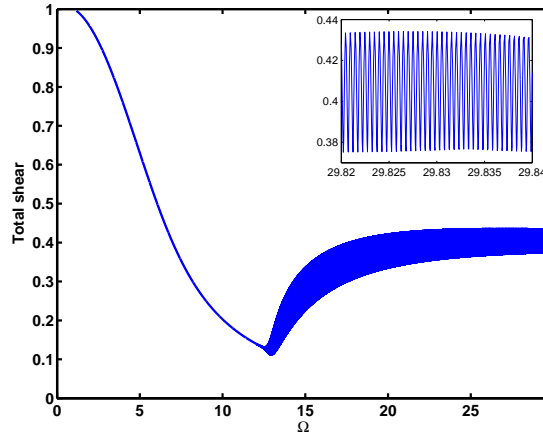


Figure 4.5: Total shear  $1 + w_0$  as a function of rotation rate  $\Omega$ .

### 4.3.5 The $|B|$ - Age Relationship

Figure 4.6(a) depicts the behavior of magnetic field strength,  $|B|$ , with dimensionless time. We find that  $|B|$  is fluctuating (doubly periodic) for time up to  $t \approx 4200$  followed by an increasing behavior until it attains a maximum value

around 7313. After this  $|B|$  is found to decrease with time. In Fig. 4.6(b) the magnetic field strength is shown as a function of age where we have presented the age on  $x$ -axis in physical units by scaling our dimensionless time by the age of present Sun of  $4 \times 10^9$  years with initial age of  $3 \times 10^7$  years. The magnetic field strength  $|B|$  is observed to maintain almost the same mean value fluctuating with finite amplitude for very young fast rotating stars of age up to 590 Myrs (Mega years). This fluctuation is due to the presence of two different modes, as is discussed in subsection (4.3.1). The magnetic activity is noticed to increase with age in the range  $\in [590, 830]$  Myrs as  $|B| \sim t^s$  with a power law exponent  $s = 0.53$ , after which the magnetic activity remains almost constant in the age interval  $\in [830, 1100]$  Myrs. Beyond this value the magnetic activity decreases very rapidly with increasing age. We find that the power law exponent,  $s$ , varies with different values for stars with different ages and are provided in Table (4.3). This decrease in magnetic activity becomes steeper as the star ages and is in good agreement with observations carried out by Pace et al. (2009). In their observational analysis of a sample of almost 40 stars, which includes Hyades and Praesepe (both 0.7 Gyrs) along with five open clusters IC4756, NGC5822, NGC 3680, IC4651, and M67 with ages 1.2, 1.4, 1.7 and 4.3 in Gyrs, respectively, they concluded that after 700 Myrs there is no correlation between magnetic activity and age. They also observed a rapid transition from active to inactive branch between the ages of 1.2 Gyrs to 1.4 Gyrs with a fast drop in magnetic activity between these ages. It is imperative to highlight that the sample size studied in above mentioned observations is very small and Pace et al. (2009) have particularly emphasised that owing to the small sample size and the method of calculating the ages of the stars, high end observations of larger sample size are required for accurate results (Pace, 2010).

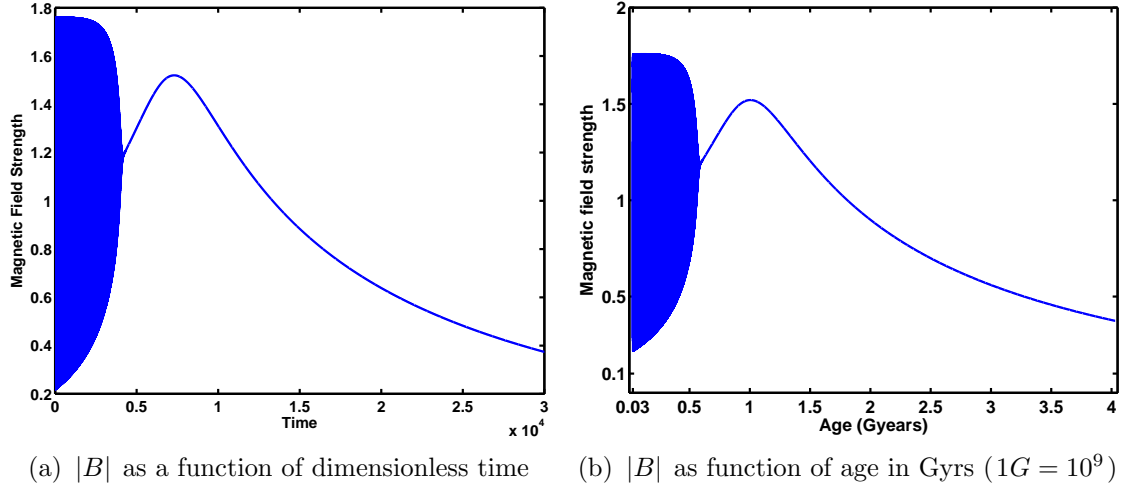


Figure 4.6: Magnetic field strength  $|B|$  is shown as function of dimensionless time in (a) while (b) depicts the magnetic field strength as a function of age in physical units by scaling the  $x$ -axis with age of the Sun.

Table 4.3: Power law exponent  $s$  for magnetic activity with age  $t$  of stars  $\in [1.066, 4]Gyrs$

$s$	Age (Gyrs)
-0.61	$t \in [1.100, 1.363]$
-0.97	$t \in [1.363, 2.030]$
-1.13	$t \in [2.030, 2.697]$
-1.25	$t \in [2.697, 3.364]$
-1.40	$t \in [3.364, 4.03]$

### 4.3.6 The time-scale for spindown

In order to quantify the time scale of spindown, we numerically compute the characteristic spindown time,  $\tau = |\Omega/\partial_t\Omega|$ , by using Eq. (4.5) as we evolve the system, and then show the suitable averaged value in Fig. 4.7(a) and Fig. 4.7(b) by using linear and log scales, respectively. The time on the  $x$ -axis is given in physical time unit by scaling our dimensionless time<sup>1</sup> by the age of present Sun of  $4 \times 10^9$  years. In Fig. 4.7(a), red color depicts the mean value<sup>2</sup> of timescale over time. Clearly, we observe a spindown timescale of 300 Mega years (Myrs) for very

<sup>2</sup>This mean value is obtained over the  $\frac{1}{420}$  fraction of the interval.

young fast rotating stars of ages from 30 Myrs to 590 Myrs approximately, beyond which the spindown timescale decreases with increasing age for a short interval [590, 900]. This decline in spindown time reaches a minimum of approximately 233 Myrs for age 900 Myrs. After this, the spindown timescale starts increasing with the age of the stars. Specifically, the spindown timescale increases linearly for solar type stars with ages approximately 4 Giga years (Gyrs). The shortest spindown timescale is obtained in the region [590, 1100] Myrs ( $\Omega \in [5.8, 12.5]$ ) noted previously, and interestingly corresponds to V-P gap, transition region between fast and slow rotators, i.e., this is the region where a star suddenly jumps from active to inactive branch staying for a short timescale due to the fast spin down. To summarise, our results show that the spindown time for fast rotating stars in that region is shorter than the spindown time for slow rotating stars while the spindown timescale for stars in the transition region is even much shorter than the spindown timescale for fast rotating stars. These results are in good agreement with observations for spindown timescale (Barnes, 2003).

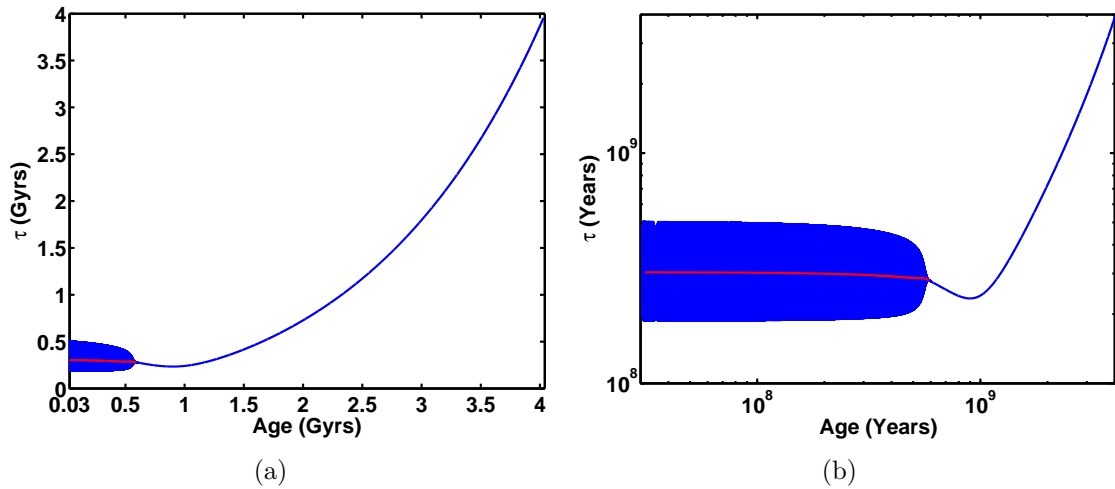


Figure 4.7: Spindown timescale as function of age in Gyrs ( $1G = 10^9$ ) depicted in linear- and log-scale respectively.

### 4.3.7 Summary of results

Investigations of  $\Omega - t$ ,  $|B|$ ,  $\omega_{cyc}$ ,  $1 + w_0$ , with  $\Omega$ , magnetic activity and spindown timescale with age show that all the results are consistent with observations for spindown process for fast and slow rotating stars, respectively. Abrupt transition of stars from active ( $A$ ) to inactive branch ( $I$ ) and its underlying physics are still an unsolved issue. There have been different reasons proposed to explain the exponential spindown for fast rotators and power law spindown for slow rotators, for instance, as a consequence of changes in dynamo due to various nonlinear transport coefficients. During most of the pre-main sequence evolution, the changing internal structure of star dominates other effects and star spins up to become differentially rotating object (Keppens et al., 1995). This differential rotation produced beneath the outer convection zone leads to mild turbulent diffusion and an angular momentum is transported from interior to the outer convection zone. For rapidly rotating stars the convection zone is not large and stellar layers are not very deep where dynamo operates (Böhm-Vitense, 2007). Since the star is differentially rotating, it experiences back reaction of shear produced by Lorentz force and  $\alpha$ -effect is quenched as a result of rapid rotation. Thus, the growth of magnetic field is inhibited by various transport coefficients and dynamo action is saturated for rapid rotators. In the case of slow rotating old stars there are deeper surface layers and large convection zones where the magnetic field strength produced is strong enough to sustain its linear growth against rotation rate despite the back reaction of shear and other quenching mechanisms. Even without incorporating these other effects, our dynamical model coupled to spindown successfully captures the V-P gap.

## 4.4 Conclusions

We investigate a dynamical model of dynamo and rotation for spindown. The motivation of our work stems from the idea that the generation of magnetic field

and spindown are closely inter-linked processes, i.e., the generation of magnetic fields depends on rotation of stars and, thus spindown, while spindown process crucially depends upon the magnetic field (e.g. generation, destruction) and differential rotation. For the first time our model evolves magnetic field and rotation rate in spindown at the same time by taking into account various feedback mechanisms that are important in generation and destruction of magnetic fields during the spindown of stars.

We have already mentioned the importance of nonlinear transport coefficients in the evolution of magnetic field and self-regulation of dynamo (Sood and Kim, 2013, 2014). Based upon our previous results and recent investigations we provide an explanation for linear increase of magnetic field strength in case of slow rotating stars and flattening of magnetic field strength in case of fast rotating stars. These nonlinear transport coefficients capture the effect of generation and destruction of magnetic fields and control the growth of magnetic field strength for higher rotation rate. Strong shear quenching in our model is also responsible for inhibition of magnetic fields. We note that evolution of magnetic fields and rotation rate is a self-regulated process which depends upon various internal and structural changes during star formation. Shear is thought to produce among the layers for stars with developed radiative cores which causes the generation of large scale magnetic fields essential for dynamo action (Barnes, 2003). Fast rotating stars being fully convective have weak differential rotation dependence on rotation rate (Donati and Collier Cameron, 1997) and an unstable magnetic field is produced beneath the surface layers which does not sustain a linear dynamo or in other words, dynamo is saturated.

Despite being a simple parameterised model our working framework successfully reproduces the observations for spindown of stars which cannot be explained by full 3D MHD simulations. In particular, we have found exponential spindown, saturation of magnetic field strength and power law dependence of frequency of magnetic fields of active and inactive branches for rapidly rotating stars. For

slow rotators, we obtained power law spindown, linear increase of magnetic field strength and power law relationship of  $\omega_{cyc}$  on  $\Omega$  with power law scaling 1.16 for inactive branch. The transition from fast to slow rotating stars is quantitatively shown to occur very rapidly, thereby providing an explanation for the V-P gap.

# Chapter 5

## Regulation of kinematic dynamo by shear flow

Magnetic fields and shear flows play an important role in many systems including astrophysical, geophysical and laboratory plasmas. Here we investigate how the growth of magnetic fields is modified by large-scale shear flow by investigating a kinematic dynamo in a spherical shell of highly conducting fluid surrounded by an insulator. A small scale prescribed velocity field is taken to be axisymmetric, steady and strongly helical. Small-scale flow is chosen in such a way that it allows the dipole/quadrupole decoupling for magnetic field  $\mathbf{B}$ . On the other hand, large-scale shear flows are taken to be in radial or latitudinal directions. By numerically solving the induction equation with the prescribed small-scale flow and large-scale shear flow, we investigate the effects of large scale shear on dynamo for different azimuthal  $m$  modes for large magnetic Reynolds number  $R_m$  such as the growth rate and structures of magnetic field  $\mathbf{B}$ . In all the cases, the growth rate of the magnetic field is found to decrease as the strength of shear flow increases, which indicates that the dynamo is suppressed in the presence of shear.



## 5.1 Introduction

Sun and stars possess small scale and large scale magnetic fields maintained by the inductive motion of conducting fluid known as dynamo process (Parker, 1955). This dynamo process is thought to produce the magnetic activity cycle of 11 years and generation of sunspots at the surface of the Sun. Theoretically, the dynamo process is categorised in two regimes: linear and nonlinear. In linear regime the induction equation is solved in the presence of prescribed velocity field such that the magnetic field is very small as compared to the velocity field and does not alter the flow. The dynamos studied in this framework are known as kinematic dynamos. The kinematic theory is no longer valid if the magnetic field becomes strong enough to alter the velocity field and the Lorentz force acts back on the velocity field and induction then becomes nonlinear. These types of dynamos are known as nonlinear dynamos. Due to the complex nature of the equation and being computationally expensive in time, generally the induction equation is solved in the framework of kinematic dynamo theory. Further, dynamos are divided into two categories namely large scale and small scale dynamos. For large scale dynamos the flows are chosen to be large scale, i.e., the fields are evolved on large scale by averaging and considering the mean part of the governing equations, specifically, the induction equation and are known as mean field dynamos. To study small scale dynamos, the flows are chosen to be small scale and these type of dynamos work under fully isotropic conditions. Small scale or fluctuating dynamos play a crucial role in understanding of the fundamental physical processes in astrophysical bodies as these are common to random flows in conducting fluid (Brandenburg and Subramanian, 2005). Small scale dynamos could be fast or slow depending upon the nature of the growth rate of magnetic field with magnetic Reynolds number (Childress and Gilbert, 1995). A small scale dynamo is assumed to be fast dynamo if the growth rate of the magnetic field becomes constant for large  $R_m$ , that is, advection dominates the process, otherwise, a

small scale dynamo is considered to be a slow dynamo.

It is revealed through high end observations that shear is produced in the base of convection zone near tachocline and is the main ingredient in the working of a solar dynamo. In traditional  $\alpha$ - $\Omega$  dynamo theory, shear is believed to play an important role for the generation of toroidal field from poloidal field whereas helicity is thought to produce poloidal field from toroidal field (Moffatt, 1978). Dynamo action in the presence of shear is investigated numerically in a number of studies (Yousef et al., 2008a,b; Käpylä and Brandenburg, 2009; Hughes and Proctor, 2009, 2013; Heinemann et al., 2011; Mitra and Brandenburg, 2012; Proctor and Hughes, 2011) indicating that the presence of shear enhances the growth rate of large scale magnetic field which helps in the working of a dynamo. However, theoretical studies, by taking a stable shear flow parallel to the large scale magnetic field (Leprovoist and Kim, 2008) and by considering no direct interaction of large scale shear with magnetic field in kinematic limit without backreacting on the velocity field (Leprovoist and Kim, 2009), predict the quenching of  $\alpha$  effect and other turbulent transport coefficients. Recently, Tobias and Cattaneo (2013) considered interaction between helical flow and shear, and observed that shear reduces the generation of magnetic fields at small scale instead of enhancing the generation of magnetic fields at large scale.

Most of the numerical studies noted above are carried out in the periodic box domain by imposing uniform shear in the presence of different set of conditions such as forced helical/nonhelical turbulence (Yousef et al., 2008a,b). Our investigations of dynamo action in spherical shell are more realistic and relevant to the astrophysical bodies, specifically, the Sun and helps us to provide valuable insight in the working of dynamo. Previously, the dynamo action in spherical shell by taking small scale flows has been studied by Hollerbach et al. (1995) which turns out to be a fast dynamo. Transition from large scale to small scale dynamos in spherical geometry was investigated by Richardson et al. (2012). We know that a large scale radial shear is produced at the base of solar convection zone and a

strong latitudinal shear also works at the same time. Therefore, it is compelling to investigate the effect of large scale radial and latitudinal shear on small scale flows in spherical geometry to enhance the understanding of how large scale shear effects the properties of small scale flows.

The remainder of the chapter is arranged as follows. In Section 5.2 we discuss the mathematical formulation of the problem and governing equations. Section 5.3 discusses the results obtained from numerical simulations followed by conclusions in Section 5.4.

## 5.2 Governing Equations

In the framework of kinematic dynamo theory, we solve induction equation

$$\frac{\partial \mathbf{B}}{\partial t} = \nabla \times (\mathbf{u}_t \times \mathbf{B}) + R_m^{-1} \nabla^2 \mathbf{B}, \quad (5.1)$$

in a spherical shell where  $R_m$  represents magnetic Reynolds number and is defined as  $R_m = UL/\eta$ . Here,  $U$  is the characteristic velocity scale,  $\eta$  is the magnetic diffusivity and  $L$  is the characteristic length scale equivalent to the radius of shell. The prescribed velocity field,  $\mathbf{u}_t$ , is axisymmetric and is chosen in such a way that we have small scale cells separated by large scale.

$$\mathbf{u}_t = v_t \hat{\mathbf{e}}_\varphi + \nabla \times (\psi_s \hat{\mathbf{e}}_\varphi). \quad (5.2)$$

Here  $v_t$  represents the zonal flow,  $\psi_s$  represents the meridional circulation and  $\hat{\mathbf{e}}_\varphi$  is the unit vector in azimuthal direction. The nature of flow is steady and strongly helical such that the cells are like Roberts flow near equator (Roberts, 1970, 1972). The total zonal flow is given by

$$v_t = v_s + S_p r \sin \theta v_l, \quad (5.3)$$

where,  $v_s$  is the small scale velocity field similar to Richardson et al. (2012)<sup>1</sup> represents large scale shear in the azimuthal direction and  $S_p$  is the shear strength of large scale shear. Here

$$v_s = \sin \left( \frac{(r - r_i)}{(r_o - r_i)} N_r \pi \right) \sin \theta \cos(N_\theta \theta), \quad (5.4)$$

$$v_t = \begin{cases} (r - 0.75), \text{ is the radial shear,} \\ (\cos^2 \theta - 0.5), \text{ is the latitudinal shear,} \end{cases} \quad (5.5)$$

$\psi_s$  is the small scale meridional circulation

$$\psi_s = \frac{1}{N_\theta} r \cos \theta \sin \left( \frac{(r - r_i)}{(r_o - r_i)} N_r \pi \right) \sin \theta \cos(N_\theta \theta), \quad (5.6)$$

Here,  $v_s$  has equatorial symmetry whereas the factor of  $\cos \theta$  in  $\psi_s$  changes the equatorial symmetry of  $\psi_s$  to be opposite of  $v_s$ . Hence, we have dipole/quadrupole decoupling for  $B$ . In addition,  $r_i$  and  $r_o$  are the inner boundary and outer boundary of the shell, respectively.  $N_\theta = 4N_r$ , where  $N_r$  and  $N_\theta$  are the number of cells in  $r$  and  $\theta$ , respectively. Therefore, we investigate two flows in the current simulations: Flow1 and Flow2. Flow1 is the small scale flow in the presence of large scale radial shear and equation is given as

$$\mathbf{u}_t = (v_s + S_p r \sin \theta (r - 0.75)) \hat{\mathbf{e}}_\varphi + \nabla \times (\psi_s \hat{\mathbf{e}}_\varphi). \quad (5.7)$$

Flow2 is the small scale flow in the presence of large scale latitudinal shear with equation of the flow noted as

$$\mathbf{u}_t = (v_s + S_p r \sin \theta (\cos^2 \theta - 0.5)) \hat{\mathbf{e}}_\varphi + \nabla \times (\psi_s \hat{\mathbf{e}}_\varphi). \quad (5.8)$$

---

<sup>1</sup>Our  $v_s$  is similar to Richardson et al. (2012) but  $\psi_s$  has an extra term of  $\cos \theta$  so that  $\psi_s$  has opposite symmetry to  $v_s$ .

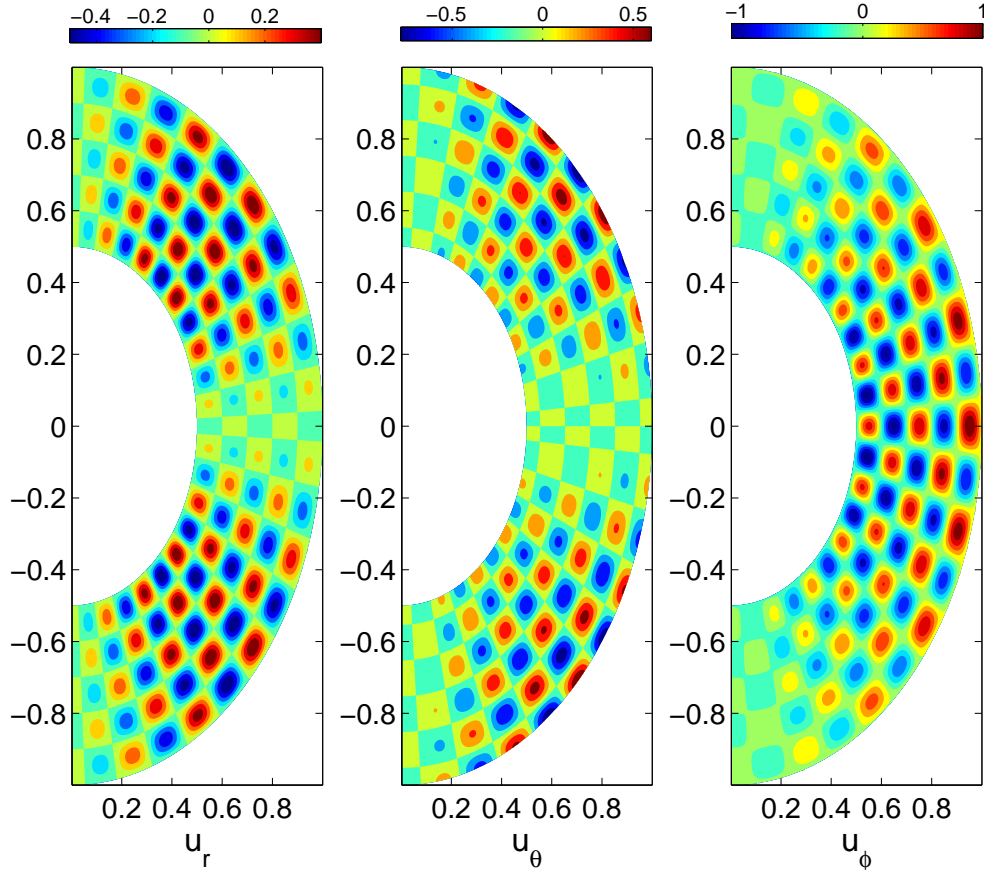


Figure 5.1: Here we represent the dimensionless velocity components  $u_r$ ,  $u_\theta$  and  $u_\phi$  of the flow in the presence of radial shear in azimuthal direction depicted in first, middle and last panel, respectively. Clearly,  $u_r$  is symmetric,  $u_\theta$  is antisymmetric while  $u_\phi$  is symmetric.

We use the spherical-shell MHD code described by Hollerbach (2000) to investigate the above flows numerically. The brief details of the code are noted here. This code solves the induction equation in kinematic regime for axisymmetric velocity field by decomposing the magnetic field into its poloidal and toroidal components such that  $\mathbf{B} \propto \exp(im\phi)$  where  $m \neq 0$ . The decomposition of the magnetic field in toroidal and poloidal components is given as:

$$\mathbf{B} = \nabla \times g\hat{\mathbf{e}}_r + \nabla \times \nabla \times h\hat{\mathbf{e}}_r, \quad (5.9)$$

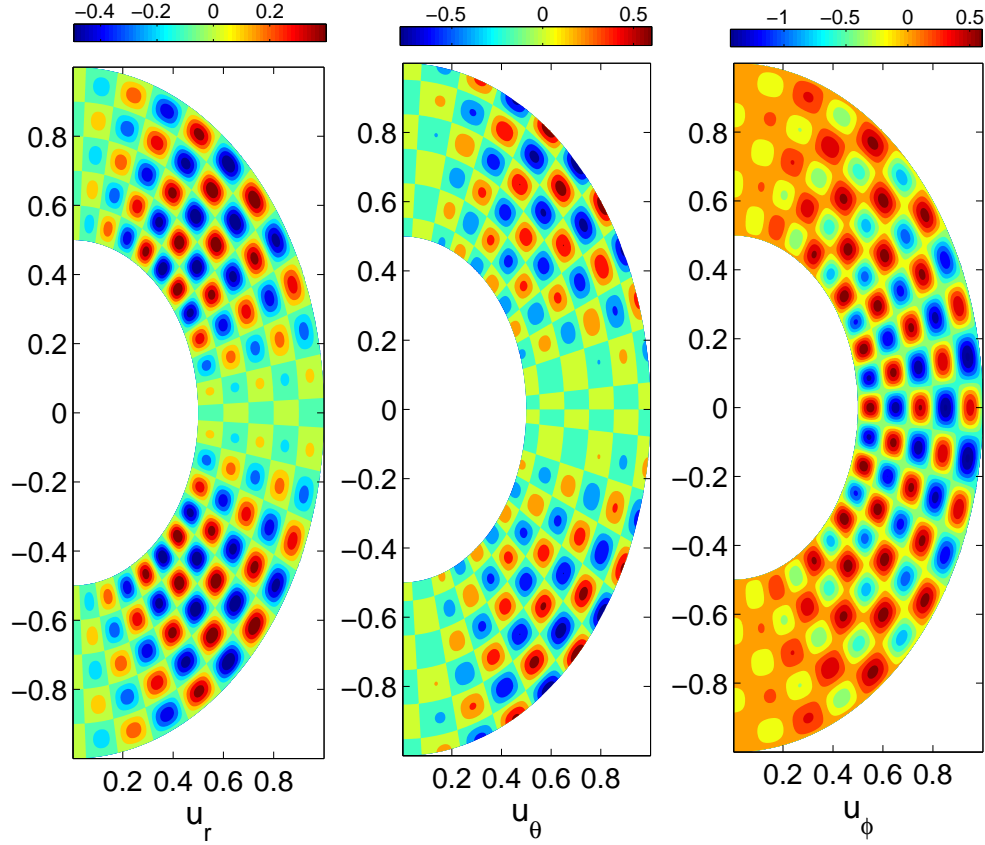


Figure 5.2: Here we represent the dimensionless velocity components  $u_r$ ,  $u_\theta$  and  $u_\varphi$  of the flow in the presence of latitudinal shear in azimuthal direction illustrated in first, middle and last panel, respectively. Clearly,  $u_r$  is symmetric,  $u_\theta$  is antisymmetric while  $u_\varphi$  is symmetric.

where  $g$  and  $h$  are the toroidal and poloidal scalar fields, respectively and  $\hat{\mathbf{e}}_r$  is the unit vector in radial direction. Further, the toroidal and poloidal parts of the magnetic field are expanded in their spectral coefficients such as Legendre function in  $\theta$  and Fourier expansion in  $\varphi$  as follows:

$$g = \sum_{l=m}^{L_{max}} g_{lm}(r) P_l^m(\cos \theta) \exp(im\varphi), \quad (5.10)$$

$$h = \sum_{l=m}^{L_{max}} h_{lm}(r) P_l^m(\cos \theta) \exp(im\varphi), \quad (5.11)$$

where  $m$  is fixed and  $L_{max}$  represents the largest value of  $l$  for which the sums are truncated. The radial structures of  $g$  and  $h$  are expanded in Chebyshev polynomial series with maximum Chebyshev collocation point  $K_{max}$ . Since the shell is fully conducting, the inner and outer regions of the shell are considered to be insulating with boundary condition

$$\begin{aligned}
 g_{lm} = 0 & \quad \left( \frac{\partial}{\partial r} - \frac{l+1}{r} \right) h_{lm} = 0, & \text{for } r = r_i, \\
 g_{lm} = 0 & \quad \left( \frac{\partial}{\partial r} - \frac{l}{r} \right) h_{lm} = 0, & \text{for } r = r_o.
 \end{aligned}$$

The inner boundary of the shell is  $r_i = 0.5$  and outer boundary of the shell is  $r_o = 1$ , which are in dimensionless units with characteristic lengthscale  $L$ , considered to be the radius of the shell.

## 5.3 Results

In this section we summarise the results from the numerical simulation for two flows, i.e., in the presence of radial shear and latitudinal shear. For  $(N_r, N_\theta) = (5, 20)$ , the numerical simulations are performed by varying the magnetic Reynolds number from  $R_m \in [100, 10000]$  and  $m \in [1, 50]$  with times step  $dt = 0.002$ ,  $K_{max} = 180$  and  $L_{max} = 360$ . For  $(N_r, N_\theta) = (10, 40)$ , we have carried out the numerical simulations by varying  $R_m$  in same range as above, with  $m \in [1, 20]$ ,  $dt = 0.001$ ,  $K_{max} = 300$  and  $L_{max} = 360$ .

### 5.3.1 Growth rate as a function of $R_m$

This section studies the growth rates evaluated in terms of eigenmodes as a function of magnetic Reynolds number,  $R_m$ , for  $(N_r, N_\theta) = (5, 20)$  and  $(N_r, N_\theta) = (10, 40)$ , respectively, for different  $m$  modes by considering the velocity field in the absence/presence of shear. First, we study the behavior of growth rate for  $(N_r, N_\theta) = (5, 20)$  in Fig. 5.3 in the absence of shear flow by taking  $R_m$  on

logarithmic scale. The growth rates are found to increase initially showing the onset of the dynamo for small  $R_m$ . After attaining a maximum value for a critical magnetic Reynolds number  $R_{mc}$ , the growth rates are observed to decrease with increasing  $R_m$  in Fig. 5.3(a) indicating a slow dynamo.  $m = 10$  is noticed to be the most excited mode in this case beyond which peak amplitude of the growth rate starts decreasing with increasing the  $m$  value. Addition of radial (Flow1) or latitudinal shear (Flow2) in the flow shows almost similar behavior of growth rates with  $R_m$  and can be seen in Fig. 5.3(b-c) for shear strength 3, i.e., the amplitude of growth rate is reduced in the presence of both shears, however, latitudinal shear is found to suppress the growth rates more as compared to radial shear. Modes with  $m = 15, 20$  are the most excited modes in case of Flow1 and Flow2 which ensures that if we further increase the value of  $m$ , it will show a decline in the amplitude of the growth rate. Almost similar results are obtained for  $(N_r, N_\theta) = (10, 40)$  in the absence/presence of shear (see Fig.5.4(a-c)). Therefore, we conclude that presence of the large scale shear suppresses the small scale flows depicting the quenching of dynamo.

### 5.3.2 Growth rates with shear strength

Here, we study the behavior of growth rates with shear strength (Fig. 5.5(a-b)) for  $N_r = 5, 10$ , respectively, with fixed  $R_m = 1000$  and fixed modes  $m = 5, 10$  in case of Flow1 and Flow2. Clearly, the amplitude of growth rate is observed to decrease with shear strength in both flows for  $N_r = 5$  for mode  $m = 5$  and  $m = 10$  in Fig. 5.5(a), when the shear strength is increased in positive or negative direction. Similar results have been obtained in case of  $N_r = 10$  (cf. Fig. 5.5(b)), i.e., the growth rate is found to decrease in the case of increasing shear strength. This trend indicates that the small scale flows are suppressed with increased shear parameter in the presence of large scale radial and latitudinal shear in the direction of azimuthal velocity field.

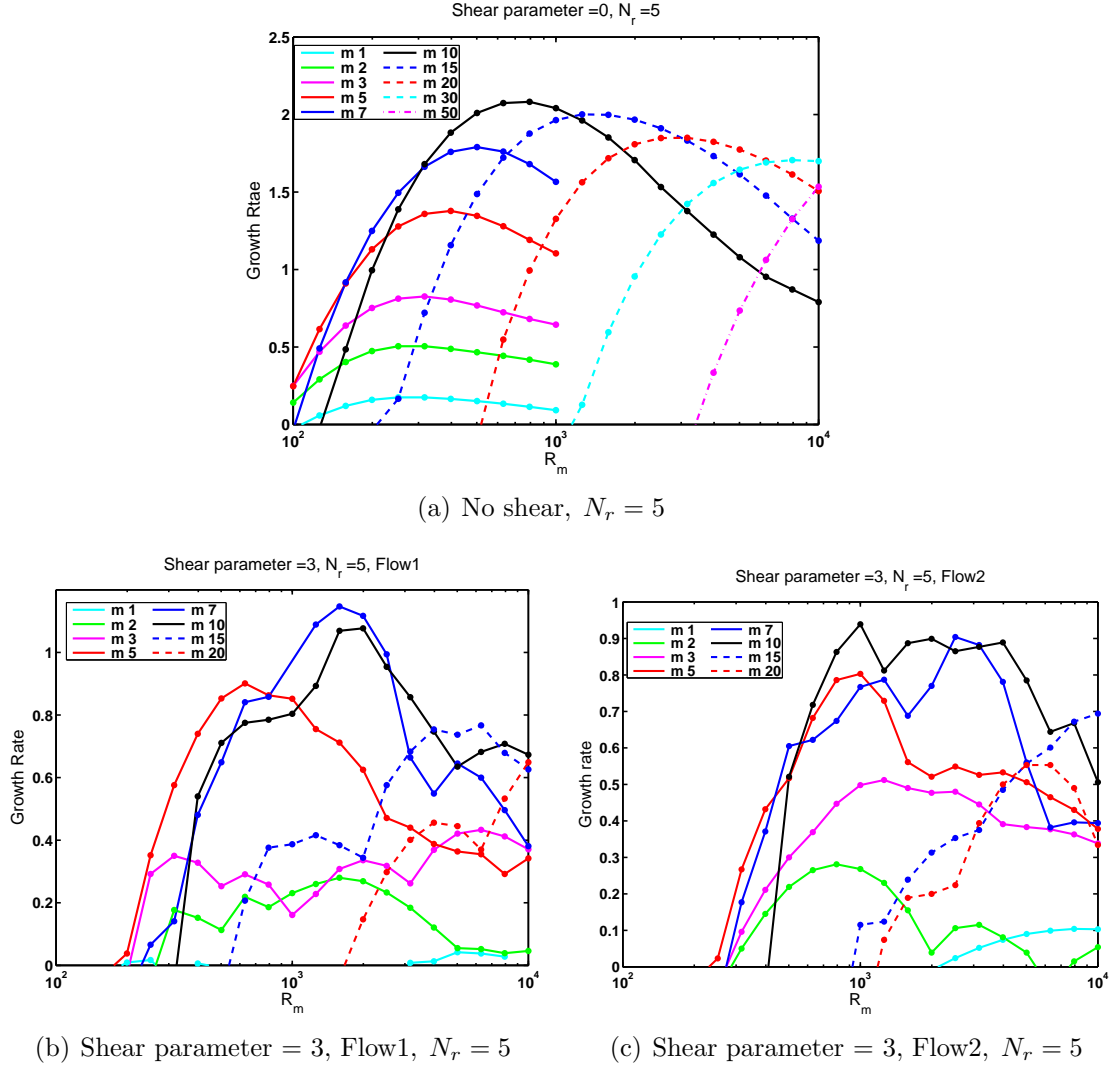


Figure 5.3: Here we plot the behavior of growth rates for  $(N_r, N_\theta) = (5, 20)$ . Fig. 5.3(a) shows the behavior of growth rates with no shear while 5.3(b) and 5.3(c) show the behavior of growth rates with  $R_m$  for Flow1 and Flow2, respectively, for shear strength 3. The decreasing behavior of growth rates with increasing  $R_m$  ensures the slow dynamo in the presence of either shear.

### 5.3.3 Contour plots and energy spectrum

Here, we investigate the generation of magnetic field for different combinations of  $m$  and  $N_r$  for  $R_m = 1000$  in case of Flow1 and Flow2 for shear strengths 1, 3 and 7. Note that we choose  $m = 5, 10$  and  $N_r = 5, 10$ .

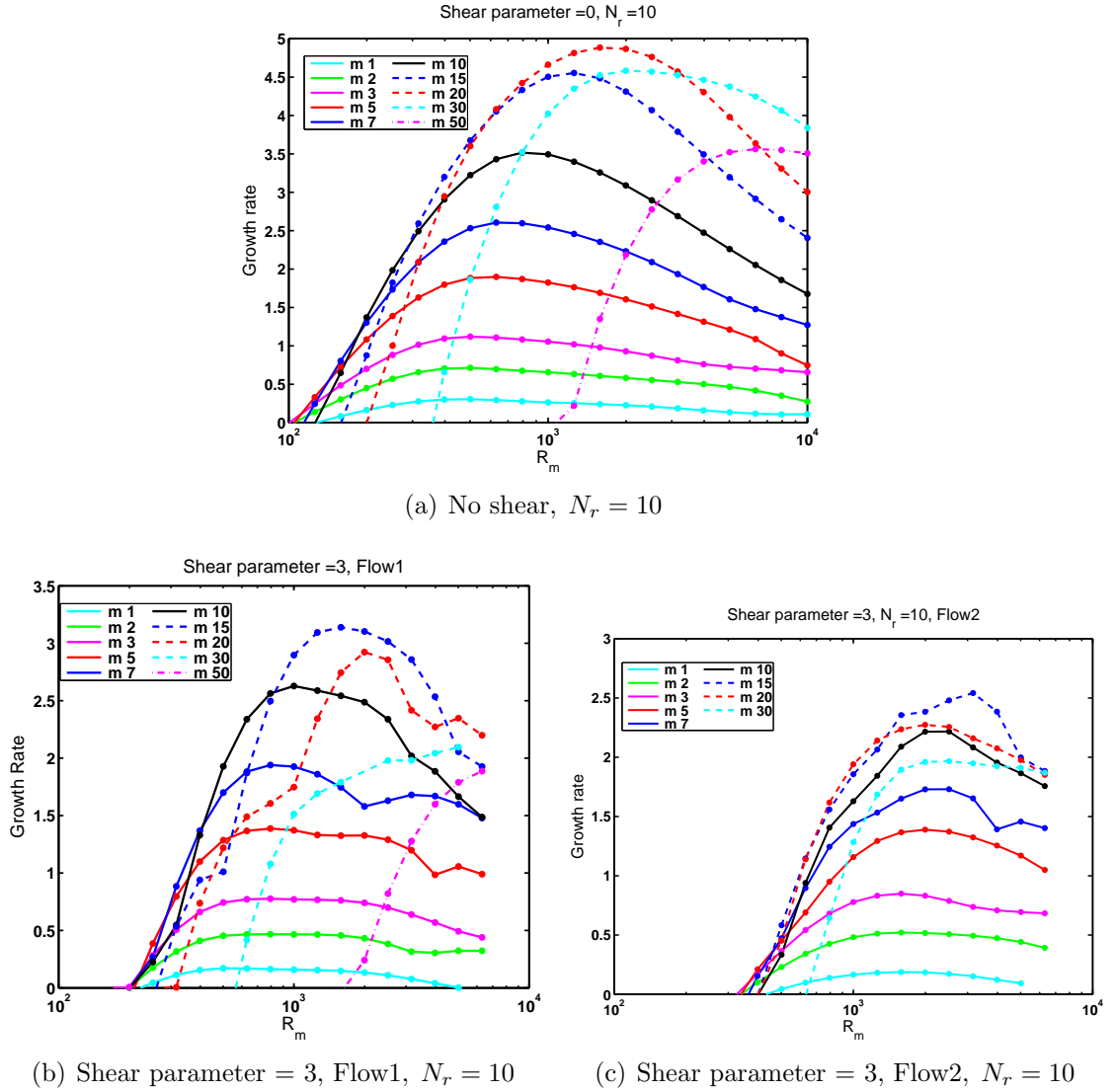


Figure 5.4: The same as in Fig. (5.3), but here  $(N_r, N_\theta) = (10, 40)$ .

**I.**  $m = 5, N_r = 5, N_\theta = 20, R_m = 1000$

The magnetic field structures of  $\varphi$  component of  $B$  for Flow1 and Flow2 can be seen in Fig. (5.6 (a-f)) with color coding on a spectrum of blue to red representing a range of negative to positive values, respectively. Fig. (5.6(a)) shows the contour plot of  $B_\varphi$  for shear strength 1 for Flow1 and we find that magnetic field is generated near the edge of the shell. Cells are distorted and concentrated at the inner boundary of the shell. Similar trend is noticed in case of shear

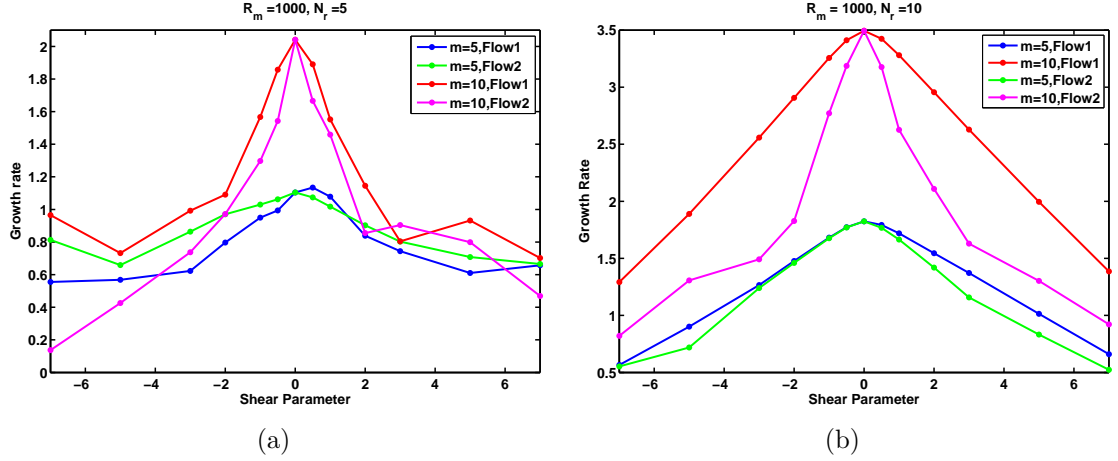


Figure 5.5: Growth rate as a function of shear strength for  $(N_r, N_\theta) = (5, 20)$  and  $(N_r, N_\theta) = (10, 40)$  for fixed values of  $R_m$  and  $m$  as  $R_m = 1000$ ,  $m = 5, 10$  for Flow1 and Flow2.

strengths 3 and 7 in Fig. 5.6(b) and 5.6(c), for Flow1. Fig.5.6(d-f) represent the behavior of magnetic field structures in case of Flow2 which are again shown to be distorted and pushed towards the middle of inner boundary of the shell in case of shear strengths 1, 3 & 7. The toroidal magnetic energy for Flow1 and Flow2 is plotted as a function of  $L$  in Fig.5.7(a-b) for different shear strengths represented in different colors, for example, blue color depicts shear strength 1, red illustrates shear strength 3 and cyan represents shear strength 7. Fig. 5.7(a) clearly shows a decline in magnetic energy with  $L$  for all shear strengths in case of Flow1. A similar trend of energy can be seen in Fig.5.7(b) in the case of Flow2.

## II. $m = 5, N_r = 10, N_\theta = 20, R_m = 1000$ .

We investigate the  $\varphi$  component of  $B$  for Flow1 and Flow2 for  $m = 5, N_r = 10, R_m = 1000$  with shear strengths = 1, 3, 7, respectively (cf. Fig.5.8(a-f)), with dark blue to bright red colors representing negative to positive values on the color bar, respectively. For Flow1, the magnetic field is again generated above the edge of the shell which is found to be pushed towards the inner boundary of the shell with distorted structures in case of all shear strengths in Fig.5.8(a-c). For Flow2, the magnetic field generation is almost the same for shear strengths 1 & 3, that is,

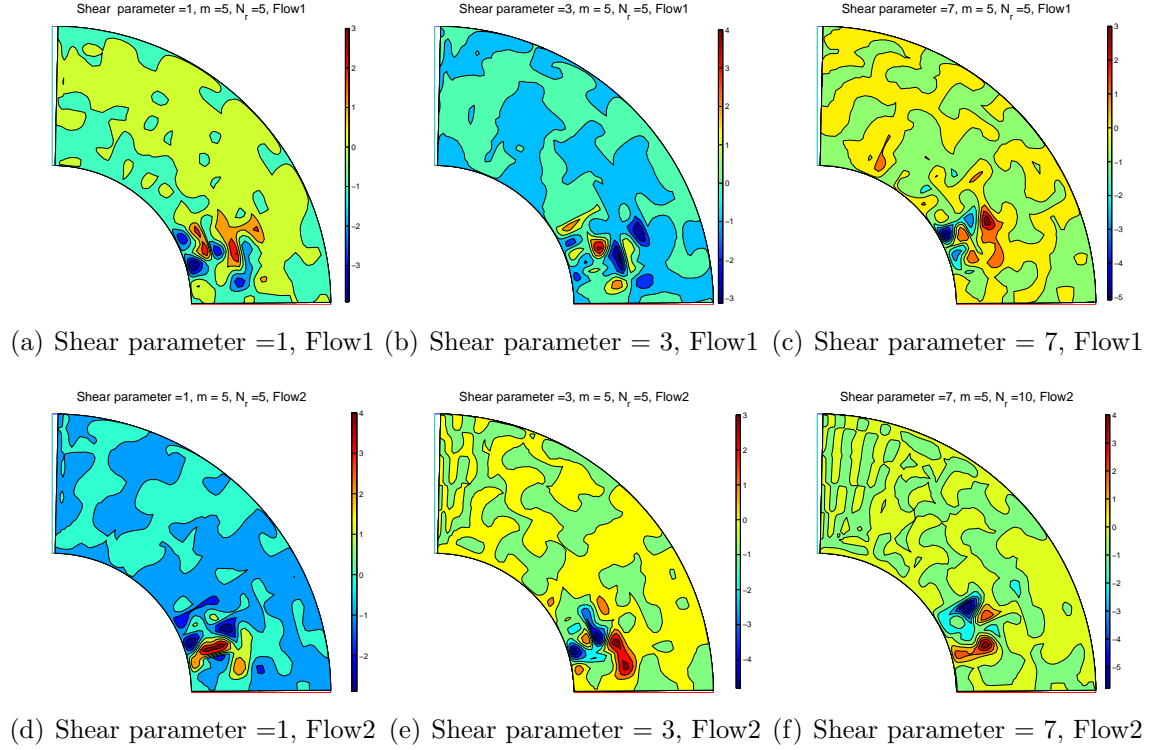


Figure 5.6: Contour plots for  $B_\varphi$  component of magnetic field for Flow1 (a-c) and Flow2 (d-f) for shear parameters 1,3, and 7, respectively, by taking  $m = 5$ ,  $N_r = 5$ ,  $R_m = 1000$ .

the magnetic field is distorted, concentrated near the inner boundary of the shell (Fig.5.8(d-e)). Interestingly, for shear strength 7, the magnetic field is generated exactly near the edge of the shell which can be seen in Fig. 5.8(f). Though the structures are distorted but they are not pushed towards the inner boundary of the shell which is quite different from the behavior observed in Fig. 5.7(a-f) and Fig. 5.8(a-d). Again, the toroidal magnetic energy for Flow1 and Flow2 is plotted against  $L$  in Fig. 5.9(a-b) for shear strengths 1, 3 & 7 illustrated in blue, red and cyan colors respectively. The magnetic energy is noticed to decrease with increasing  $L$  in case of Flow1 as shown in Fig. 5.9(a) followed by scattered behaviour whereas the magnetic energy in case of Flow2 is found to decrease smoothly with different shear strengths in Fig. 5.9(b).

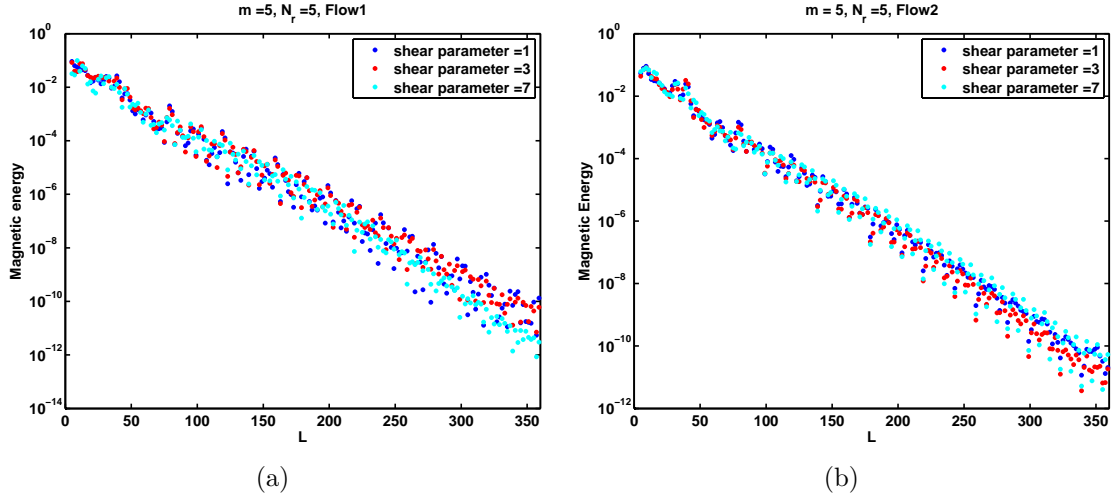


Figure 5.7: Energy spectrum for Flow1 and Flow2 is depicted in (a) and (b) respectively, by taking  $m = 5$ ,  $N_r = 5$ ,  $R_m = 1000$ .

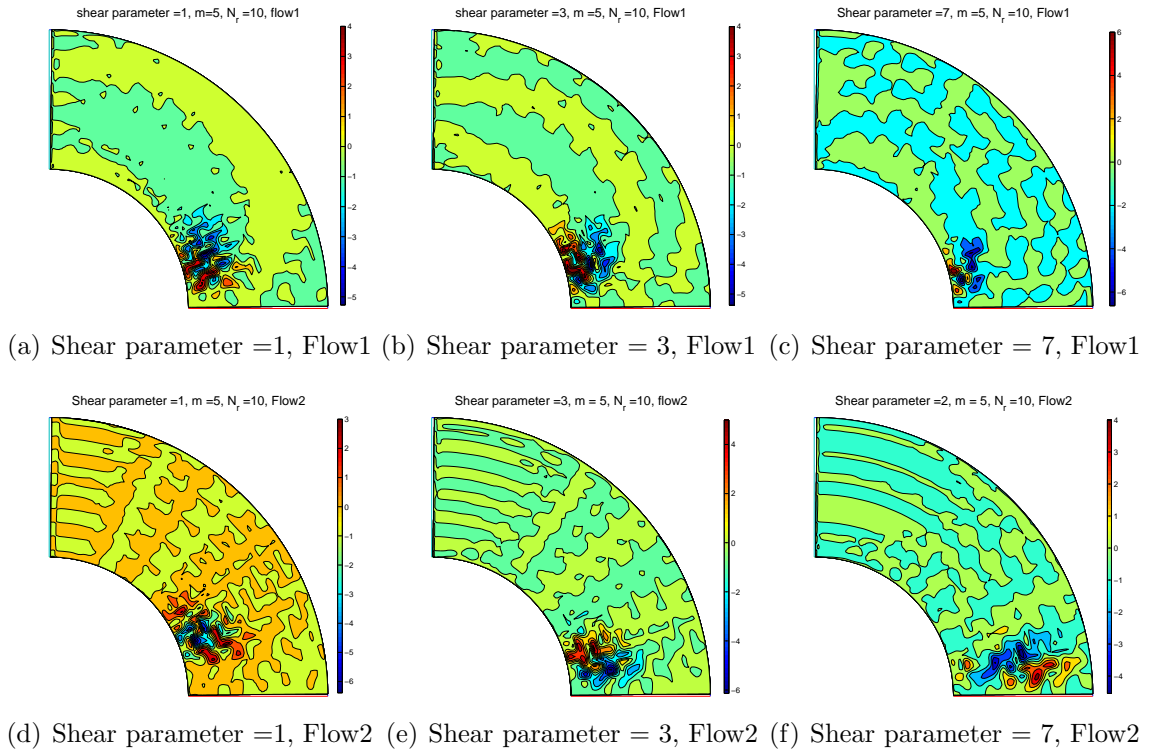


Figure 5.8: Contour plots for  $B_\phi$  component of magnetic field for Flow1 (a-c) and Flow2 (d-f) for shear parameters 1,3, and 7, respectively, by taking  $m = 5$ ,  $N_r = 10$ ,  $R_m = 1000$ .

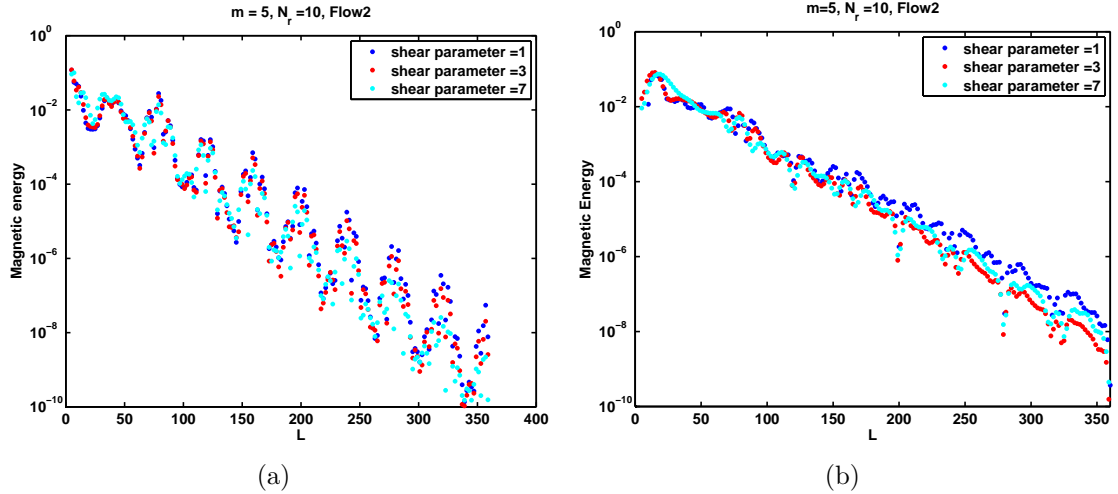


Figure 5.9: Energy spectrum for Flow1 and Flow2 is depicted in (a) and (b) respectively, by taking  $m = 5, N_r = 10, R_m = 1000$ . We note that the resolution is marginal here.

### III. $m = 10, N_r = 5, N_\theta = 10, R_m = 1000$ .

Since  $m = 10$  is observed to be the most excited mode in case of  $N_r = 5$ , it would be compelling to know how magnetic field structures and energy spectrum behave for Flow1 and Flow2 for shear strengths 1, 3, & 7 in this case (cf. Fig. 5.10 (a-f)). In case of Flow1, for shear strength 1, the magnetic field is generated near the middle of the shell which is found to be distorted and concentrated near the inner boundary of the shell (see Fig. 5.11(a)). Further, for shear parameter 3, the magnetic field is observed to generate in the middle of the shell far from the edges of the shell which can be seen in Fig. 5.11(b) in case of Flow1. Interestingly, the structures are distorted and concentrated in the middle of the shell instead of the inner boundary. Fig. 5.11(c) shows the magnetic field structure for shear strength 7 for Flow1, and we find that in this case magnetic field is generated in the middle of the shell but pushed towards the outer boundary of the shell. The magnetic field is not as strong as observed in Fig 5.11(a-b). We find almost similar trends of magnetic field generation in case of Flow2 for shear strengths 1, 3&7 in Fig. 5.11(d-f) and conclude that the presence of radial/latitudinal shear

suppresses the magnetic field generation for larger shear strength which further quenches the dynamo action. Again, the magnetic energy is shown to decrease with increasing  $L$  in case of both flows for said shear strength in Fig. 5.12(a-b).

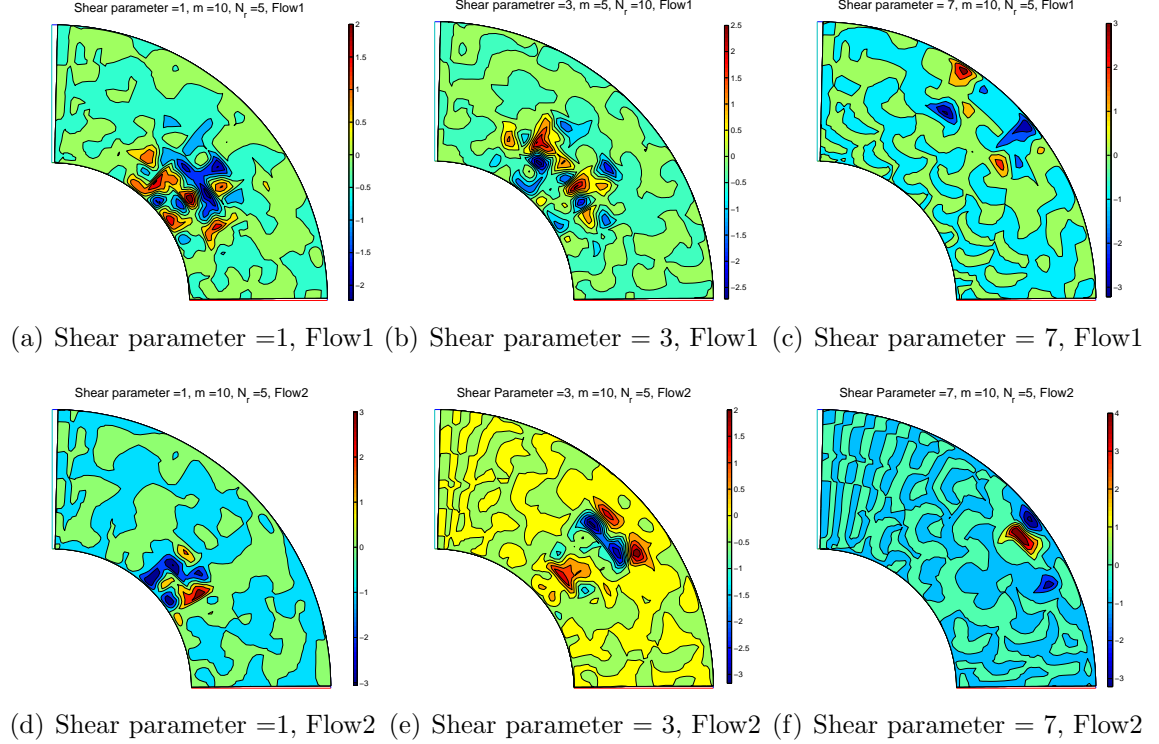


Figure 5.10: Contour plots for  $B_\phi$  component of magnetic field for Flow1 (a-c) and Flow2 (d-f) for shear parameters 1,3, and 7, respectively, by taking  $m = 10, N_r = 5, R_m = 1000$ .

#### IV. $m = 10, N_r = 10, N_\theta = 40, R_m = 1000$

Magnetic field structures in case of Flow1 are depicted in Fig. 5.12(a-c) for shear strengths 1, 3, & 7. Clearly, the magnetic field is generated far from edges of the shell and is found to be concentrated almost at the middle of shell. Also, the cells are distorted and pushed towards the inner boundary of the shell. Similar magnetic field generation is observed in case of Flow2 for shear strengths 1, 3, & 7 (cf. Fig. 5.12(d-f)). The behavior of magnetic energy can be seen in Fig. 5.13(a-b) for Flow1 and Flow2. The magnetic energy is found to decrease with  $L$  in both the cases for shear strengths 1, 3, & 7. The scattering of energy is

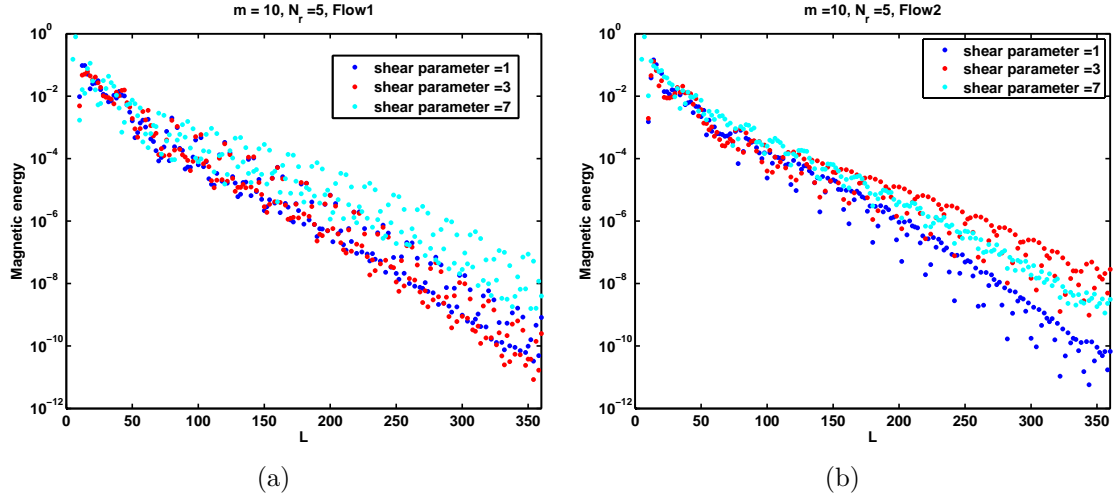


Figure 5.11: Energy spectrum for Flow1 and Flow2 is depicted in (a) and (b) respectively, by taking  $m = 10$ ,  $N_r = 5$ ,  $R_m = 1000$ .

more in case of Flow1 as compared to Flow2.

We investigate a small scale flow in the presence of large scale shear to observe the behavior of growth rate with  $R_m$  for different modes, growth rates against shear strength and magnetic field structures at different shear strengths and the results indicate that a slow dynamo works in the presence of large scale radial/latitudinal shear by suppressing the small scale flows, and by distorting and concentrating the magnetic field structures near the edge of inner boundary of the shell. All these results are in agreement with the predictions of Leprovost and Kim (2008) and Leprovost and Kim (2009).

## 5.4 Conclusions

The problem is studied in kinematic regime according to which the amplitude of magnetic field is small compared to the velocity field and does not alter the velocity field. The nature of flow is strongly helical and steady and flow is chosen to be small scale with large scale separation. The addition of large scale shear in radial/latitudinal direction alters the growth of magnetic field by quenching

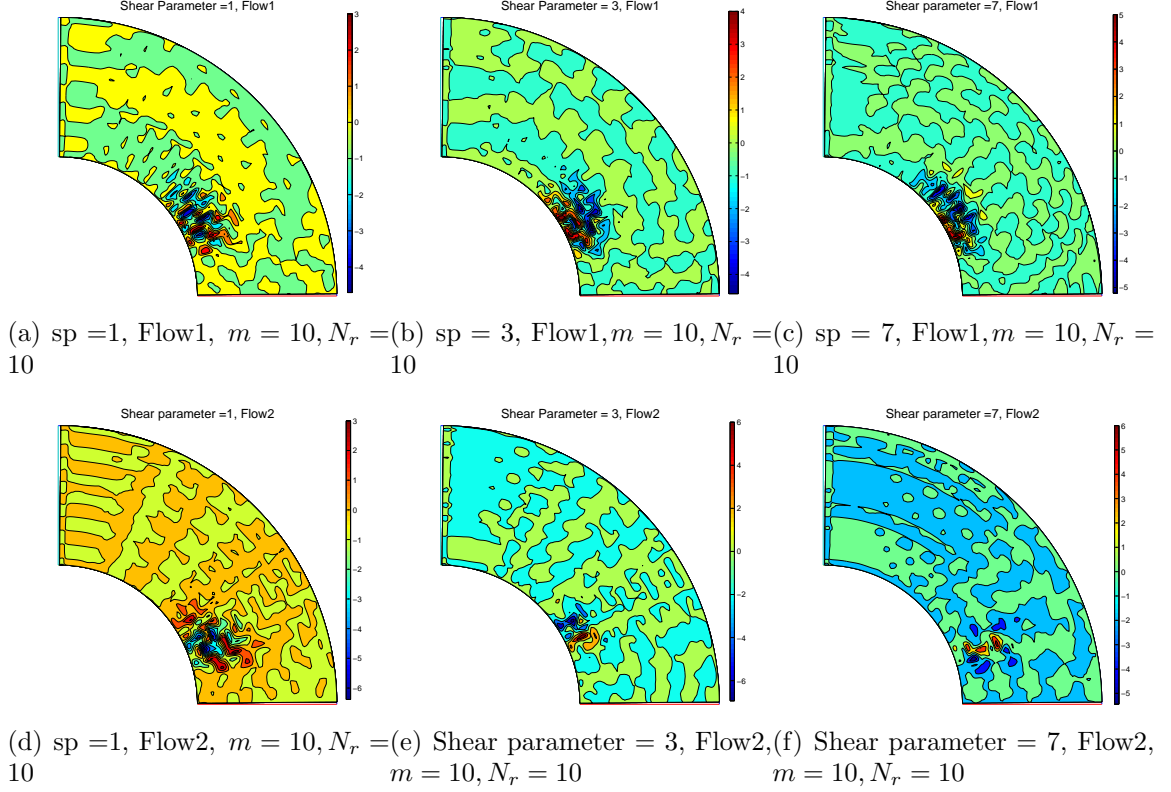


Figure 5.12: Contour plots for  $B_\varphi$  component of magnetic field for Flow1 (a-c) and Flow2 (d-f) for shear parameters 1,3, and 7, respectively, by taking  $m = 10$ ,  $N_r = 10$ ,  $R_m = 1000$ .

the amplitude and properties of small scale flows by distorting the magnetic field structures and pushing them towards the middle of spherical shell near the inner boundary. In all the cases we have investigated, the dynamo is observed to be a slow dynamo as growth is found to decrease for large value of magnetic Reynolds number, that is, the process is dominated by magnetic diffusivity instead of advection. The results obtained so far, such as, quenching of growth rate with high  $R_m$ , the decrease in magnetic energy and decline in the amplitude of growth rate with shear strength support the theoretical prediction, that the presence of large scale shear quenches the turbulent flows, made by Leprovost and Kim (2008, 2009). It is clear from these investigations that small scale magnetic fields are suppressed by large scale shear and could help in the manifestation of large

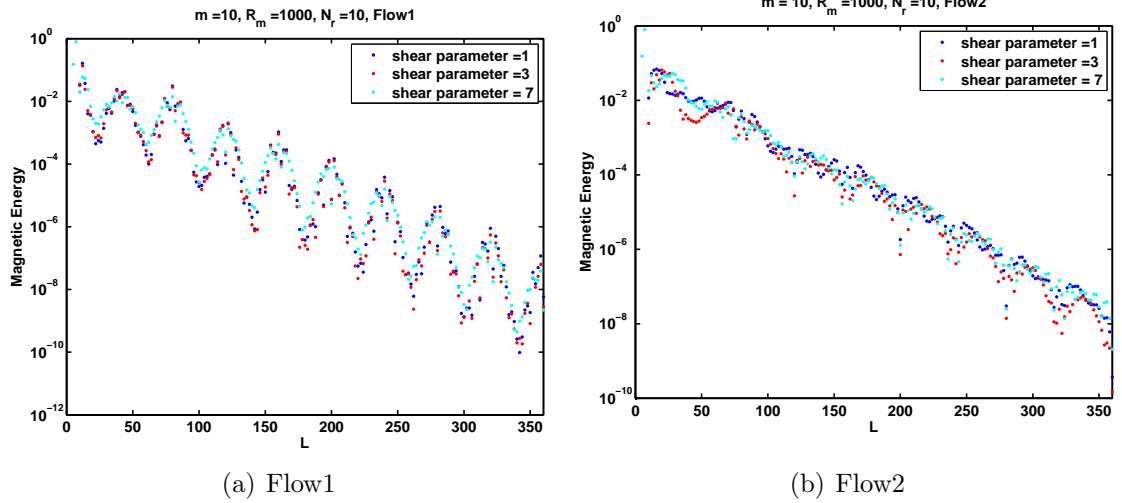


Figure 5.13: Energy spectrum for Flow1 and Flow2 is depicted in (a) and (b) respectively, by taking  $m = 10$ ,  $N_r = 10$ ,  $R_m = 1000$ . We note that the resolution is marginal here. Shear parameter is denoted by sp in some of the plots.

scale magnetic fields as noted by Tobias and Cattaneo (2013). For this problem, the feedback from Lorentz force is not taken into account, therefore it would be interesting to investigate the problem by extending it into nonlinear regime for future work. The tendency of magnetic field structures to concentrate near the inner boundary of shell could be due to some other effects that come into play due to magnetic diffusion such as turbulent pumping. Sun has both small scale and large scale dynamos working together and there is no clear line of demarcation between the two. Therefore, further investigations in this problem in nonlinear regime will help us to understand the various physical mechanisms in the working of solar dynamo.

# Chapter 6

## Conclusions

### 6.1 Summary of the results

In the second chapter we investigate a dynamic model of dynamo which comprises of seven coupled nonlinear differential equations. Specifically, we include the effects of  $\alpha$ -quenching, flux losses through poloidal and toroidal magnetic fields and Lorentz force on mean/fluctuating differential rotation. We unfold how frequency of magnetic fields, magnetic field strength and total shear depends upon the rotation rate. We find that the results are in good agreement with observations if the  $\alpha$ -quenching and both flux losses are taken in equal amount with quadratic dependence on  $B$  along with the effects of mean/fluctuating differential rotation. We find that our model is able to reproduce the linear increase in frequency of magnetic field with rotation, flattening of magnetic energy as well as quenching of total shear for higher rotation. These results further suggest the necessity of a dynamic balance in the generation and destruction of magnetic fields as well as mean and fluctuating differential rotations for the working of stellar dynamo.

The third chapter is an extension of second chapter where the role of nonlinear transport coefficients in the self-regulation of a dynamo process and generation/destruction of magnetic fields is emphasized in detail by studying the model

analytically and numerically. We find that in the absence of effects of mean and fluctuating differential rotations the magnetic field strength and frequency of magnetic field keeps on growing with rotation rate. Although analytic and numerical results are in agreement with each other, yet, the results obtained are not in good agreement with observations. In the presence of mean shear, we find a severe quenching in total shear, which in turn, quenches the growth rate of magnetic field and frequency which is further responsible for the shutting down of the dynamo. The presence of fluctuating shear shows opposite results to the case where only mean shear is taken into account and we notice that fluctuating shear is accountable for the chaos in the system. Though the addition of nonlinear transport coefficients is able to control the chaos and indefinite growth of magnetic fields up to an extent, but is incapable to reproduce the observation. Therefore, self-regulatory behavior of the system is represented in the presence of mean and fluctuating differential rotations in the presence of equal amount of all nonlinear transport coefficients to emphasize the importance of dynamic balance among all nonlinear terms to the working of a stellar dynamo.

We extend our seventh-order system by adding equation of evolution in rotation rate in the fourth chapter to understand the spindown of solar type stars. In particular, we prescribe the angular momentum loss dynamically through equation of evolution and explain the existence of two branches of frequency, two different spindown mechanisms, that is, exponential spindown for fast rotators and power law spindown for slow rotators, decrease in magnetic activity with increasing age and shorter spindown timescale for fast rotators while larger spindown timescale for slow rotators. The shortest spindown timescale in our system constantly explains the V-P gap. For the first time a model is proposed which provides an explanation for V-P gap in the framework of  $\alpha - \Omega$  dynamo.

The fifth chapter summarises the results of a kinematic dynamo in the presence of large scale shear. In this chapter, the induction equation is solved numerically to understand the effects of large scale shear on the working of the dynamo. In

particular, an axisymmetric, steady, helical small scale velocity field is considered, to which a large scale radial/latitudinal shear in the azimuthal velocity field is added. The decreasing behavior of growth rates for larger Reynolds number,  $R_m$ , suggests a slow dynamo in the presence of radial as well as latitudinal shear. The growth rate is found to decline with shear strength while the magnetic field structures are found to be distorted and concentrated near inner or outer boundaries depending upon the values of  $m$  and  $N_r$ . Our investigations clearly show that large scale shear suppresses the small scale flows and quenches the kinematic dynamo.

## 6.2 Future Work

The spin evolution of stars is an important problem in astrophysics since it has a direct impact on, e.g., asteroseismology, disk and planet formation, magnetic field generation, and a host of observational signatures. For solar-type stars, a magnetic stellar wind is thought to be the primary source of angular momentum loss and hence spin-down of stars. Therefore, future studies will be conducted on the spin-down of Sun-like stars by extending my previous work in 2D MHD by investigating the effects of various instabilities caused by shear, in spherical geometry and to investigate the ‘gap’ between two branches of stars commonly known as ‘Vaughan–Preston Gap’.

# Appendix A

## Derivation of nonlinear dynamical system represented by Eqs. (2.1) - (2.4)

This appendix provides the detailed derivation of Eqs. (2.1)-(2.4) as noted in Weiss et al. (1984). In nonlinear dynamo theory, the induction equation

$$\frac{\partial \mathbf{B}}{\partial t} = \nabla \times (\mathbf{u} \times \mathbf{B}) + \eta \nabla^2 \mathbf{B}, \quad (\text{A.1})$$

and the equation of motion

$$\rho \left[ \frac{\partial \mathbf{u}}{\partial t} + (\mathbf{u} \cdot \nabla) \mathbf{u} \right] = \rho \mathbf{g} - \nabla p + \mathbf{j} \times \mathbf{B} + \rho \nu \nabla^2 \mathbf{u}, \quad (\text{A.2})$$

are solved together with energy equation for magnetic field,  $\mathbf{B}$ , and velocity field,  $\mathbf{u}$ , where other symbols have their usual definitions. An axisymmetric magnetic field in spherical polar coordinates  $(r, \theta, \Phi)$  is given by

$$\mathbf{B} = \mathbf{B}_p + \mathbf{B}_t, \quad (\text{A.3})$$

where,  $\mathbf{B}_p = \nabla \times [A(r, \theta, t)] \hat{\Phi}$  is the poloidal magnetic field,  $\mathbf{B}_t = B(r, \theta, t) \hat{\Phi}$  is the toroidal magnetic field and  $\hat{\Phi}$  is a unit vector in  $\Phi$ -direction. It is assumed that in rapidly rotating system, no mean motions exist except rotation, and in that case velocity is given by  $\mathbf{u} = (0, 0, \Omega r \sin \theta)$  (Parker, 1955; Moffatt, 1978), and decomposition of induction equation in its mean field poloidal and toroidal parts can be written as follows:

$$\frac{\partial A}{\partial t} = \alpha B + \eta[\nabla^2 - (r \sin \theta)^{-2}]A, \quad (\text{A.4})$$

$$\frac{\partial B}{\partial t} = r \sin \theta \mathbf{B}_p \cdot \nabla \Omega + \eta[\nabla^2 - (r \sin \theta)^{-2}]B. \quad (\text{A.5})$$

In a nonlinear dynamo model, the effect of Lorentz force on fluid motions is taken into account and the growth of magnetic field is thus inhibited. Therefore, the azimuthal component of velocity,  $v$ , can be written as

$$\frac{\partial v}{\partial t} = \mathbf{F}(\mathbf{r}) + \rho^{-1} \mathbf{j} \times \mathbf{B} \cdot \hat{\Phi} + \nu[\nabla^2 - (r \sin \theta)^{-2}]v, \quad (\text{A.6})$$

where volume force,  $\rho \mathbf{F}$ , and diffusivity,  $\nu$ , specify the turbulent transport of angular momentum. If  $V(r)$  and  $w(r, t)$  are the mean and fluctuating parts of  $v$ , then it can be written as  $v = \mathbf{V}(\mathbf{r}) + \mathbf{w}(\mathbf{r}, \mathbf{t})$ . Since convection drives mean flow  $V$ , therefore

$$\mathbf{F} + \nu[\nabla^2 - (r \sin \theta)^{-2}]V = 0, \quad (\text{A.7})$$

while the fluctuating part is driven by Lorentz force and becomes

$$\frac{\partial w}{\partial t} = \frac{1}{\mu_0 \rho} [\nabla \times (\mathbf{B} \hat{\Phi})] \times \mathbf{B}_p \hat{\Phi} + \nu[\nabla^2 - (r \sin \theta)^{-2}]w. \quad (\text{A.8})$$

Weiss et al. (1984) considered a thin spherical shell with local cartesian coordinates  $x$ -,  $y$ - and  $z$ -axis pointing northward, westward and radially outward,

respectively. By considering magnetic field,  $\mathbf{B}$ , and velocity,  $\mathbf{u}$ , in plane layer as:

$$\mathbf{B} = \nabla \times [A(z, x, t)\hat{\mathbf{y}}] + B(z, x, t)\hat{\mathbf{y}}, \quad (\text{A.9})$$

$$\mathbf{u} = [0, V(z), 0], \quad (\text{A.10})$$

they obtained Eqs. (A.11) and (A.12) as follows

$$\frac{\partial A}{\partial t} = \alpha B + \eta \nabla^2 A, \quad (\text{A.11})$$

$$\frac{\partial B}{\partial t} = \frac{\partial A}{\partial x} \frac{dV}{dz} + \eta \nabla^2 B, \quad (\text{A.12})$$

To eliminate the  $z$ -dependence of  $A$  and  $B$ , they averaged Eqs. (A.11) and (A.12) vertically over the layer and considered a plane wave solutions propagating in  $x$ -direction (Parker, 1979), in the presence of azimuthal velocity  $\mathbf{v} = (V(z) + W(x, z, t))\hat{\mathbf{y}}$ , where the rotation velocity is represented by  $V = \Omega z$  while the differential rotation due to back reaction is represented by  $W(x, z, t)$ . By assuming the periodic boundary conditions in terms of fourier mode and  $k$ -mode of magnetic field as  $\mathbf{B} = (0, B(t)e^{ikx}, ikA(t)e^{ikx})$ , the dynamo Eqs. (A.11) and (A.12) reduce to

$$\frac{dA}{dt} = \alpha B + \eta k^2 A, \quad (\text{A.13})$$

$$\frac{dB}{dt} = ikV' A + \eta k^2 B, \quad (\text{A.14})$$

where  $V'$  represents the value of the velocity shear  $\frac{dV}{dz}$ . Equations (A.13) and (A.14) represent a linear system and if the perturbations are considered to vary as  $exp(st)$ , this system possesses a linear dispersion relation,  $s = \eta k^2 [-1 \pm (1 + i)D^{1/2}]$ , as noted by Weiss et al. (1984), where  $D$  is the dynamo number and is given by

$$D = \frac{\alpha V'}{2\eta^2 k^3}. \quad (\text{A.15})$$

Further, if  $A = B = 0$ , then linear system (A.13) and (A.14) is stable for  $|D| < 1$  and a Hopf bifurcation occurs at  $D = 1$ , while the system grows exponentially for  $D > 1$ . To induce the nonlinear effects, the system was subjected to nonlinearities such as saturation of  $\alpha$ -effect, magnetic buoyancy loss and quenching of velocity by choosing  $\alpha = \alpha_0 f(|\mathbf{B}|^2)$ ,  $g(\mathbf{B})^2$  and  $v' = v'_0 f(|\mathbf{B}|^2)$  then following nonlinear system is obtained

$$\frac{dA}{dt} = \alpha_0 f(|\mathbf{B}|^2)B + \eta k^2 A, \quad (\text{A.16})$$

$$\frac{dB}{dt} = ikv' A + \eta k^2 g(\mathbf{B})^2 B, \quad (\text{A.17})$$

where  $f(b^2) = (1 + \kappa b^2)^{-1}$  and  $g(b^2) = (1 + \lambda b^2)$  with  $\kappa$  and  $\lambda$  as constants. Differential rotation is generated by the Lorentz force which takes the form  $\frac{\partial W}{\partial z} = w_0(t) + w(t) \exp(2ikx)$ , where  $w_0(t)$  and  $w(t)$  are mean and fluctuating differential rotation. A net torque,  $G$ , with a value  $\nu_0 V'$ , is exerted during the generation of  $V'$  as a result of which spatially uniform and varying components of velocity shear obtained by Weiss et al. (1984) are

$$\frac{dw_0}{dt} = \mu^2 k (A_2 B_1 - A_1 B_2) - \nu_0 w_0, \quad (\text{A.18})$$

$$\frac{dw}{dt} = -\mu^2 ki AB - \nu w, \quad (\text{A.19})$$

where  $\nu_0$  and  $\nu$  are the viscosities of mean and fluctuating differential rotation. The quantities  $A_1, B_1, A_2$  and  $B_2$  are arisen during the evaluation of nonlinear terms (Weiss et al., 1984) where terms with prefix 1 represent real parts of poloidal/toroidal magnetic fields while terms with prefix 2 represent imaginary part of poloidal/toroidal magnetic fields in Eq. (A.12). Further, the toroidal magnetic field,  $B$ , is affected by the presence of time dependent velocity shear and Eq. (A.17) takes the form

$$\frac{dB}{dt} = ik(V' + w_0)A - \frac{1}{2}kA^*w - \eta k^2 [1 + \lambda |B|^2]B. \quad (\text{A.20})$$

Eventually, Eqs. (A.16), (A.20), (A.18) and (A.19) were reduced to dimensionless form by Cattaneo et al. (1983) and Weiss et al. (1984) where various variables are rescaled and transformed appropriately as follows.

$$\begin{pmatrix} A \\ B \\ w_0 \\ w \end{pmatrix}_{new} = \begin{pmatrix} \mu A / \eta k \\ AB / V' \\ w_0 / V' \\ w / V' \end{pmatrix}, \quad \begin{pmatrix} \kappa \\ \lambda \\ \nu_0 \\ \nu \end{pmatrix}_{new} = \begin{pmatrix} \mu^2 V' \kappa / \eta^4 K^4 \\ \mu^2 V' \lambda / \eta^4 K^4 \\ nu_0 / \eta k^2 \\ nu / \eta k^2 \end{pmatrix}. \quad (\text{A.21})$$

The seventh order system in the dimensionless form is thus given as (Cattaneo et al., 1983; Weiss et al., 1984):

$$\dot{A} = 2D(1 + \kappa|B|^2)^{-1}B - A, \quad (\text{A.22})$$

$$\dot{B} = i(1 + w_0)A - \frac{1}{2}iA^*w - B(1 + \lambda|B|^2), \quad (\text{A.23})$$

$$\dot{w}_0 = \frac{1}{2}i(A^*B - AB^*) - \nu_0 w_0, \quad (\text{A.24})$$

$$\dot{w} = -iAB - \nu w. \quad (\text{A.25})$$

The system (A.22) - (A.25) is further reduced by setting  $\kappa = \lambda = 0$  to

$$\dot{A} = 2DB - A, \quad (\text{A.26})$$

$$\dot{B} = i(1 + w_0)A - \frac{1}{2}iA^*w - B, \quad (\text{A.27})$$

$$\dot{w}_0 = \frac{1}{2}i(A^*B - AB^*) - \nu_0 w_0, \quad (\text{A.28})$$

$$\dot{w} = -iAB - \nu w. \quad (\text{A.29})$$

Equations (A.26) - (A.29) represent Eqs. (2.1) - (2.4) which are further modified to investigate the effects of nonlinear transport coefficients in the present thesis.

# Bibliography

- Allain, S. *Modelling the angular momentum evolution of low-mass stars with core-envelope decoupling*. *A&A*, 333:629–643, 1998.
- Arlt, R. and Fröhlich, H.-E. *The solar differential rotation in the 18th century*. *A&A*, 543:A7, 2012.
- Barnes, J. R., Collier Cameron, A., Donati, J.-F., James, D. J., Marsden, S. C., and Petit, P. *The dependence of differential rotation on temperature and rotation*. *MNRAS*, 2005.
- Barnes, S. A. *On the Rotational Evolution of Solar- and Late-Type Stars, Its Magnetic Origins, and the Possibility of Stellar Gyrochronology*. *ApJ*, 586: 464–479, 2003.
- Barnes, S. A. *A Simple Nonlinear Model for the Rotation of Main-sequence Cool Stars. I. Introduction, Implications for Gyrochronology, and Color-Period Diagrams*. *ApJ*, 722:222–234, 2010.
- Barnes, S. A. and Kim, Y.-C. *Angular Momentum Loss from Cool Stars: An Empirical Expression and Connection to Stellar Activity*. *ApJ*, 721:675–685, 2010.
- Böhm-Vitense, E. *Chromospheric Activity in G and K Main-Sequence Stars, and What It Tells Us about Stellar Dynamos*. *ApJ*, 657:486–493, 2007.

- Brandenburg, A. and Subramanian, K. *Astrophysical magnetic fields and nonlinear dynamo theory. Physics Reports*, 417:1 – 209, 2005.
- Brandenburg, A., Saar, S. H., and Turpin, C. R. *Time Evolution of the Magnetic Activity Cycle Period. ApJL*, 498:L51–L54, 1998.
- Brown, T. M. *The Metastable Dynamo Model of Stellar Rotational Evolution. The Astrophysical Journal*, 789(2):101, 2014.
- Cattaneo, F., Weiss, N. O., and Jones, C. A. *Periodic and aperiodic behaviour in stellar dynamos. In Solar and Stellar Magnetic Fields: Origins and Coronal Effects*, volume 102 of *IAU Symposium*, pages 307–309, 1983.
- Childress, S. and Gilbert, A. D. *Stretch, twist, fold: the fast dynamo*. Berlin: Springer, 1995.
- Delfosse, X., Forveille, T., Perrier, C., and Mayor, M. *Rotation and chromospheric activity in field M dwarfs. A&A*, 331:581, 1998.
- Dikpati, M. and Charbonneau, P. *A Babcock-Leighton Flux Transport Dynamo with Solar-like Differential Rotation. ApJ*, 518:508–520, 1999.
- Donahue, R. A., Saar, S. H., and Baliunas, S. L. *A Relationship between Mean Rotation Period in Lower Main-Sequence Stars and Its Observed Range. ApJ*, 466:384, 1996.
- Donati, J.-F. and Collier Cameron, A. *Differential rotation and magnetic polarity patterns on AB Doradus. MNRAS*, 291:1–19, 1997.
- Durney, B. R., Mihalas, D., and Robinson, R. D. *A preliminary interpretation of stellar chromospheric CA II emission variations within the framework of stellar dynamo theory. PASP*, 93:537–543, 1981.
- Fröhlich, H.-E., Küker, M., Hatzes, A. P., and Strassmeier, K. G. *On the differential rotation of CoRoT-2a. aap*, 506:263–268, 2009.

- Gallet, F. and Bouvier, J. *Improved angular momentum evolution model for solar-like stars. A&A*, 556:A36, 2013.
- Gilman, P. A. *Dynamos of the sun and stars, and associated convection zone dynamics*. In *Solar and Stellar Magnetic Fields: Origins and Coronal Effects*, volume 102 of *IAU Symposium*, pages 247–269, 1983a.
- Gilman, P. A. *Dynamically consistent nonlinear dynamos driven by convection in a rotating spherical shell. II - Dynamos with cycles and strong feedbacks. ApJS*, 53:243–268, 1983b.
- Hale, G. E. *Solar-Vortices. ApJ*, 28:100, 1908a.
- Hale, G. E. *On the probable existence of a magnetic field in sun-spots. ApJ*, 28: 315, 1908b.
- Heinemann, T., McWilliams, J. C., and Schekochihin, A. A. *Large-scale magnetic field generation by randomly forced shearing waves. PRL*, 2011.
- Henry, T., Soderblom, D., Donahue, R., and Baliunas, S. *A Survey of Ca II H and K Chromospheric Emission in Southern Solar-Type Stars. Astron. J.*, 111: 439, 1996.
- Hollerbach, R. *A spectral solution of the magneto-convection equations in spherical geometry. IJNMF*, 32:773–797, 2000.
- Hollerbach, R., Galloway, D. J., and Proctor, M. R. E. *Numerical Evidence of Fast Dynamo Action in a Spherical Shell. PRL*, 74:3145–3148, 1995.
- Hotta, H. and Yokoyama, T. *Modeling of Differential Rotation in Rapidly Rotating Solar-type Stars. ApJ*, 740:12, 2011.
- Hughes, D. W. and Proctor, M. R. E. *Large-Scale Dynamo Action Driven by Velocity Shear and Rotating Convection. Physical Review Letters*, 102(4):044501, 2009.

- Hughes, D. W. and Proctor, M. R. E. *The effect of velocity shear on dynamo action due to rotating convection. Journal of Fluid Mechanics*, 717:395–416, 2013.
- Ivanova, T. S. and Ruzmaikin, A. A. *A nonlinear magnetohydrodynamic model of the solar dynamo. SoVAST*, 21:479–485, 1977.
- Jepps, S. A. *Numerical models of hydromagnetic dynamos. Journal of Fluid Mechanics*, 67:625–646, 1975.
- Käpylä, P. J. and Brandenburg, A. *Turbulent Dynamos with Shear and Fractional Helicity. ApJ*, 699:1059–1066, 2009.
- Keppens, R., MacGregor, K. B., and Charbonneau, P. *On the evolution of rotational velocity distributions for solar-type stars. aap*, 294:469–487, 1995.
- Knobloch, E. and Landsberg, A. S. *A new model of the solar cycle. MNRAS*, 278:294, 1996.
- Knobloch, E., Tobias, S. M., and Weiss, N. O. *Modulation and symmetry changes in stellar dynamos. MNRAS*, 297:1123, 1998.
- Labonte, B. J. and Howard, R. *Torsional waves on the sun and the activity cycle. Solar Physics*, 75:161–178, 1982.
- Larmor, J. *How could a rotating body such as the Sun become a magnet. Rep. Brit. Assoc. Adv. Sci.*, 159:160, 1919.
- Leprovost, N. and Kim, E. *Dynamo Quenching Due to Shear Flow. PRL*, 100 (14):144502, 2008.
- Leprovost, N. and Kim, E. *Dynamo Efficiency with Shear in Helical Turbulence. ApJL*, 696:L125–L128, 2009.

- Leprovost, N. and Kim, E. *On a Stochastic Model for the Spin-down of Solar-type Stars*. *ApJ*, 719:287–298, 2010.
- Lopes, I. and Passos, D. *Evidence for a long-term variation of the dynamo action responsible for the solar magnetic cycle*. *MNRAS*, 397:320–324, 2009.
- Love, J. J. *Reversals and excursions of the geodynamo*. *Astronomy & Geophysics*, 40(6):6.14–6.19, 1999.
- MacGregor, K. B. and Brenner, M. *Rotational evolution of solar-type stars. I - Main-sequence evolution*. *ApJ*, 376:204–213, 1991.
- Matt, S. P., Brun, A. S., Baraffe, I., Bouvier, J., and Chabrier, G. *The Mass-dependence of Angular Momentum Evolution in Sun-like Stars*. *ApJL*, 799:L23, 2015.
- Mininni, P. D., Gomez, D. O., and Mindlin, G. B. *Simple Model of a Stochastically Excited Solar Dynamo*. *solphys*, 201:203–223, 2001.
- Mitra, D. and Brandenburg, A. *Scaling and intermittency in incoherent  $\alpha$ -shear dynamo*. *MNRAS*, 420:2170–2177, 2012.
- Moffatt, H. K. *Magnetic Field Generation in Electrically Conducting Fluids*. Cambridge: Cambridge University Press, 1978.
- Newton, A. P. L. and Kim, E. *Determining the temporal dynamics of the solar  $\alpha$  effect*. *aap*, 551:A66, 2013.
- Newton, A. P. L., Kim, E., and Liu, H. L. *On the self-organizing process of large scale shear flows*. *Phys. Plasmas*, 420(092306), 2013.
- Noyes, R. W., Hartmann, L. W., Baliunas, S. L., Duncan, D. K., and Vaughan, A. H. *Rotation, convection, and magnetic activity in lower main-sequence stars*. *ApJ*, 279:763, 1984.

- Noyes, R. W., Weiss, N. O., and Vaughan, A. H. *The relation between stellar rotation rate and activity cycle periods.* *ApJ*, 287:769–773, 1984.
- Ostriakov, V. M. and Usoskin, I. G. *On the dimension of solar attractor.* *Sol. Phys.*, 127:405–412, 1990.
- Ott, E. *Chaos in dynamical systems.* Cambridge University Press, first edition, 1993. ISBN 0521437997.
- Pace, G. *The discontinuous nature of chromospheric-activity evolution.* *APSS*, 328:307–311, 2010.
- Pace, G., Melendez, J., Pasquini, L., Carraro, G., Danziger, J., François, P., Matteucci, F., and Santos, N. C. *An investigation of chromospheric activity spanning the Vaughan-Preston gap: impact on stellar ages.* *A&A*, 499:L9–L12, 2009.
- Parker, E. N. *Cosmic Magnetic Fields: their origin and activity.* Oxford: Clarendon Press, 1979.
- Passos, D. and Lopes, I. *Grand minima under the light of a low order dynamo model.* *Journal of Atmospheric and Solar-Terrestrial Physics*, 73:191–197, 2011.
- Passos, D. and Lopes, I. *A Low-Order Solar Dynamo Model: Inferred Meridional Circulation Variations Since 1750.* *ApJ*, 686:1420–1425, 2008.
- Pizzolato, N., Maggio, A., Micela, G., Sciortino, S., and Ventura, P. *The stellar activity-rotation relationship revisited: Dependence of saturated and non-saturated X-ray emission regimes on stellar mass for late-type dwarfs.* *A&A*, 397:147, 2003.
- Pontieri, A., Lepreti, F., Sorriso-Valvo, L., Vecchio, A., and Carbone, V. *A Simple Model for the Solar Cycle.* *solphys*, 213:195–201, March 2003.

- Popova, E. P. and Potemina, K. A. *Modeling of the solar activity double cycle using dynamical systems. Geo. & Aeronomy*, 53:941, 2013.
- Pouquet, A., Frisch, U., and Leorat, J. *Strong MHD helical turbulence and the nonlinear dynamo effect. Journal of Fluid Mechanics*, 77:321–354, September 1976.
- Proctor, M. R. E. and Hughes, D. W. *Competing kinematic dynamo mechanisms in rotating convection with shear. In IAU Symposium*, 2011.
- Reiners, A. and Mohanty, S. *Radius-dependent Angular Momentum Evolution in Low-mass Stars. I. ApJ*, 746:43, 2012.
- Reiners, A. and Schmitt, J. H. M. M. *Rotation and differential rotation in field F- and G-type stars. aap*, 398:647–661, 2003.
- Rempel, M. *Flux-Transport Dynamos with Lorentz Force Feedback on Differential Rotation and Meridional Flow: Saturation Mechanism and Torsional Oscillations. ApJ*, 647:662–675, 2006.
- Richardson, K. J., Hollerbach, R., and Proctor, M. R. E. *From large-scale to small-scale dynamos in a spherical shell. Physics of Fluids*, 24(10):107103, 2012.
- Roberts, G. O. *Spatially Periodic Dynamos. Philos. Trans. R. Soc. London, Ser. A*, 266:545, 1970.
- Roberts, G. O. *Dynamo action of fluid motions with two-dimensional periodicity. Philos. Trans. R. Soc. London, Ser. A*, 271:411, 1972.
- Roberts, P. H. *In Lectures on Solar and Planetary Dynamos. Cambridge University Press, Cambridge*, 1994.
- Ruzmaikin, A. *The solar cycle as a strange attractor. Comments on Astrophysics*, 9:85, 1981.

- Saar, S. H. . In the 11th Cool Stars: Stellar System and the Sun, volume 223 of 292, 2002.
- Saar, S. H. and Brandenburg, A. *Time Evolution of the Magnetic Activity Cycle Period. II. Results for an Expanded Stellar Sample.* *ApJ*, 524:295–310, 1999.
- Scholz, A. Stellar spindown: From the ONC to the Sun. In Stempels, E., editor, *15th Cambridge Workshop on Cool Stars, Stellar Systems, and the Sun*, volume 1094 of *American Institute of Physics Conference Series*, pages 61–70, 2009.
- Serre, T. and Nesme-Ribes, E. *Nonlinear analysis of solar cycles.* *A&A*, 360:319, 2000.
- Simon, L. *The life of the cosmos.* OXFORD UNIVERSITY PRESS, 1997.
- Skumanich, A. *Time Scales for CA II Emission Decay, Rotational Braking, and Lithium Depletion.* *ApJ*, 171:565, 1972. doi: 10.1086/151310.
- Soderblom, D., Duncan, D., and Johnson, D. *The Chromospheric Emission-Age Relation for Stars of the Lower Main Sequence and its Implications for the Star Formation Rate.* *ApJ*, 375:722, 1991.
- Sood, A. and Kim, E. *Dynamic model of dynamo (magnetic activity) and rotation.* *A&A*, 555:A22, 2013.
- Sood, A. and Kim, E. *Detailed mathematical and numerical analysis of a dynamo model.* *A&A*, 563:A100, 2014.
- Spada, F., Lanzafame, A. C., Lanza, A. F., Messina, S., and Collier Cameron, A. *Modelling the rotational evolution of solar-like stars: the rotational coupling time-scale.* *MNRAS*, 416:447–456, 2011.
- Steenback, M., Kruuse, F., and Rädler, H. *A calculation of the mean electromotive force in an electrically conducting fluid in turbulent motion, under the influence of Coriolis forces.* *Z. NAturef.*, A21:369, 1966.

- Thomas, J. H. and Weiss, N. O. *Sunspots and Starspots*. Cambridge University Press, 2008.
- Tobias, S. M. *The solar dynamo*. *Philosophical Transactions of the Royal Society of London A: Mathematical, Physical and Engineering Sciences*, 360(1801): 2741–2756, 2002.
- Tobias, S. M. and Cattaneo, F. *Shear-driven dynamo waves at high magnetic Reynolds number*. *Nature*, 497:463–465, 2013.
- Tobias, S. M., Weiss, N. O., and Kirk, V. *Chaotically modulated stellar dynamos*. *MNRAS*, 273:1150–1166, 1995a.
- Tobias, S. M., Weiss, N. O., and Kirk, V. *Chaotically modulated stellar dynamos*. *MNRAS*, 273:1150–1166, April 1995b.
- Vainshtein, S. and Zel'dovich, Y. *Origin of magnetic fields in astrophysics*. *Sov. Phys. Usp.*, 15:159, 1972.
- Vaughan, A. H. and Preston, G. W. *A Survey of Chromospheric Ca II H and K Emission in Field Stars of the Solar Neighborhood*. *PASP*, 922:385, 1980.
- Weiss, N. O., Cattaneo, F., and Jones, C. A. *Periodic and aperiodic dynamo waves*. *Geophysical and Astrophysical Fluid Dynamics*, 30:305–341, 1984.
- Wilmot-Smith, A. L., Martens, P. C. H., Nandy, D., Priest, E. R., and Tobias, S. M. *Low-order stellar dynamo models*. *MNRAS*, 363:1167–1172, 2005.
- Wright, J. T., Marcy, G. W., Butler, R. P., and Vogt, S. S. *Chromospheric Ca II Emission in Nearby F, G, K, and M Stars*. *ApJ Suppl. Ser.*, 152:261, 2004.
- Wright, N. J., Drake, J. J., Mamajek, E. E., and Henry, G. W. *The Stellar-activity-Rotation Relationship and the Evolution of Stellar Dynamos*. *ApJ*, 743:48, 2011.

Yoshimura, H. *A model of the solar cycle driven by the dynamo action of the global convection in the solar convection zone.* *ApJs*, 29:467–494, 1975.

Yoshimura, H. *Nonlinear astrophysical dynamos - The solar cycle as a nonlinear oscillation of the general magnetic field driven by the nonlinear dynamo and the associated modulation of the differential-rotation-global-convection system.* *ApJ*, 220:692–711, 1978.

Yousef, T. A., Heinemann, T., Rincon, F., Schekochihin, A. A., Kleeorin, N., Rogachevskii, I., Cowley, S. C., and McWilliams, J. C. *Numerical experiments on dynamo action in sheared and rotating turbulence.* *Astronomische Nachrichten*, 329:737, 2008a.

Yousef, T. A., Heinemann, T., Schekochihin, A. A., Kleeorin, N., Rogachevskii, I., Iskakov, A. B., Cowley, S. C., and McWilliams, J. C. *Generation of Magnetic Field by Combined Action of Turbulence and Shear.* *Physical Review Letters*, 100(18):184501, 2008b.